PROBABILISTIC CALIBRATION OF UNREINFORCED MASONRY WALL PROPERTIES: FROM CONSTITUTIVE MATERIAL MODELS TO STRUCTURAL PERFORMANCE

A Dissertation

by

QUDAMA JASIM MOHAMMED ALBU-JASIM

Submitted to the Office of Graduate and Professional Studies of
Texas A&M University
in partial fulfillment of the requirements for the degree of

DOCTOR OF PHILOSOPHY

Chair of Committee,	Zenon Medina-Cetina
Co-Chair of Committee,	Anastasia Muliana
Committee Members,	Arash Noshadravan
	Eduardo Gildin
Head of Department,	Robin Autenrieth

August 2020

Major Subject: Civil Engineering

ABSTRACT

Unreinforced masonry walls are structural elements consisting of brick units and mortar layers, which show brittle and nonlinear inelastic response with regards to their mechanical behavior. Brick and mortar components show large variations in their mechanical responses, which are attributed to variabilities in the processing conditions, compositions and types of constituents, and testing methods. The mechanical responses of brick and mortar 'components' strongly influence the performance and load bearing capabilities of masonry walls thought as 'systems'. Thus, developing appropriate constitutive models and calibration of material parameters in the constitutive models are important tasks for scientists in order to generate accurate model-based predictions. Determining material parameters of a constitutive model for a nonlinear inelastic response, while being a key factor to predict its mechanical response, is a tedious task. This difficulty is due to the limited experimental tests that can be performed. Thus, a proper determination of these material parameters is necessary to improve the predictions of the overall response of masonry walls. A Bayesian probabilistic calibration is conducted to investigate the effects of the uncertainty of concrete damage plasticity model parameters in masonry wall components, i.e., brick, mortar, and concrete. For this purpose, experimental tests are simulated using finite element method (FEM) and their responses are integrated to the probabilistic calibration algorithm. Markov Chain Monte-Carlo and Metropolis-Hastings algorithms are used to integrate the material parameters using random variables. A Neural Network Optimization algorithm is proposed to identify and characterize the material parameters for describing the mechanical response of unreinforced masonry walls.

Unreinforced masonry wall models are validated using the optimal material parameters that provide the best fitting between the simulation results of a masonry prism and the corresponding experimental data taken from the literature. From the tangential shear stress and normal stress distributions between brick units and mortar layers during lateral loading and vertical compression stress, potential failure modes along with their failure criteria are determined. The influence of vertical compressive stress, length-to-height "aspect ratio", and material parametric sensitivity (e.g., flexural tensile strength, compressive strength, coefficient of friction and cohesion stress) is investigated.

DEDICATION

I would like to dedicate my dissertation to my dad and my mom whom I love dearly. Here I am finishing my PhD and feel unhappy for not being beside my mom who passed away in 2017 from a severe disease; I wish I were there for you while you were struggling with the pain. My life would never be better when I listen to your voice praying and wishing the best for me. But I know you are there in heaven praying with angels and righteous. I am grateful to God for giving me such a great mom, and her unconditional love and support. I hope you with me to witness my accomplishments. I love you more than life itself and I love you to infinity and beyond.

Here I am again talking about the man behind the scenes, “my dad”. Words cannot be enough to how grateful you were supporting me. You were always there for me. I thank God for you every day. You blessed me far beyond what I could have ever hoped for in a father. You have taught me some much in my 35 years of life, and I appreciate every lesson you have offered me. Also, I would like to dedicate my dissertation to my wife and my kids Adam and Rayan. I appreciate all your hard work and love; you've always believed in me and wished to be a better person and a better engineer. Words can never tell how grateful I am. Words cannot even begin to express how much you mean to me. Thank you for the patience while I pursue my dream.

Also, I would like to thank my brothers and sisters; who love and guidance are with me in whatever I pursue. To my supportive wife; your encouragement when the times got rough, are much appreciated and noted.

ACKNOWLEDGEMENTS

I would like to acknowledge to several individuals who volunteered their time and effort to provide their wisdom toward the successful completion of my dissertation. All of these individuals were willing to offer whatever was needed to have this work completed.

This work would not have been possible without the support of my committee Chair, Dr, Zenon Medina-Cetina and my Co-Chair Dr. Anastasia Muliana, who provided me with extensive personal and professional guidance and taught me a great deal about both scientific research and life in general. Also, when I had a question, I always have their answers and advise available. Dr. Medina-Cetina and Dr. Muliana provided me significant guideline on my research in both aspects as an engineer and a scientist. Thank you, both of you, for believing in me and being such wonderful persons.

I would also like to extend my appreciation to my committee members, Dr. Arash Noshadravan and Dr. Eduardo Gildin, for consistently providing advice whenever I needed.

I would like to thank Dr. Papazafeiropoulos for providing significant information and support on the software "Abaqus2Matlab" (A2M). Also, when I have a question regarding to the software, he always answers my questions immediately. Thank you so much, Dr. Papazafeiropoulos, for your help and support. He was such a good friend during my Ph.D. journey.

I would like to thank Dr. Alma Rosa Pineda, who assisted me from the beginning until the end of the academic journey. Dr. Pineda provided significant suggestions and advice to help me with my research. I appreciate her help and support.

My special thanks to Dr. Martha Dannenbaum, who never hesitated to help and encourage me to continue and be always there when I need support. She was one of the greatest persons I have ever met in my life.

To my colleagues, I will never find another great teamwork like you during my degree.

Also, special thank for my friend Dr. Ali Alansari, who was always encouraging me and providing significant advice during my academic journey.

My special thanks to my country Iraq especially University of Misan whose support me financially during my academic journey.

CONTRIBUTORS AND FUNDING SOURCES

Contributors

This work was supervised by a dissertation committee consisting of Professor Medina-Cetina [advisor] Department of Civil and Environmental Engineering and Dr. Muliana [co-advisor] of the Department of Mechanical Engineering and two committee members: Dr. Arash Noshadravan of the Department of Civil and Environmental Engineering, and Dr. Eduardo Gildin of the Department of Petroleum of Engineering. All other work conducted for the dissertation was completed independently by the student.

Funding Sources

I am writing to acknowledge with deep gratitude to the Ministry of Higher Education and Scientific Research (MoHESR) of Iraq through University of Misan for supporting my graduate study at Texas A&M University.

NOMENCLATURE

A2M	Abaqus2Matlab
ANN	Artificial Neural Network
CDP	Concrete Damaged Plasticity
URM	Unreinforced Masonry
MCMC	Monte Carlo Markov Chain
NNO	Neural Network Optimization
Std	Standard Deviation

TABLE OF CONTENTS

Page

LIST OF FIGURES

Page

LIST OF TABLES

Page

1. INTRODUCTION

1.1. Problem Statement

Unreinforced masonry (URM) walls are widely used in many countries in the world, owing to their cultural and historical context and architectural charm. URM walls are a structural element consisting of brick and mortar 'components' which play a vital role in the resistance of structures against vertical and lateral loads. Because of the variation in their material properties and failure modes between the masonry layers, the mechanical response of this structural component becomes difficult to predict. Physical models of unreinforced masonry walls have the capability to reproduce all possible combinations of components, material parameters, and geometrical characteristics in order to provide a clear understanding of the mechanical responses of the URM walls under different load combinations 'thought as systems'. The physical models rely on appropriate constitutive material behaviors for all components of the masonry walls. Therefore, predicting accurately the model response through calibration of model parameters is a key process for obtaining realistic model-based predictions. The present study uses a Concrete Damaged Plasticity (CDP) model, which is available in ABAQUS FE analysis software, to simulate the nonlinear inelastic behavior of brick, mortar, and concrete, which are the components of an URM wall system (Hillerborg, Modéer, & Petersson, 1976; Lee & Fenves, 1998; J Lubliner, Oliver, Oller, & Oñate, 1989).

Design criteria of URM walls is effectively included into the International Building Code (IBC) due to the risk posed on this type of buildings found before the issuing of the most recent code seismic provisions. However, due to the uncertainty of the material

parameters an inherent vulnerability is present and small safety factors are anticipated according to IBC. This uncertainty depends on different aspects such as the inherent variation in the material behaviors and the wall system responses. The inverse problem of obtaining the URM system wall material properties by minimizing the error between the numerical and the experimental results has been implemented based on a probabilistic formulation. An early study of an inverse probability analysis was adapted to infer the actual values of the model parameters (Tarantola, 2005). Chisari, Macorini, Amadio, and Izzuddin (2015) identify and characterize material parameters using inverse problem for unreinforced masonry walls. A proper determination of the material parameters becomes necessary in order to obtain better predictions of the overall response of masonry walls systems. The probabilistic calibration also ensured that the material properties for each component fall within certain limits to better predict their behavior and be integrated into a full system of URM walls assemblages. The feasibility of the deterministic and calibration procedure is examined through correlation with the results of experimental work done by Blackard, Kim, Citto, Willam, and Mettupalayam (2007) , Mehrabi (1996), and Epperson and Abrams (1990).

Safety of URM walls systems has been a major concern in past decades due to many defects of resisting a possible earthquake or strong wind load which can cause severe failures. Generally, the material parameters govern the strength limit which is possible to affect the failure modes due to high or low vertical compressive stress Xu and Abrams (1992). FEMA 306 p.138 claim that variation of material properties (e.g., compression and tensile strength, young's modulus, shear moduli and shear strength) is an essential factor for in-plane capacity and masonry strength (Council, Response, & Agency, 1999). Therefore,

increasing the lateral resistance capacity by deterministic material parameters can provide a significant enhancement in the entire building during extensive loads. Also, evaluating the shear strength can provide a significant understanding of failure mechanisms. Many researchers have widely investigated the failure mechanisms of masonry, which mainly depend on the material parameter, under uniaxial compression, combined shear and compression, and tension in both experimental and theoretical analysis. Yokel and Fattal (1976) verified their hypotheses on failure mechanisms in URM walls systems, such as joint separation and splitting of four wall masonry panels, through experimental studies of 32 URM walls. Magenes and Calvi (1997) evaluate the strength, deformability, and energy dissipation capacity within in-plane loads of existing buildings. Recently, Rahman and Ueda (2014) investigated the shear stress through parametric studies of various parameters such as cohesion and friction angle by experiment and numerical analysis. Xu and Abrams (1992) evaluated the post cracking behavior of masonry walls tested by others subjected to vertical and lateral loads. These studies showed the variations in the masonry failure modes and failure criteria such as shear sliding, compressive splitting, and diagonal failure.

1.2. Research Objectives

The objectives of this research are:

- *To identify* & *characterize* key parameters of CDP influencing the strength and mechanical response for masonry's three independent components: Mortar, Bricks and Concrete in a Finite Element Method (FEM) simulation framework.
- *To assess* key parameters and experimental uncertainty which can be associated with the experimental observations using *probabilistic calibration* approach for Mortar and Bricks.

- *To investigate* the effects of material heterogeneity in masonry prism by randomly varying degrees of material parameters to predict the overall behavior.
- *To investigate* the effect of various parameters on lateral strength of unreinforced masonry walls (e.g., compressive strength, flexural strength, and coefficient of friction and cohesion stress)
- *To investigate* the relationship between shear strength and lateral displacement in term of the length-to-effective height "aspect ratio (l / h_{eff})".

1.3. Research Outline

Chapter 2 presents the collection of data to investigate the masonry infill wall component (e.g., brick, mortar and concrete), study material parametric sensitivity of seven parameters in CDP model, and obtain optimal parameters of masonry components using nonlinear least square optimization. Chapter 3 introduces the Bayesian probabilistic calibration of the optimal parameters for mortar and brick units using the Markov Chain Monte Carlo approach coupled with Metropolis Hastings criteria (MCMC- MH) to infer the statistical results. Chapter 4 illustrates the validation of the CDP model that is established through comparison of its numerical results related to FE analysis of a masonry prism to corresponding experimental stress strain curves using the NNO algorithm. Chapter 5 presents the study of material heterogeneity of masonry prisms and the development of a neural network optimization (NNO) algorithm to obtain the optimal constitutive parameters of the Abaqus CDP model which fit best the experimental stress strain response of the masonry prism. Afterwards, the optimal parameters of a CDP model established in chapter 4 will be used in chapter 6 to validate the experimental wall tests and investigate the shear

strength of the masonry walls in term of a relation between a vertical compressive stress and lateral load-displacement. Chapter 7 discusses the conclusions and future work.

1.4. References

Blackard, B., Kim, B., Citto, C., Willam, K., & Mettupalayam, S. (2007). Failure issues of brick masonry. Paper presented at the Proceedings of the Sixth International Conference on Fracture Mechanics of Concrete and Concrete Structures.

Chisari, C., Macorini, L., Amadio, C., & Izzuddin, B. (2015). An inverse analysis procedure for material parameter identification of mortar joints in unreinforced masonry. Computers & Structures, 155, 97-105.

Council, A. T., Response, P. f., & Agency, U. S. F. E. M. (1999). Evaluation of Earthquake Damaged Concrete and Masonry Wall Buildings: Basic Procedures Manual: The Agency.

Epperson, G. S., & Abrams, D. P. (1990). Nondestructive evaluation of masonry buildings (Vol. 89): University of Illinois at Urbana-Champaign.

Hillerborg, A., Modéer, M., & Petersson, P.-E. (1976). Analysis of crack formation and crack growth in concrete by means of fracture mechanics and finite elements. Cement and Concrete Research, 6(6), 773-781.

Lee, J., & Fenves, G. L. (1998). Plastic-damage model for cyclic loading of concrete structures. Journal of Engineering Mechanics, 124(8), 892-900.

Lubliner, J., Oliver, J., Oller, S., & Oñate, E. (1989). A plastic-damage model for concrete. International journal of solids and structures, 25(3), 299-326.

Magenes, G., & Calvi, G. M. (1997). In-plane seismic response of brick masonry walls. Earthquake engineering & structural dynamics, 26(11), 1091-1112.

Mehrabi, A. B. (1996). Behavior of masonry infilled reinforced concrete frames subjected to lateral loadings.

Rahman, A., & Ueda, T. (2014). Experimental investigation and numerical modeling of peak shear stress of brick masonry mortar joint under compression. Journal of Materials in Civil Engineering, 26(9), 04014061.

Tarantola, A. (2005). Inverse problem theory and methods for model parameter estimation (Vol. 89): siam.

Xu, W., & Abrams, D. P. (1992). Evaluation of Lateral Strength and Deflection for Cracked Unreinforced Masonry Walls. Retrieved from

Yokel, F. Y., & Fattal, S. G. (1976). Failure hypothesis for masonry shear walls. Journal of the Structural Division, 102(3), 515-532.

2. OPTIMIZING THE MATERIAL PARAMETERS IN A CONCRETE DAMAGE PLASTICITY MODEL IN MASONRY INFILL WALLS

2.1. Introduction

This chapter discusses the identification and characterization of material parameters in a concrete damage plasticity constitutive model that is being used for describing the mechanical responses of brick, mortar, and concrete in an unreinforced masonry infill wall. Each of the above components exhibits a nonlinear and inelastic response, which requires a number of material parameters to capture its response. Experimental data also show large variations in their mechanical responses, which are attributed to various material compositions, processing conditions, and specimen types. Thus, a proper determination of these material parameters becomes necessary in order to obtain better predictions of the overall responses of the masonry wall. In this study, a concrete damage plasticity model was used to describe the stress-strain relationship in each constituent of an unreinforced masonry infill wall under uniaxial compression. Extensive datasets of the material properties of mortar, brick, and concrete, as well as the associated stress-strain curves, were collected from the literature. A parametric analysis is first conducted to evaluate the correlated and uncorrelated parameters in representing the overall compressive responses of the constituents, in order to engage in proper calibration. In this study, Abaqus2Matlab (A2M) is used as an interface for linking ABAQUS and MATLAB. The A2M application serves for transferring results from ABAQUS to MATLAB and vice versa, allowing for an integrated programing and simulation environment. The post-processing algorithm A2M (Papazafeiropoulos, Muñiz-Calvente, & Martínez-Pañeda, 2017) and an inverse method

were used to optimize the parameters and minimize the differences between the experimental observations and numerical predictions. The A2M optimization algorithm was then employed to fit the stress-strain curves associated with the uncertainties, allowing for a comparison with the data observations.

2.2. Background

Unreinforced masonry (URM) walls are structural elements consisting of brick and mortar, which show brittle and nonlinear inelastic responses with regards to their mechanical behaviors. Formulating constitutive models and calibrating material parameters in the constitutive models are essential in order to provide reliable predictions of the responses of materials. Typical constitutive models for nonlinear inelastic materials include a number of material parameters that are usually determined from experimental tests. Examples of constitutive models that have been formulated for masonry walls and their constituents as well as a discussion on validating the calibrated material parameters can be found in the following literature (Gambarotta & Lagomarsino, 1997; Grassl & Jirásek, 2006; Lee & Fenves, 1998; Lotfi & Shing, 1991; Jacob Lubliner, 1991; J Lubliner et al., 1989). Several studies have discussed a wide variety of the material parameters calibrated from experimental data and provided a typical range for different parameters, e.g., the dilatancy angle , ψ, (0-36°), biaxial strength ratio , $^{fb}/_{fc'}$ (1.10-1.16) and deviatoric plane in the yield surfaces , κ, (0.5-1) (Jankowiak & Lodygowski, 2005; Kmiecik & Kamiński, 2011; J Lubliner et al., 1989). An alternative approach has been on identifying material parameters by determining the parameters using forward calibration process instead of inverse problem techniques to validate experimental parameters by using a constitutive models and try to

minimize the errors between the model and the experiment(Cecchi & Sab, 2002; Chisari, Macorini, Amadio, & Izzuddin, 2018; Jankowiak & Lodygowski, 2005; Renata Morbiducci, 2003; R Morbiducci & Shing, 1998; Sarhosis & Sheng, 2014). To minimize errors between the observation-based datasets and model parameters, inverse methods have been applied to identify and characterize the material properties in the constitutive models (Carmeliet, 1999; Chisari, 2015, 2019; Chisari et al., 2015; Chisari et al., 2018; Fadale, Nenarokomov, & Emery, 1995; Muñoz-Rojas, Cardoso, & Vaz, 2010; Nazari & Sanjayan, 2015; Rechea, Levasseur, & Finno, 2008; Sarhosis & Sheng, 2014; V. V. Toropov & van der Giessen, 1993). In this paper, the objective function was applied using the least-squares technique suggested by Legendre and Gauss in the 1800s, which minimizes the sum of the square of the difference between experiment-based measurements and the calculated response of a model.

The present study uses a concrete damage plasticity (CDP) model, which is available in ABAQUS FE analysis, to simulate the nonlinear inelastic behavior of brick, mortar, and concrete, which are the constituents of a masonry wall (Hillerborg et al., 1976; Lee & Fenves, 1998; J Lubliner et al., 1989). The CDP model has two components: the plasticity and damage mechanics with the typical failure modes (i.e., cracking in tension and crushing in compression). The CDP model is first examined in capturing the mechanical response of brick, mortar and concrete. For this purpose, experimental data from (Blackard et al., 2007) and (Mehrabi, 1996) are used. Models for the brick, mortar, and concrete are generated using 3D continuum element in order to mimic the tested specimens (cylindrical specimens for mortar and concrete and a rectangular cuboid for the brick) in the experiments. In order to safe computational cost during the optimization, we also consider an axisymmetric element

to represent the cylinder specimen and a one-eight symmetric model for the brick. Responses from different elements are assessed for their numerical accuracy and cost efficiency. A sensitivity analysis is also performed for the material parameters in the CDP (e.g., $E, \upsilon, f'c, \psi, {}^{fb}/_{fc}, \epsilon, \kappa, \mu$) for the mortar in order to understand the influence of each of these parameters on the overall mechanical response.

In this research, experimental data, in terms of stress-strain relations, were collected for mortar, brick, and concrete under a uniaxial compression in order to study variations in material properties with different material compositions (e.g., the cement type, lime contents, and water-to-cement ratio), processing conditions, and specimen shapes (C. Barbosa, Lourenço, Mohamad, & Hanai, 2007; C. S. Barbosa, Lourenço, & Hanai, 2010; Ciornei, 2012; Fiorato, Sozen, & Gamble, 1970; Gonçalves, Tavares, Toledo Filho, Fairbairn, & Cunha, 2007; Illampas, Ioannou, & Charmpis, 2014; Kaushik, Rai, & Jain, 2007; McNary & Abrams, 1985; Mohamad, Lourenço, & Roman, 2006; Nguyen, 2014; Singh & Munjal, 2017; Venkatarama Reddy & Gupta, 2006; Xavier & Francisco, 2015) (See Appendixes A). Variations in the material properties became very useful in the optimization strategies for selecting the range of material properties based on the data population. Because of variations in the stress-strain curves that appear in the literature, the empirical cumulative density (ECD) function was considered. This study employed a new optimization algorithm based on the Abaqus2Matlab software (A2M), which is an interface process used to calibrate the proper parameters through inverse problem analysis. The extensive variations in the stress-strain experimental data allow to test capability for optimizing the appropriate

material parameters in the CDP (e.g., $E, \upsilon, f'c, \psi, {}^{fb}/_{fc}, \epsilon, \kappa, \mu$), by setting the upper and lower bounds of each parameter.

2.3. Data Collection for Mortar, Concrete, and Brick

Various combinations of cement, lime, sand, and water produce either strong or weak mortar. Early studies found that Portland cement provides strong mortar compared to pozzolanic cement. However, the water-to-cement ratio and amount of lime more directly control mortar's hardness or softness. Soft mortar can offer a good cohesion bond with the masonry unit as well as weak strength, while strong mortar can easily be separated under a load. Figure 2.1 lists uniaxial compressive stress-strain responses of mortar under various conditions discussed above. These variations result in different material parameters in the CDP model.

Early studies investigated concrete cylinders or cubes in an effort to understand the distribution of stress through a compression zone and the general stress-strain relationship (Desayi & Krishnan, 1964; Fiorato et al., 1970; Hognestad, Hanson, & McHenry, 1955; Mehrabi, 1996; Mosalam, 1996; Smith & Young, 1956; Stavridis, 2009) (see Figure 2.2). These data were used to validate the accuracy of the parameters embedded in ABAQUS and simulate the concrete frame of a URM wall.

Brick is the most common type of masonry in the world. There can be substantial variations in brick strength due to the material type, geometric effect, and manufacturing process. Several studies have tested these individual components, seeking to understand the behavior of brick under compression loads (C. S. Barbosa et al., 2010; Blackard et al., 2007; Blackard, Willam, & Mettupalayam, 2009; Kaushik et al., 2007; Mohamad, Fonseca,

Vermeltfoort, Martens, & Lourenço, 2017; Mosalam, 1996; Singh & Munjal, 2017; Stavridis, 2009; Yang, Lee, & Hwang, 2019) (see Figure 2.3).

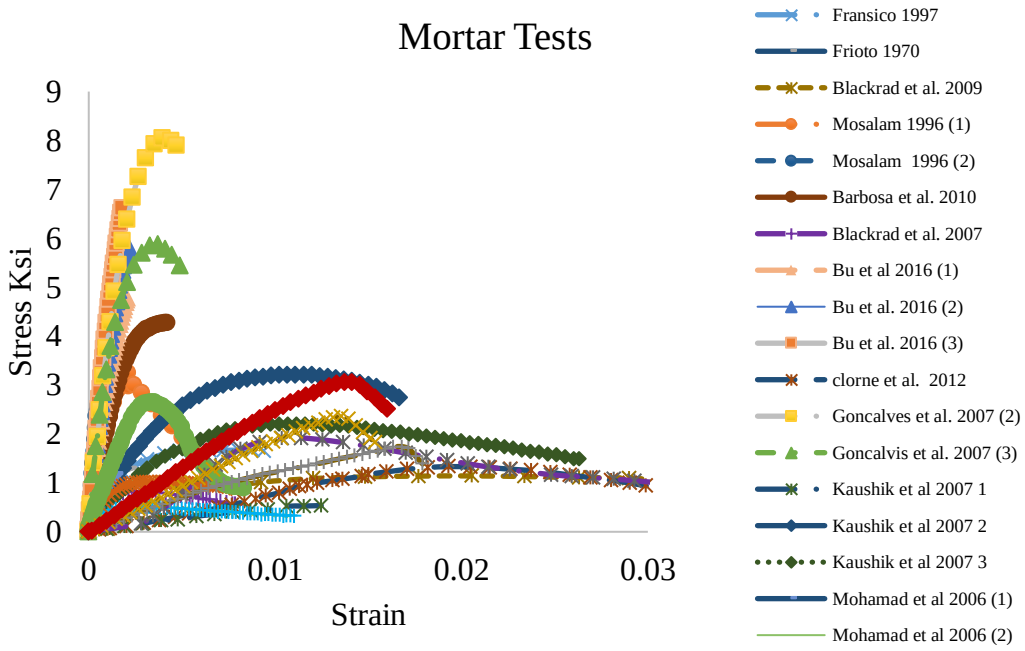

Figure 2.1 Mortar data collections(Fiorato, et al. 1970; Mosalam 1996; Fransico 1997; Blockrad et. al 2009; Blockrad et. al 2007; Barbosa et al. 2010; Cheng & Khoo 1972; Gonçalves et al., 2007; Mohamad et al. 2006 ; Mohamad et al., 2016 ; Ciornei 2012; Nguyen 2014; Kaushik, et. al. 2007; Bu.et al., 2016; Singh & Munjal 2016)

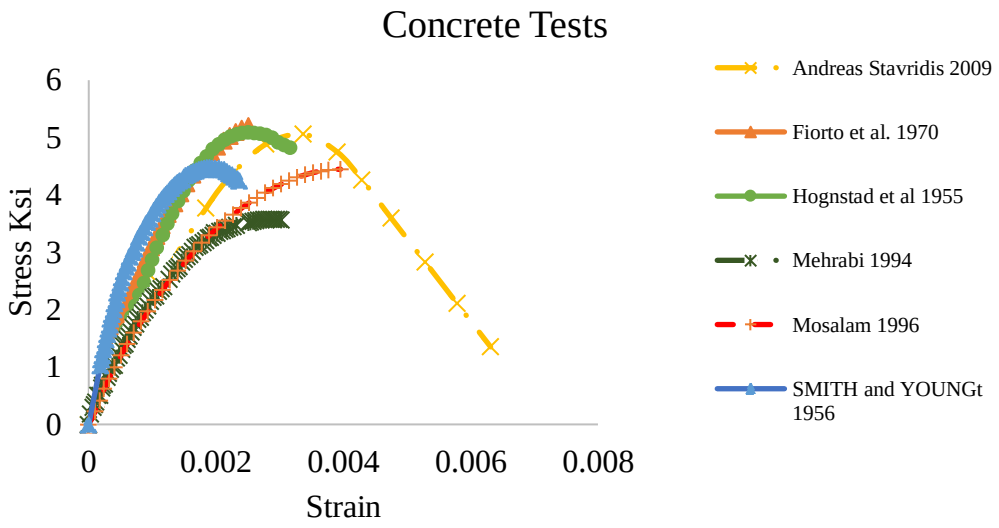

Figure 2.2 Concrete data collections (Fiorato 1970; Mehrabi 1996; Stavridis 2009; Nguyen 2014; Hognstad et al., 1955; Smith & Young 1956)

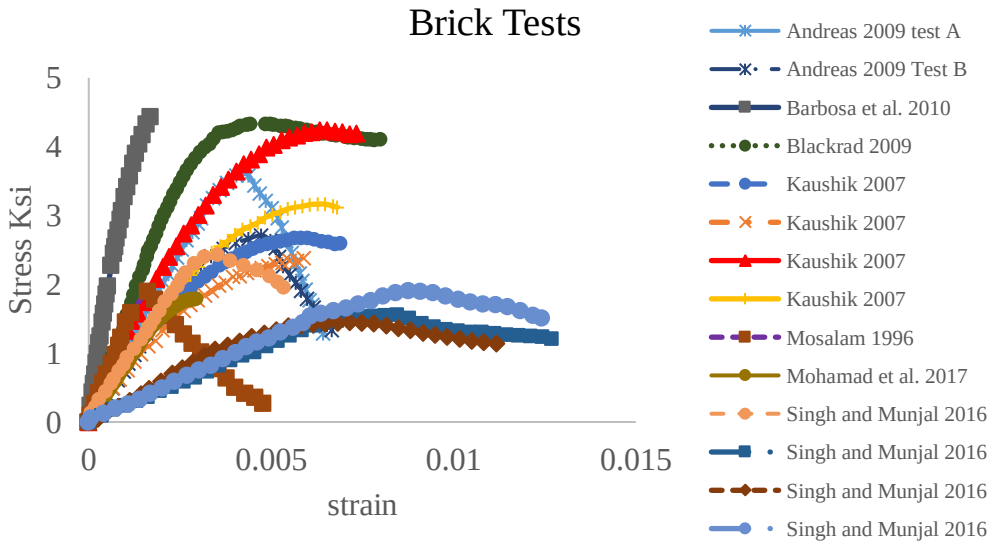

Figure 2.3 Brick data collections (Mosalam 1996; Barbosa et al. 2010; Andreas 2009; Mohamad et al., 2016; Singh & Munjal 2016; Kaushik et al., 2007; Blockrad et. al., 2009; Blockrad et. al., 2007; Singh & Munjal 2016)

2.4. Concrete Damage Plasticity Model

The identification of constitutive parameters is a fundamental phase of replicating experimental tests of stress-strain curves. The constitutive model for concrete materials is expressed within the framework of plasticity theory and the theory of damage mechanics, both of which have been investigated since the 1970s (A. C. Chen & Chen, 1975; Demin & Fukang, 2017; Feenstra & De Borst, 1996; Grassl, 2004; Grassl, Xenos, Nyström, Rempling, & Gylltoft, 2013; Hillerborg et al., 1976; Pramono & Willam, 1989). Concrete material is a complex phenomenon reflecting elastic and inelastic behaviors of brittle materials. The typical failure modes of concrete materials include crushing under compression and cracking under tension. In this study, to analyze the mechanical response of masonry structures a CDP constitutive model that describes both plasticity modes and damage behaviors, J Lubliner et al. (1989), is used.

For brittle materials that undergo small deformation, the elastic and inelastic strains are additively decomposed:

$$\boldsymbol{\varepsilon} = \boldsymbol{\varepsilon}^{e} + \boldsymbol{\varepsilon}^{p} \qquad (1)$$

The superscript ‘e’ and ‘p’ denotes elastic and inelastic components of strain. The model introduces two types of stresses, the actual stress $\bar{\boldsymbol{\sigma}}$ and the apparent stress $\boldsymbol{\sigma}$, which is the stress defined based on the degraded elastic fourth order tensor (stiffness matrix) $\boldsymbol{C}$. The actual and apparent stresses are related though the damage variable d, whose values are between 0 (no damage) and 1 (complete damage), as follow:

$$\boldsymbol{\sigma} = (1-d)\bar{\boldsymbol{\sigma}} \qquad (2)$$

The general stress-strain relationship can be written as:

$$\boldsymbol{\sigma} = \boldsymbol{C} : (\boldsymbol{\varepsilon} - \boldsymbol{\varepsilon}^p) = (1-d)\boldsymbol{D}^e : (\boldsymbol{\varepsilon} - \boldsymbol{\varepsilon}^p) \qquad (3)$$

where $\boldsymbol{D}^e$ is the initial (undamaged) elasticity tensor. For an isotropic material $\boldsymbol{D}^e$ is expressed in terms of the elastic modulus E and Poisson's ratio ν.

In order to determine the inelastic strain component, a plastic flow potential G and the associated yield function (in this case failure surface) F need to be defined. In brittle and granular materials like mortar and concrete, significant volume changes during inelastic deformation can induce distortion. Such an effect can be incorporated by having the flow potential G to depend on the dilatancy angle ψ and stress measure, see Lubliner et al. (1989). The CDP assumes a non-associated potential plastic flow and for the Drucker-Prager hyperbolic form, the following form is considered:

$$G = \sqrt{(\partial \sigma_t \tan\psi)^2 + 3J_2} + I_1/3\tan\psi \qquad (4)$$

where J_2 is the second invariant of the deviatoric stress, I_1 is the first invariant of stress. Another parameter in CDP is the eccentricity ∂ is a ratio of tensile strength to compressive strength ratio which depends on the cross-section of the deviatoric plane, and σ_t is the uniaxial tensile test to failure that is obtained from experiment.

For the CDP, Lubliner et al. (1989) considered the following form for the failure surface F:

$$F = \frac{1}{(1-\alpha)}\left[\sqrt{3J_2} + \alpha I_1 + \beta\langle\sigma_{\max}\rangle - \gamma\langle -\sigma_{\max}\rangle\right] \qquad (5)$$

where α is a dimensionless constant that depend on the ratio of the initial equibiaxial and uniaxial compressive yield stresses f_b / f_c as: $\alpha = \frac{(f_b/f_c)-1}{2(f_b/f_c)-1}$. The parameter β involves

the ratio of the uniaxial compressive yield stress to the uniaxial tensile yield stress f_t, written as $\beta=(1-\alpha)(f_c/f_t)-(1+\alpha)$. Finally, γ represents a constant from triaxial compression $\gamma=\frac{3(1-\kappa)}{2\kappa-1}$ where κ is the ratio of the distance between the hydrostatic axis and with respect to the compression meridian (CM), and the tension meridian (TM) in the deviatoric plane, known as deviatoric out of roundness. Under a uniaxial compressive test $\sigma_{\max}=1/3\left(I_1+\sqrt{3J_2}\right)$.

Finally, concrete and mortar experimental tests are usually shown softening behavior and stiffness degradation. Capturing the softening behaviors often result in numerical convergence. In ABAQUS FE, the softening behaviors are solved by introducing a viscoplastic constitutive equation in order to avoid numerical convergence. Thus, an additional material parameter, i.e., viscosity μ is required for the softening behavior.

In summary, the above CDP model involves seven material parameters (i.e., $E,\nu,f'c,\psi,f_b/f_c,\dot{o},\kappa,\mu$). The CDP was developed to represent all damage states, using the concept of fracture energy-based damage and stiffness degradation mechanics (Grassl & Jirásek, 2006; Lee & Fenves, 1998). The CDP model is available in the ABAQUS library, which has the ability to capture the appropriate nonlinear inelastic behaviors of brittle materials. The above material parameters need to be characterized from available experimental tests. For many brittle materials, such as concrete and mortar, these parameters are bounded by certain ranges, discussed below.

The compressive strength $f'c$ is the capacity of uncrack portion of the concrete structural member to carry the loads prior to cracking. Several studies tested a plain concrete and reinforced concrete to determine critical stressed which lie between 0.6 $f'c$ and 0.8 $f'c$

(Jenq & Shah, 1985; Karsan & Jirsa, 1969). Hognestad et al. (1955) studied the ultimate strength based on s flexural stress distribution and developed a stress-strain relation from the tested prism specimens under concentrated compression loads. Philleo (1955) tested and compared concrete specimens under three loads conditions (static, resonance, and pulse velocity) to determine the elastic and inelastic response and computed the Young's modulus E . The author stated that the results showed a variation in the results which are associated with the heterogeneity of the concrete, size and shape of the specimens, and equipment's accuracy. Kolluru, Popovics, and Shah (2000) tested a 3D cylinder concrete sample to determine the Young's modulus E and Poisson's ratio ν using the dynamic method.

The variable f_b/f_c is the ratio of biaxial initial yield stress to the uniaxial yield stress. J Lubliner et al. (1989) determined the value of f_b/f_c by testing a concrete specimen under biaxial compression at the yield surface $F(\sigma_{\max}) = 0$ with respect to the uniaxial compression to obtain stresses f_b/f_c . J Lubliner et al. (1989) claimed that during his experimental tests, the value for f_b/f_c was between 1.10 to 1.16 and the recommended value according to ABAQUS's manual is 1.16 (Hibbitt, Karlsson, & Sorensen, 2011).

The value of the deviatoric out of roundness κ varies from 0.5 to 1. When κ equal to 1 it means the yield surface has a circular shape which represents the Dracker-Prager yield surface criterion (W.-F. Chen & Han, 2007; J Lubliner et al., 1989).

The value of the dilatancy angle was between 0° and 36°. Michał and Andrzej (2015) recommended that the value be low as possible, in order to capture realistic model behavior. During the present study, the dilatancy angle correlated with the viscosity value used to

capture the model behavior. For the eccentricity, it is necessary to have the value of ϵ greater than 0 which means the compression meridian CM should be different than the tensile meridian TM and the eccentricity ϵ and deviatoric out of roundness κ are necessary to be greater than 0 and 0.5 to preserve the convexity condition of the failure (Jirasek & Bazant, 2002). The value of eccentricity $\grave{o}$ is affected by the shape of the deviatoric section and the load angle $r(\theta)$ between the meridians, and the recommended value in ABAQUS is 0.1 (Hibbitt et al., 2011). The formula that used to calculate the $\grave{o}$ is correlated to f_b/f_c in which is proposed by Jirasek and Bazant (2002).

$$\grave{o} = \frac{1+\beta}{2-\beta} \qquad (6)$$

where $\beta = \frac{f_t f_b^2 - f_c^2}{f_b f_c^2 - f_t^2}$, f_c and f_t are the compression and tension strength and f_b the biaxial strength. In addition, the values for $\grave{o}$ and β parameters should be greater than zero and 0.5, respectively, in order to obtain the convexity condition of the failure surface.

The viscosity μ is a parameter that can control the softening behavior is adopted in ABAQUS FE. Michał and Andrzej (2015) calibrated the viscosity μ in the ABAQUS FE for different parameters (i.e., 0, 0.0001, 0.001, and 0.01), and the recommended value for using the viscosity is 0.0001.

2.5. Model Validation

Blackard et al. (2007) tested and numerically simulated masonry prisms, including each component of cement mortar and clay brick, and subjected them to uniaxial compression loads. The compression simulations for the cement mortar, concrete, and brick were conducted on 4" × 8" cylinders of mortar and concrete, and 4.5" × 3.75" × 2.25"

samples of clay brick. The simulations were done using a CDP constitutive model available in ABAQUS and the results are compared to the experiments. 3D cylinder models have used for mortar and concrete and a 3D rectangular cuboid for brick to verify the stress-strain curves from the experiments. The CDP model is shown capable in capturing the stress-strain relations for the mortar, brick, and concrete (see Figure 2.4. The simulation in the present research showed better results and was closer to the experiment results than were other simulations (see Figure 2.5). Also, tests on concrete were conducted to validate the compressive strength of masonry infill walls (Mehrabi, 1996). The simulation shows that CDP model is capable in describing the overall stress-strain response. Table 2.1-3 is showing the calibrated material parameters performed in the present study, which are also compared to the parameters used by (Blackard et al., 2007; Mehrabi, 1996).

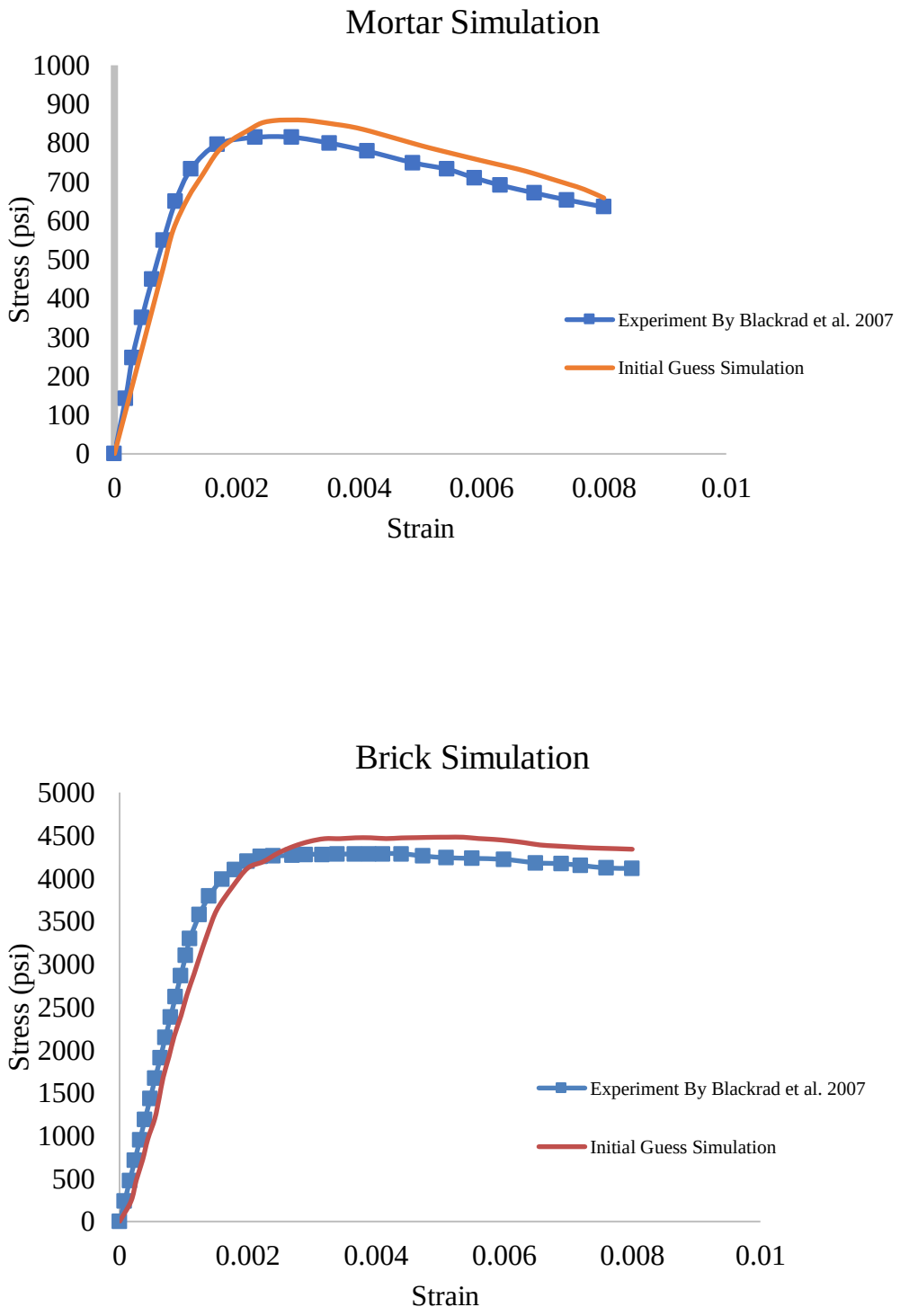

Figure 2.4 Model validation vs data from experiment and literature (Blackard et al., 2007; Mehrabi 1996)

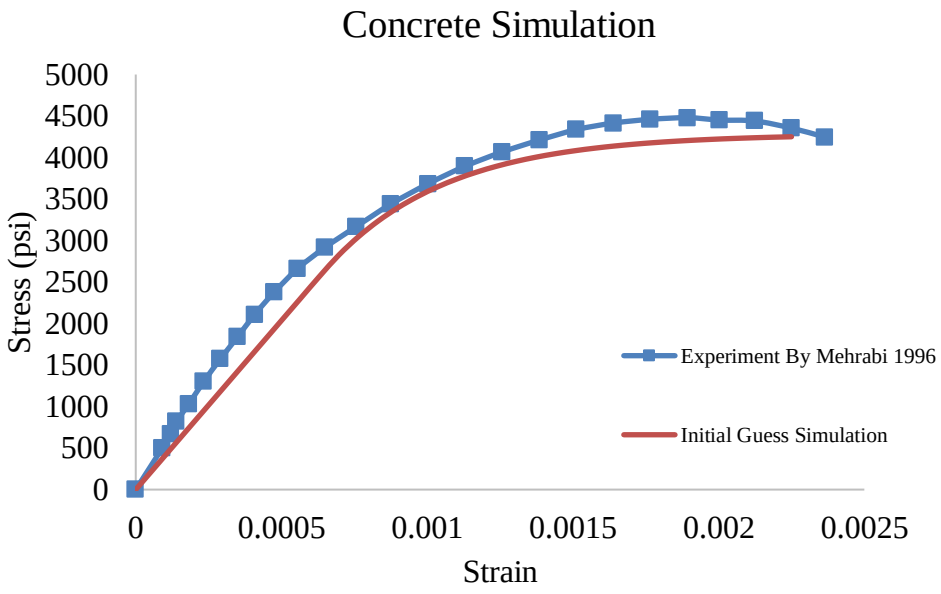

Figure 2.4 Continued

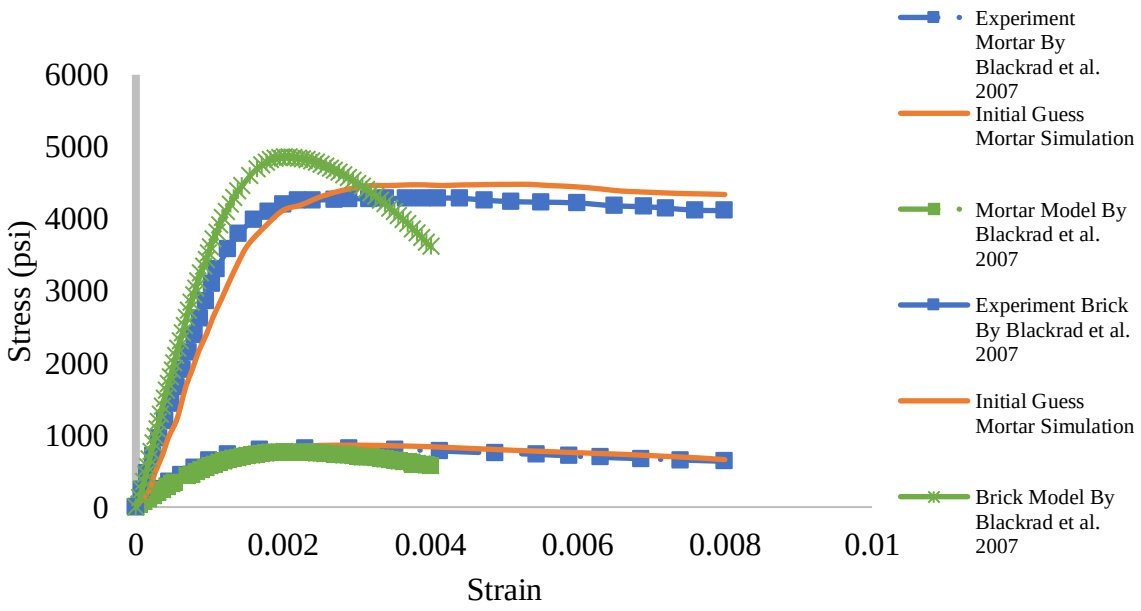

Figure 2.5 Present Simulation Compared to Experiment and simulation by Blackard et al. (2007)

Table 2.1 Model Validation Parameters Vs Previous Study Parameters for Mortar

Mortar Test	$E(psi)$	ν	ψ	f_b/f_c	$\grave{o}$	κ	μ
Blackard et al. (2007)	5×10^5	0.2	20	1.15	0.1	0.7	0
Initial Guess	5×10^5	0.2	20	1.16	0.1	0.667	0.001

Table 2.2 Model Validation Parameters Vs Previous Study Parameters for Brick

Brick Test	$E(psi)$	ν	ψ	f_b/f_c	$\grave{o}$	κ	μ
Blackard et al. (2007)	3×10^6	0.1	20	1.15	0.1	0.7	0
Initial Guess	3×10^6	0.1	20	1.16	0.1	0.667	0.001

Table 2.3 Model Validation Parameters Vs Previous Study Parameters for Concrete

Concrete Test	$E(psi)$	ν	ψ	f_b/f_c	$\grave{o}$	κ	μ
Mehrabi (1996)	3×10^6						
Initial Guess	3×10^6	0.15	36	1.16	0.1	0.667	

2.6. Model Parameters Analysis

Model parameters are the most influential component with regards to results, and they need to be identified through model analysis sensitivity. To evaluate the parameters of the CDP model a 3D cylinder mortar was simulated. The ABAQUS simulation employed a 3D model with a 4” in diameter and 8” height of a cylindrical shape. The concrete damage

plasticity (CDP) model has many parameters ($E, \nu, f'c, \psi, f_b/f_c, \dot{o}, \kappa, \mu$) that needed to be investigated to better understand their influence on the stress-strain relationship. Because there are many variations in the stress-strain curves that appear in the literature, an Empirical Cumulative Density (ECD) function was employed in the present work only for Young's modulus and compressive stress (see Figure 2.6). Other parameters (e.g, $\nu, \psi, f_b/f_c, \dot{o}, \kappa, \mu$) values were considered from the validation model to represent the main model for the parametric analysis study. These parameters were varied individually to facilitate an understanding of the sensitivity level of each. The Empirical Cumulative Density Function (ECDF) was measured for the Young's modulus E and compressive strength, $f'c$, the most sensitive parameters in the CDP model. The main model was developed based on the ECD results and parameters obtain by model validation individually for illustrating the stress-strain curves for each parameter change ($\mp$10%, 20%, and 30%). Four parameters were shown to be more sensitive ($E, f'c, \kappa, \mu$) than the others (see Figure 2.7). The process of the parametric analysis illustrates in flow chat (see Figure 2.8).

2.7. Optimization

An optimal parametric study was conducted using the Abaqus2Matlab interface (Papazafeiropoulos et al., 2017) in order to minimize the difference between the experiment-based observations and numerical predictions related to the CDP model. Abaqus2Matlab (A2M) is a post-processing algorithm connecting ABAQUS and MATLAB, which is used to simulate a finite element model (Papazafeiropoulos et al., 2017). The simulations in this study were conducted for three components – mortar, concrete, and brick – in order to obtain

the optimum parameters of the constitutive model, such as the Young's modulus, Poisson ratio, compressive strength, etc., and minimize errors in the stress-strain curves. The axisymmetric model was used to evaluate both mortar and concrete samples of cylindrical specimens, and the symmetry model was used for brick specimen (see Figure 2.9). The objective function used to simulate the model parameters was nonlinear least squares $|Min|\| f(x)\|^2 = \min \| \boldsymbol{d}_{obs} - \boldsymbol{d}_{pred} \|^2$, where $\boldsymbol{d}_{obs}$ and $\boldsymbol{d}_{pred}$ are used to identify and characterize the uncertainty associated with the stress-strain of the observations $\boldsymbol{d}_{obs}$ and the stress-strain of the predictions $\boldsymbol{d}_{pred}$ obtained from experimentation and numerical simulations respectively:

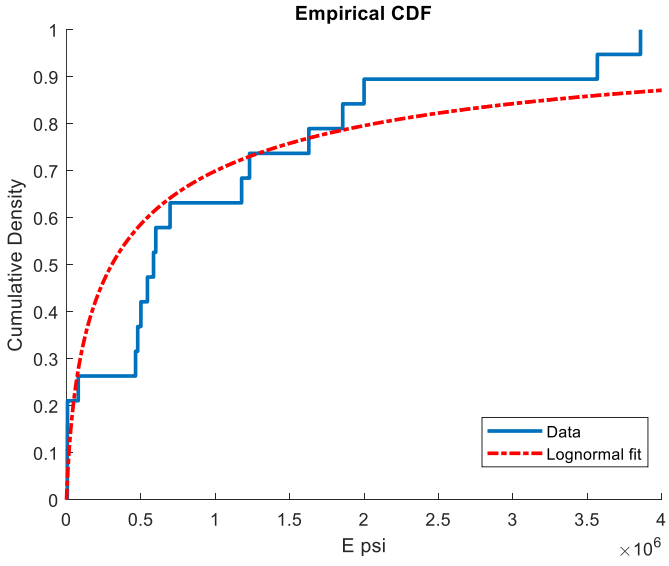

a)

Figure 2.6 Empirical Cumulative Density Function for a) compressive strength b) Young's modulus

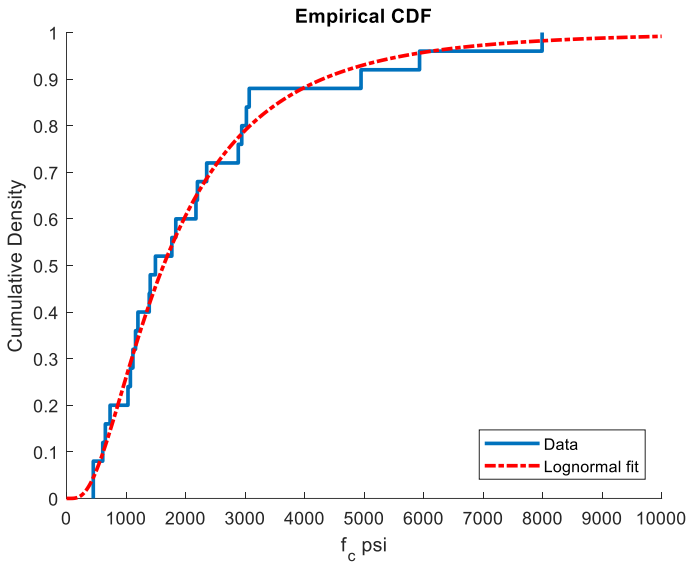

b)

Figure 2.6 Continued

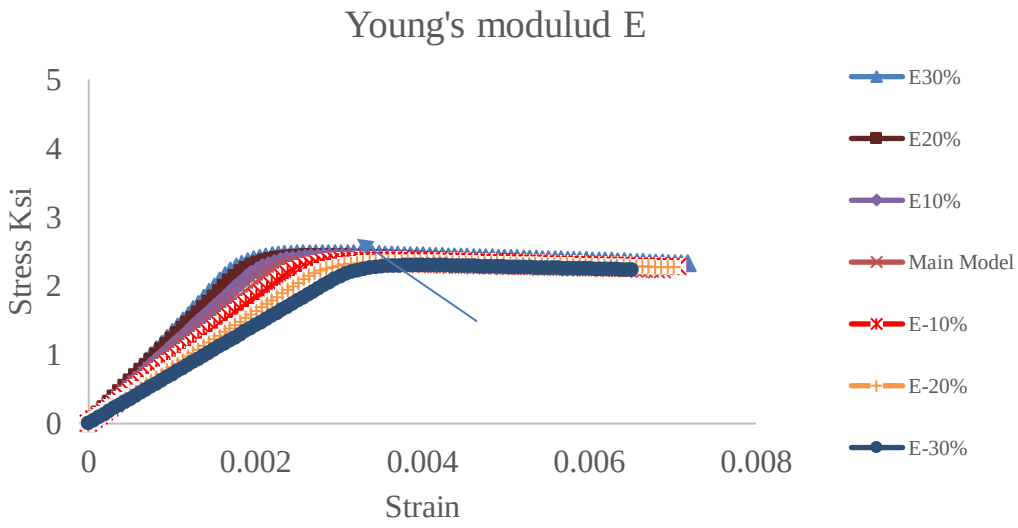

a)

Figure 2.7 Model parameters sensitivity of the CDP model for a)Young's modulus, b) Compressive Strength, c) dilatancy angle, d) Poisson's ratio, e) eccentricity, f) Biaxial to uniaxial yield stress, g) deviatoric out of roundness h) viscosity

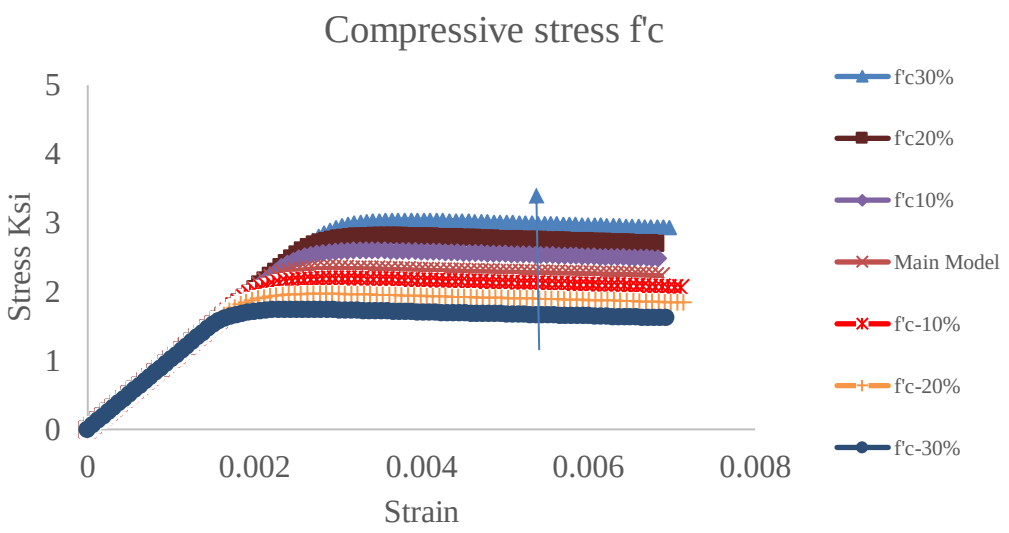

b)

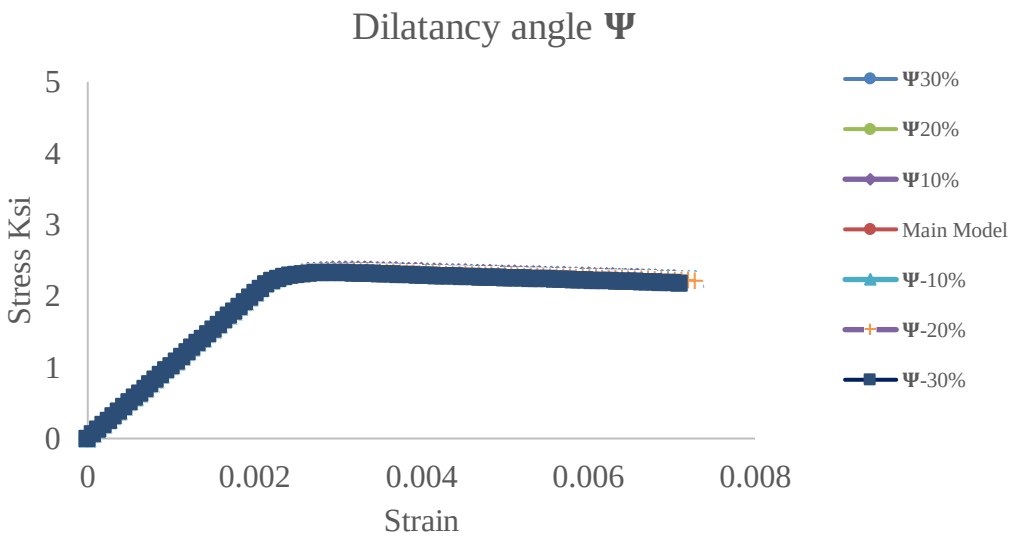

c)

Figure 2.7 Continued

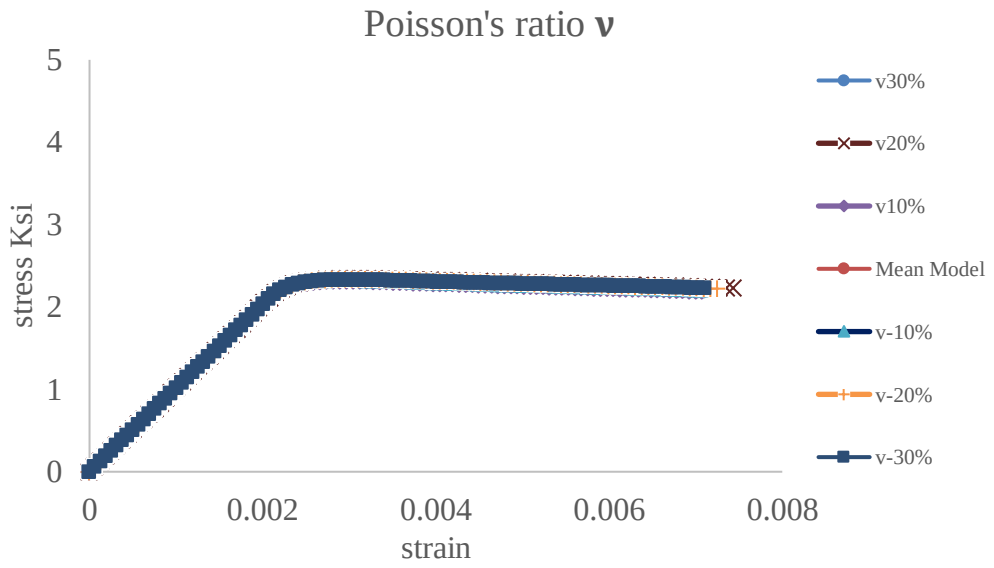

d)

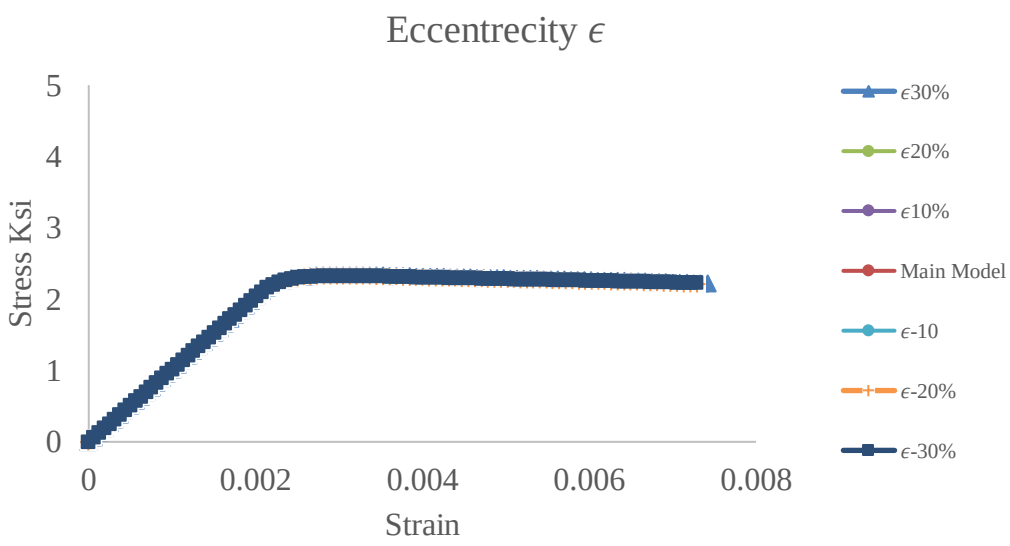

e)

Figure 2.7 Continued

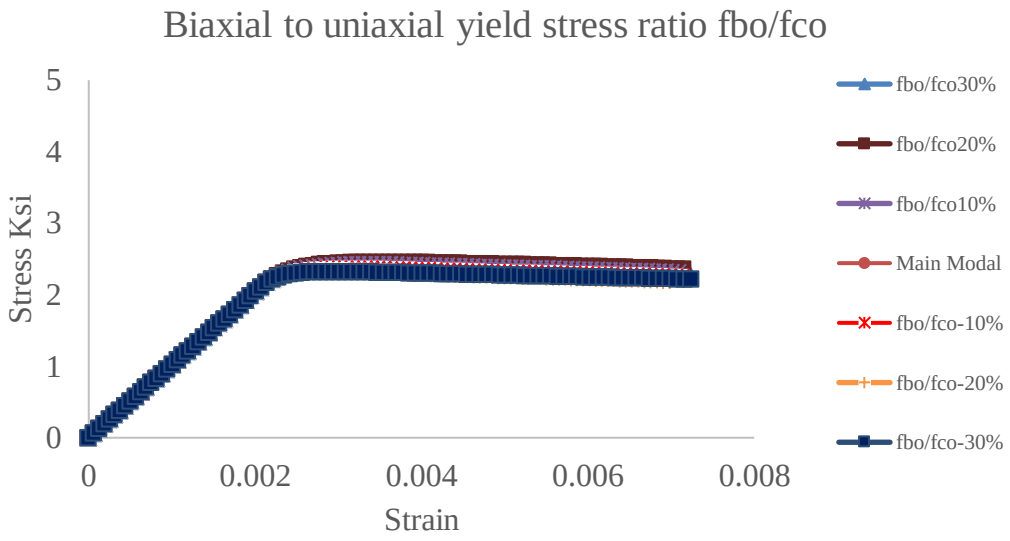

f)

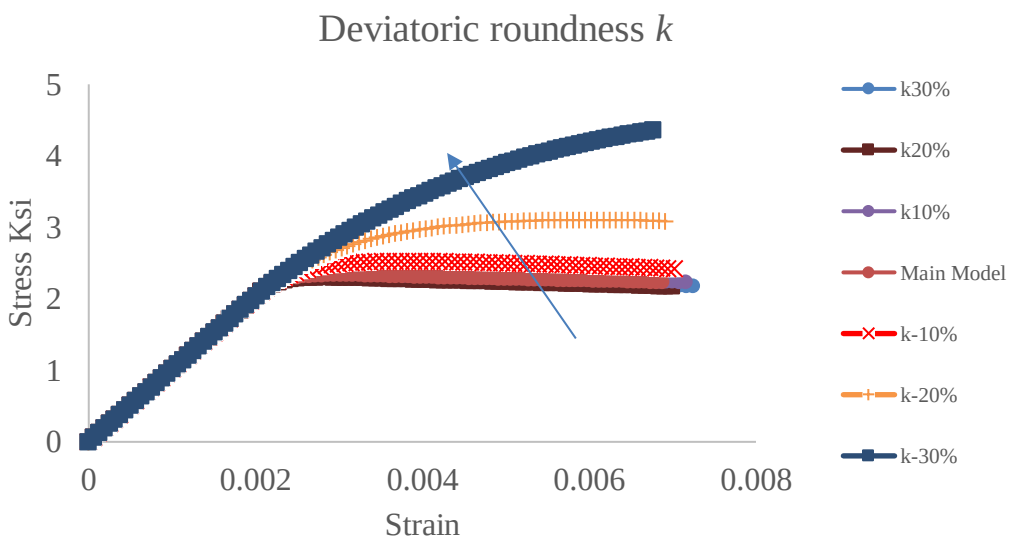

g)

Figure 2.7 Continued

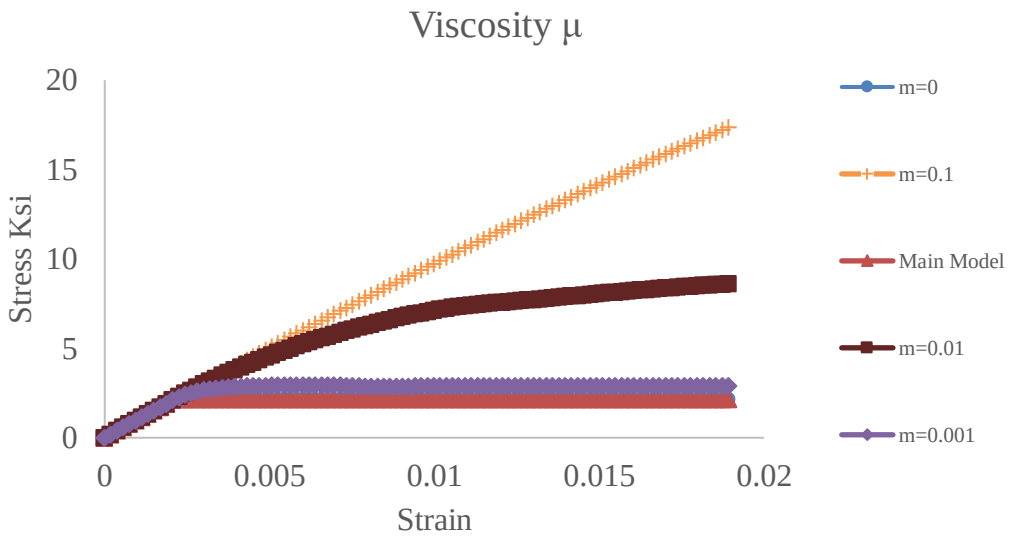

h)

Figure 2.7 Continued

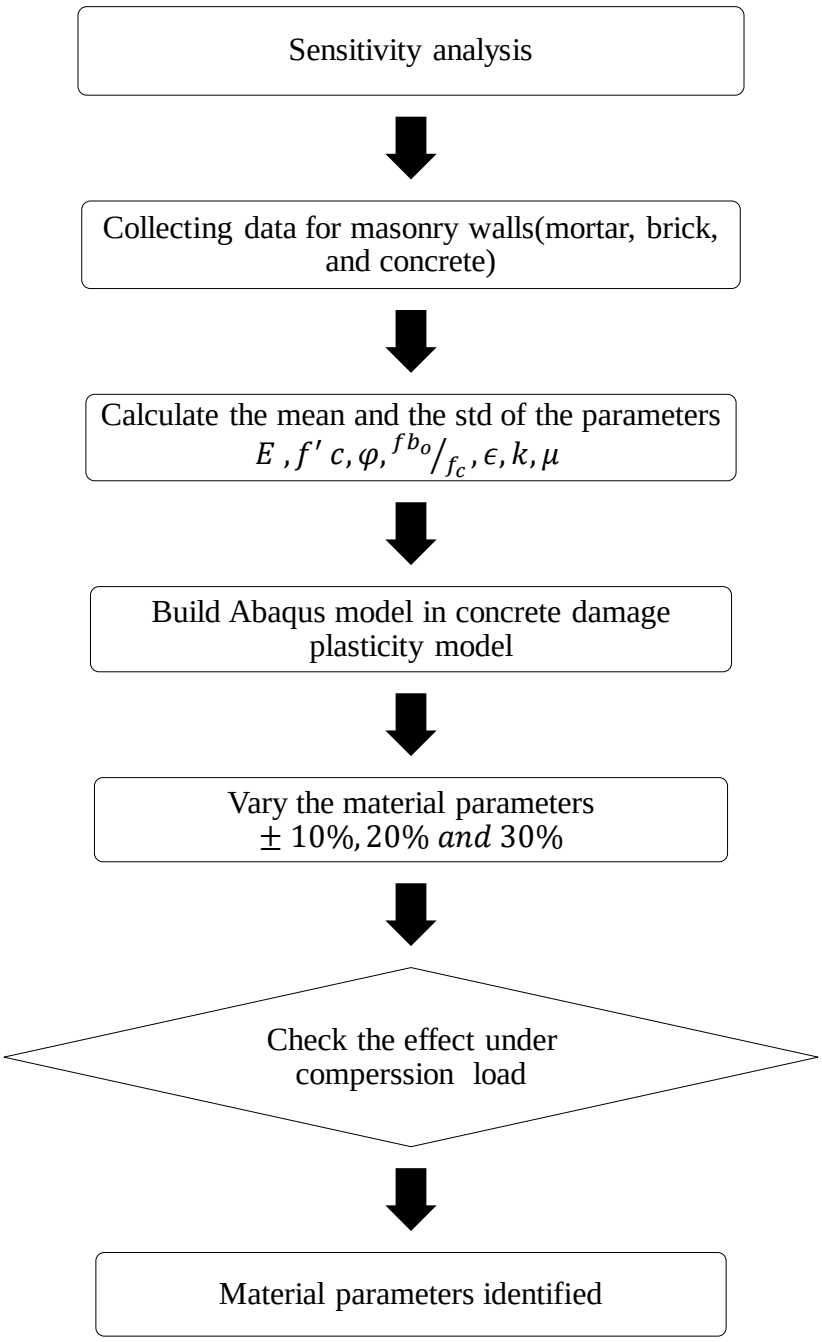

Figure 2.8 Flow chart of parametric analysis

A better way to describe the main elements of the optimization technique is by discussing the process of obtaining the appropriate model parameters through A2M. These elements are as follows:

- Initial guess: the initial model parameter values such as the Young's modulus, Poisson ratio, compressive strength, etc., implemented into ABAQUS. The values of the design variables in the initial guess can be selected randomly, or according to certain distributions. The initial sets of design variable values should be chosen so that they span a sufficiently large range, so that it includes the optimal solution. Care should be taken so that the number of initial points is neither too small nor too large with respect to the capacity of the neural network, in order to avoid overfitting or underfitting respectively.
- Objective function: the difference between the experimental stress-strain curve and the theoretical prediction of the stress-strain curve accomplished via the Abaqus simulation.
- Boundary limitations: upper and lower bound values specifying the domain for each parameter as obtained from the literature.

The flowchart in Figure 2.10 illustrates the optimization interface between ABAQUS and MATLAB. First, the model was run in ABAQUS by providing the initial guess parameters, in order to obtain a theoretical model of the stress-strain curves; this was then compared to the stress-strain from the experiment. It is noted here that the values of the initial guess parameters do not affect the result of the optimized parameters. Next, the objective function and optimization were calculated through Abaqus2Matlab, based on the nonlinear least squares function. If the optimization was less than the tolerance value, the parameters defined in the mathematical model were accepted and the iteration stopped.

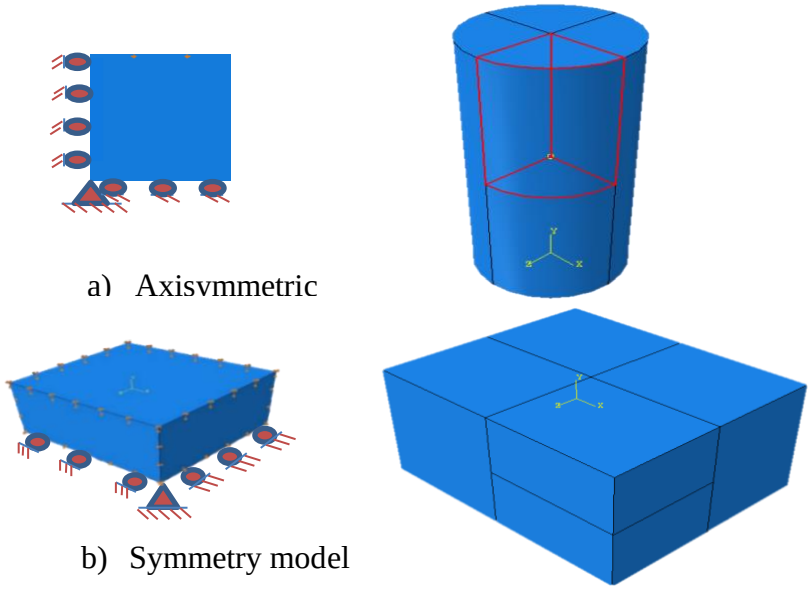

Figure 2.9 ABAQUS 3D model a) axisymmetric b) symmetry model

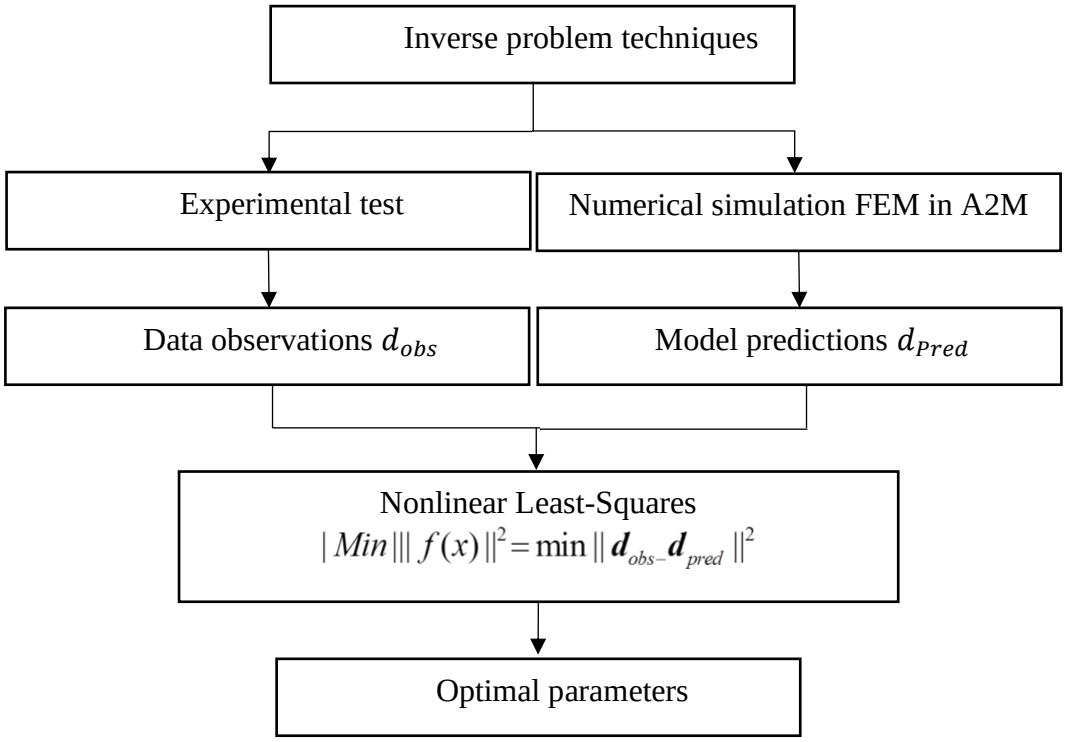

Figure 2.10 Optimization flowchart

Otherwise, the algorithm proceeded to establish a new set of parameters based on upper and lower bounds. Finally, the process was repeated iteratively until the minimum possible objective function was accomplished.

2.8. Conclusion

The parameters for three URM infill wall components were optimized by A2M and compared to the test data obtained from the literature. In other words, the optimum material parameters were determined by fitting a particularly experimental test to the CDP constitutive model under uniaxial compression loads (Blackard et al., 2007). As shown in Figure 2.11 the stress-strain models analyzed using A2M to identify the optimization parameters produced results that nearly coincided with those of actual experiment-obtained stress-strain curves found in Blackard et al. (2007) and Mehrabi (1996). The optimization process accurately fit the stress-strain relationship models, as compared to the ABAQUS (i.e., initial guess) simulation.

The tolerance value controlled the iteration number and enhanced the optimization results for the model parameters. Figure 2.12 shows the residual value versus the iteration number, which demonstrated an error approaching 1% (which is negligible). Approaching the minimum error was required for computational time, meaning the cumulative error was insignificant. Table 2.4-6 shows the optimization for all components (i.e., mortar, brick, and concrete), illustrating certain parameter results as compared to the parameters employed by Blackard et al. (2007) and Mehrabi (1996). The agreement between the objective data function with a Gaussian fit and the histogram with a normal distribution (see Figure 2.13) demonstrated a poor representation of the observations for mortar, brick, and concrete, and a small amount of bias.

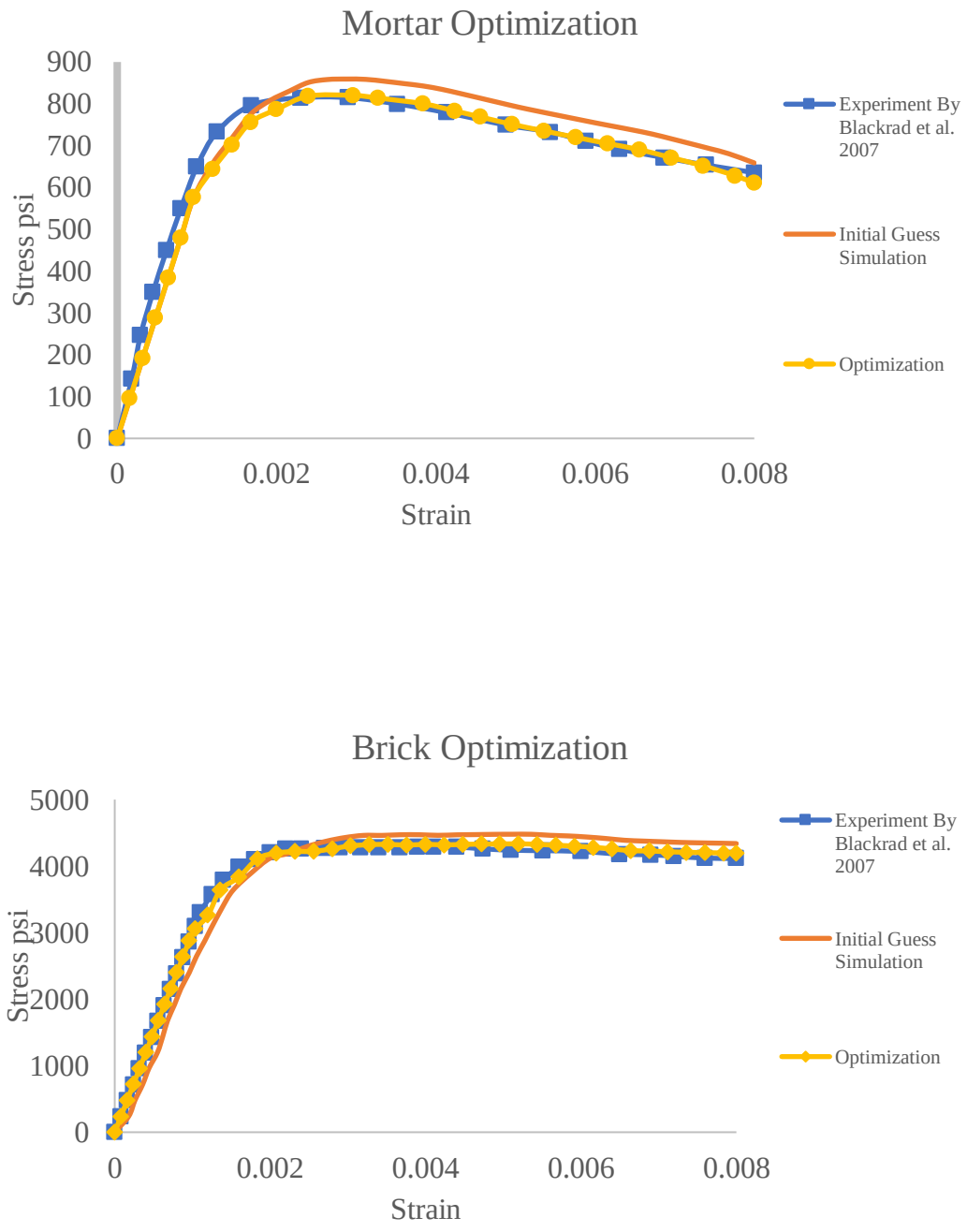

Figure 2.11 Optimization results for the CDP model compared to experiment teats (Blackard et al., 2007;Mehrabi 1996)

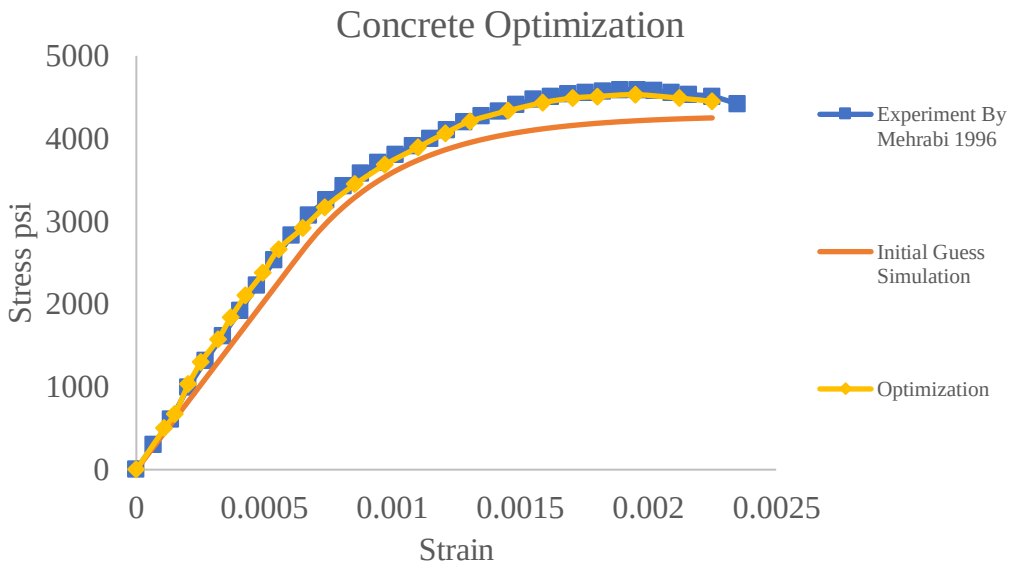

Figures 2.11 Continued

Table 2.4 Optimization Results for Mortar Compared to ABAQUS Model and Literatures

Mortar Test	$E(psi)$	ν	ψ	f_b/f_c	$\grave{o}$	κ	μ
Blackard et al. (2007)	5×10^5	0.2	20	1.15	0.1	0.7	0
Initial Guess	5×10^5	0.2	20	1.16	0.1	0.667	0.001
Optimizations	6.399×10^5	0.18	18.8153	1.088	0.108	0.6340	0.0022

Table 2.5 Optimization Results for Brick Compared to ABAQUS Model and Literatures

Brick Test	$E(psi)$	ν	ψ	f_b/f_c	$\grave{o}$	κ	μ
Blackard et al. (2007)	3×10^6	0.1	20	1.15	0.1	0.7	0
Initial Guess	3×10^6	0.1	20	1.16	0.1	0.667	0.001

Table 2.5 Continued

Optimizations	3.132×10^6	0.104	19.69	1.1418	0.0933	0.958	0.0015

Table 2.6 Optimization Results for Concrete Compared to ABAQUS Model and Literatures

Concrete Test	$E(psi)$	ν	ψ	f_b/f_c	$\grave{o}$	κ	μ
Mehrabi (1996)	3×10^6						
Initial Guess	3×10^6	0.15	36	1.16	0.1	0.667	
Optimizations	2.9491×10^6	0.147	35.7	1.143	0.094	0.659	0.0018

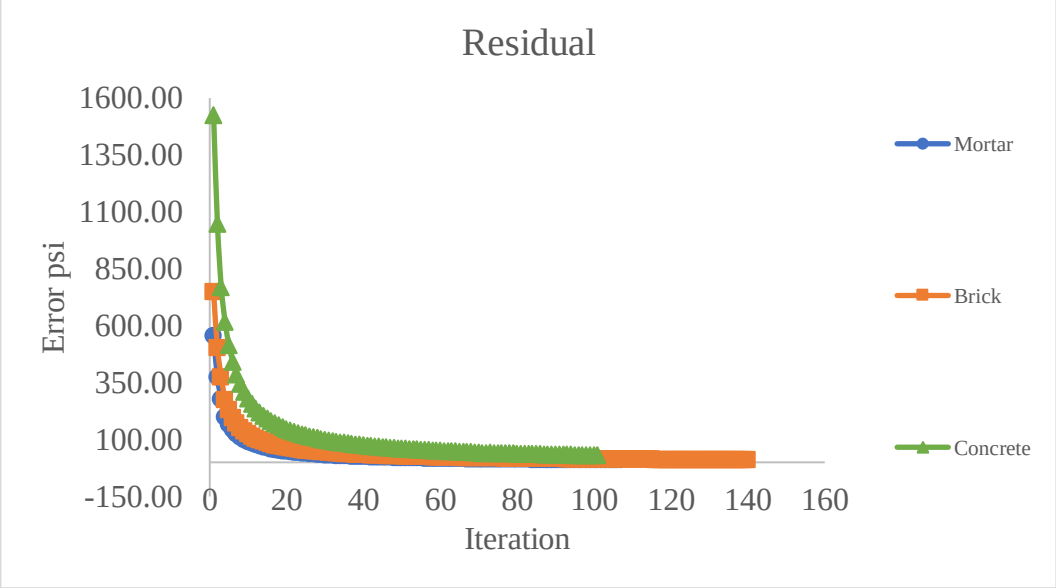

Figure 2.12 Residuals of the mortar, brick and concrete model

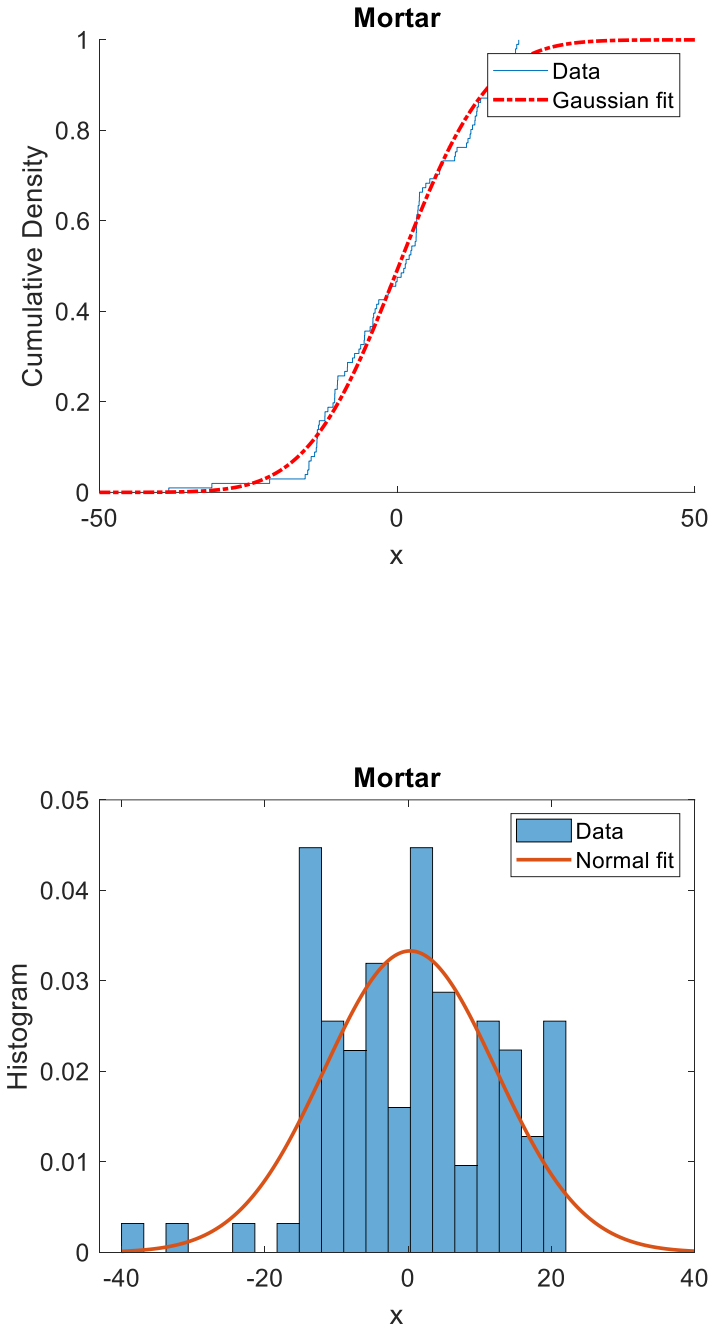

Figure 2.13 Gaussian fit and histogram of the objective function for mortar, concrete and brick, respectively.

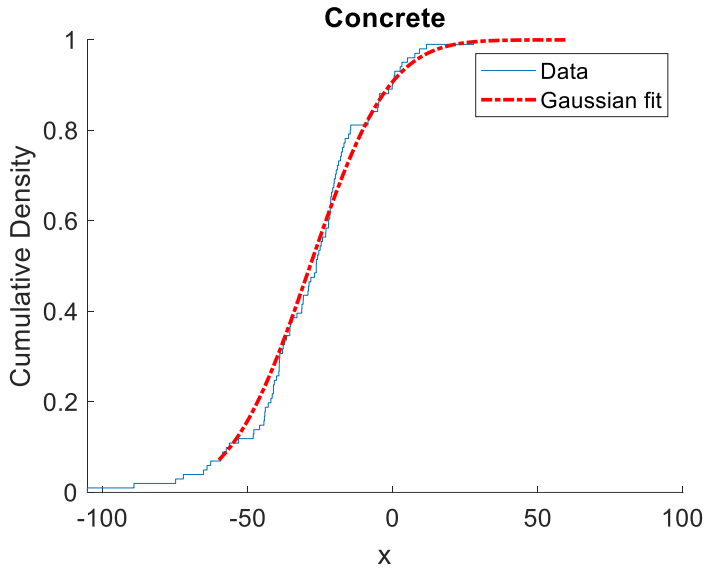

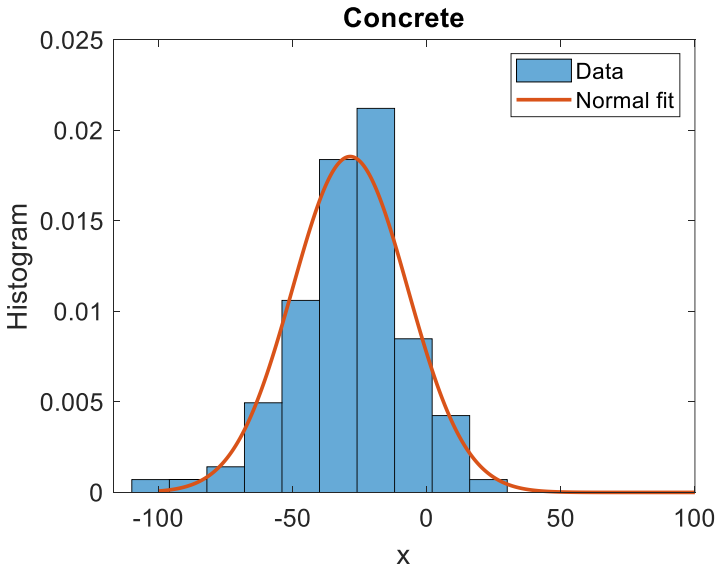

Figure 2.13 Continued

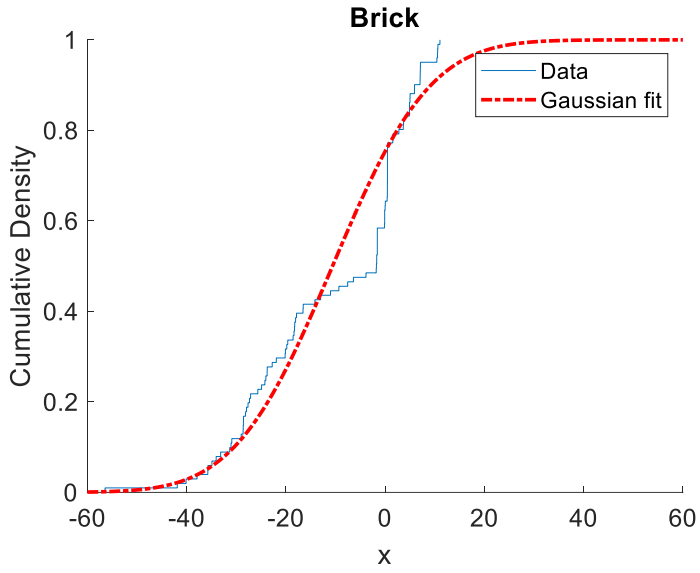

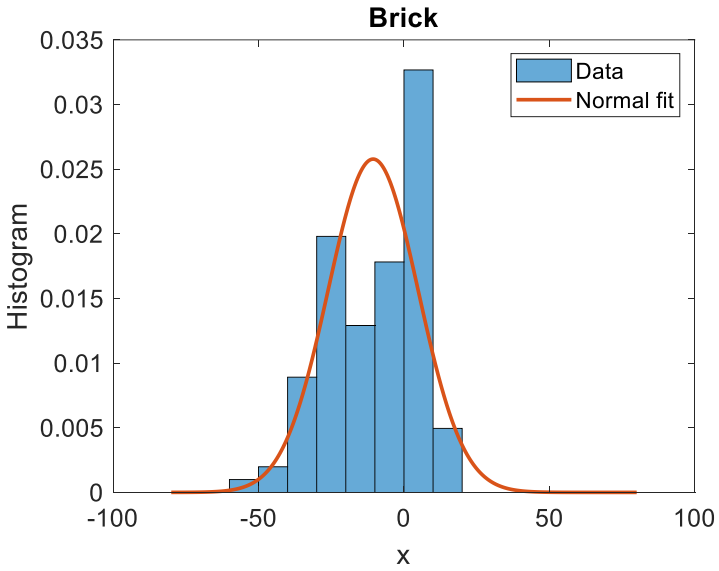

Figure 2.13 Continued

2.9. References

Barbosa, C., Lourenço, P. B., Mohamad, G., & Hanai, J. (2007). Triaxial compression tests on bedding mortar samples looking at confinement effect analysis.

Barbosa, C. S., Lourenço, P. B., & Hanai, J. B. (2010). On the compressive strength prediction for concrete masonry prisms. Materials and Structures, 43(3), 331-344.

Blackard, B., Kim, B., Citto, C., Willam, K., & Mettupalayam, S. (2007). Failure issues of brick masonry. Paper presented at the Proceedings of the Sixth International Conference on Fracture Mechanics of Concrete and Concrete Structures.

Blackard, B., Willam, K., & Mettupalayam, S. (2009). Experimental observations of masonry infilled reinforced concrete frames with openings. Special Publication, 265, 199-122.

Carmeliet, J. (1999). Optimal estimation of gradient damage parameters from localization phenomena in quasi-brittle materials. Mechanics of Cohesive-frictional Materials: An International Journal on Experiments, Modelling and Computation of Materials and Structures, 4(1), 1-16.

Cecchi, A., & Sab, K. (2002). A multi-parameter homogenization study for modeling elastic masonry. European Journal of Mechanics-A/Solids, 21(2), 249-268.

Chen, A. C., & Chen, W.-F. (1975). Constitutive relations for concrete. Journal of Engineering Mechanics, 101(ASCE# 11529 Proceeding).

Chen, W.-F., & Han, D.-J. (2007). Plasticity for structural engineers: J. Ross Publishing.

Chisari, C. (2015). Inverse techniques for model identification of masonry structures.

Chisari, C. (2019). Tolerance-based Pareto optimality for structural identification accounting for uncertainty. Engineering with Computers, 35(2), 381-395.

Chisari, C., Macorini, L., Amadio, C., & Izzuddin, B. (2015). An inverse analysis procedure for material parameter identification of mortar joints in unreinforced masonry. Computers & Structures, 155, 97-105.

Chisari, C., Macorini, L., Amadio, C., & Izzuddin, B. A. (2018). Identification of mesoscale model parameters for brick-masonry. International journal of solids and structures, 146, 224-240.

Ciornei, L. (2012). Performance of polyurea retrofitted unreinforced concrete masonry walls under blast loading: University of Ottawa (Canada).

Demin, W., & Fukang, H. (2017). Investigation for plastic damage constitutive models of the concrete material. Procedia engineering, 210, 71-78.

Desayi, P., & Krishnan, S. (1964). Equation for the stress-strain curve of concrete. Paper presented at the Journal Proceedings.

Fadale, T. D., Nenarokomov, A. V., & Emery, A. F. (1995). Uncertainties in parameter estimation: the inverse problem. International Journal of Heat and Mass Transfer, 38(3), 511-518.

Feenstra, P. H., & De Borst, R. (1996). A composite plasticity model for concrete. International journal of solids and structures, 33(5), 707-730.

Fiorato, A. E., Sozen, M. A., & Gamble, W. L. (1970). An investigation of the interaction of reinforced concrete frames with masonry filler walls. Retrieved from

Gambarotta, L., & Lagomarsino, S. (1997). Damage models for the seismic response of brick masonry shear walls. Part I: the mortar joint model and its applications. Earthquake engineering & structural dynamics, 26(4), 423-439.

Gonçalves, J., Tavares, L., Toledo Filho, R., Fairbairn, E., & Cunha, E. (2007). Comparison of natural and manufactured fine aggregates in cement mortars. Cement and Concrete Research, 37(6), 924-932.

Grassl, P. (2004). Modelling of dilation of concrete and its effect in triaxial compression. Finite elements in analysis and design, 40(9-10), 1021-1033.

Grassl, P., & Jirásek, M. (2006). Damage-plastic model for concrete failure. International journal of solids and structures, 43(22-23), 7166-7196.

Grassl, P., Xenos, D., Nyström, U., Rempling, R., & Gylltoft, K. (2013). CDPM2: A damage-plasticity approach to modelling the failure of concrete. International journal of solids and structures, 50(24), 3805-3816.

Hibbitt, H., Karlsson, B., & Sorensen, P. (2011). Abaqus analysis user's manual version 6.10. Dassault Systèmes Simulia Corp.: Providence, RI, USA.

Hillerborg, A., Modéer, M., & Petersson, P.-E. (1976). Analysis of crack formation and crack growth in concrete by means of fracture mechanics and finite elements. Cement and Concrete Research, 6(6), 773-781.

Hognestad, E., Hanson, N. W., & McHenry, D. (1955). Concrete stress distribution in ultimate strength design. Paper presented at the Journal Proceedings.

Illampas, R., Ioannou, I., & Charmpis, D. C. (2014). Adobe bricks under compression: experimental investigation and derivation of stress–strain equation. Construction and building materials, 53, 83-90.

Jankowiak, T., & Lodygowski, T. (2005). Identification of parameters of concrete damage plasticity constitutive model. Foundations of civil and environmental engineering, 6(1), 53-69.

Jenq, Y., & Shah, S. P. (1985). Two parameter fracture model for concrete. Journal of Engineering Mechanics, 111(10), 1227-1241.

Jirasek, M., & Bazant, Z. P. (2002). Inelastic analysis of structures: John Wiley & Sons.

Karsan, I. D., & Jirsa, J. O. (1969). Behavior of concrete under compressive loadings. Journal of the Structural Division.

Kaushik, H. B., Rai, D. C., & Jain, S. K. (2007). Stress-strain characteristics of clay brick masonry under uniaxial compression. Journal of materials in Civil Engineering, 19(9), 728-739.

Kmiecik, P., & Kamiński, M. (2011). Modelling of reinforced concrete structures and composite structures with concrete strength degradation taken into consideration. Archives of civil and mechanical engineering, 11(3), 623-636.

Kolluru, S. V., Popovics, J. S., & Shah, S. P. (2000). Determining elastic properties of concrete using vibrational resonance frequencies of standard test cylinders. Cement, concrete and aggregates, 22(2), 81-89.

Lee, J., & Fenves, G. L. (1998). Plastic-damage model for cyclic loading of concrete structures. Journal of Engineering Mechanics, 124(8), 892-900.

Lotfi, H., & Shing, P. (1991). An appraisal of smeared crack models for masonry shear wall analysis. Computers & Structures, 41(3), 413-425.

Lubliner, J. (1991). A simple model of generalized plasticity. International journal of solids and structures, 28(6), 769-778.

Lubliner, J., Oliver, J., Oller, S., & Oñate, E. (1989). A plastic-damage model for concrete. International journal of solids and structures, 25(3), 299-326.

McNary, W. S., & Abrams, D. P. (1985). Mechanics of masonry in compression. Journal of Structural Engineering, 111(4), 857-870.

Mehrabi, A. B. (1996). Behavior of masonry infilled reinforced concrete frames subjected to lateral loadings.

Michał, S., & Andrzej, W. (2015). Calibration of the CDP model parameters in Abaqus. Paper presented at the The 2015 World Congress on Advanced in Structural Engineering and Mechanics.

Mohamad, G., Fonseca, F. S., Vermeltfoort, A. T., Martens, D. R., & Lourenço, P. B. (2017). Strength, behavior, and failure mode of hollow concrete masonry constructed with mortars of different strengths. Construction and building materials, 134, 489-496.

Mohamad, G., Lourenço, P. B., & Roman, H. R. (2006). Poisson behaviour of bedding mortar under multiaxial stress state.

Morbiducci, R. (2003). Nonlinear parameter identification of models for masonry. International journal of solids and structures, 40(15), 4071-4090.

Morbiducci, R., & Shing, P. (1998). Parameter identification of a nonlinear interface model for masonry mortar joints. In Inverse Problems in Engineering Mechanics (pp. 273-282): Elsevier.

Mosalam, K. M. A. (1996). Experimental and computational strategies for the seismic behavior evaluation of frames with infill walls: Cornell University, August.

Muñoz-Rojas, P., Cardoso, E., & Vaz, M. (2010). Parameter identification of damage models using genetic algorithms. Experimental Mechanics, 50(5), 627-634.

Nazari, A., & Sanjayan, J. G. (2015). Modelling of compressive strength of geopolymer paste, mortar and concrete by optimized support vector machine. Ceramics International, 41(9), 12164-12177.

Nguyen, L. (2014). Confined Masonry: Theoretical Fundamentals, Experimental Test, Finite Element Models, and Future Uses. University of Colorado at Boulder,

Papazafeiropoulos, G., Muñiz-Calvente, M., & Martínez-Pañeda, E. (2017). Abaqus2Matlab: a suitable tool for finite element post-processing. Advances in Engineering Software, 105, 9-16.

Philleo, R. E. (1955). Comparison of results of three methods for determining young's modulus of elasticity of concrete. Paper presented at the Journal Proceedings.

Pramono, E., & Willam, K. (1989). Fracture energy-based plasticity formulation of plain concrete. Journal of Engineering Mechanics, 115(6), 1183-1204.

Rechea, C., Levasseur, S., & Finno, R. (2008). Inverse analysis techniques for parameter identification in simulation of excavation support systems. Computers and Geotechnics, 35(3), 331-345.

Sarhosis, V., & Sheng, Y. (2014). Identification of material parameters for low bond strength masonry. Engineering Structures, 60, 100-110.

Singh, S., & Munjal, P. (2017). Bond strength and compressive stress-strain characteristics of brick masonry. Journal of Building Engineering, 9, 10-16.

Smith, G., & Young, L. (1956). Ultimate flexural analysis based on stress-strain curves of cylinders. Paper presented at the Journal Proceedings.

Stavridis, A. (2009). Analytical and experimental study of seismic performance of reinforced concrete frames infilled with masonry walls. UC San Diego,

Toropov, V. V., & van der Giessen, E. (1993). Parameter identification for nonlinear constitutive models: Finite Element simulation—Optimization—Nontrivial experiments. In Optimal design with advanced materials (pp. 113-130): Elsevier.

Venkatarama Reddy, B., & Gupta, A. (2006). Strength and elastic properties of stabilized mud block masonry using cement-soil mortars. Journal of materials in Civil Engineering, 18(3), 472-476.

Xavier, B., & Francisco, H. (2015). The role of masonry infill in progressive collapse mitigation of multi-storey buildings.

Yang, K.-H., Lee, Y., & Hwang, Y.-H. (2019). A Stress-Strain Model for Brick Prism under Uniaxial Compression. Advances in Civil Engineering, 2019.

3. PROBABILISTIC CALIBRATION OF CONSTITUTIVE PARAMETERS OF A CONCRETE DAMAGE PLASTICITY MODEL IN MASONRY WALLS

3.1. Introduction

This study discusses a Bayesian probabilistic calibration in determining material parameters in a concrete damage plasticity constitutive model that is being used for describing the mechanical responses of brick and mortar for an unreinforced masonry wall. The main objective is to identify the uncertainty and correlation of the material parameters defined in the constitutive model to assess the confidence of the structure response containing it, which in this case would reflect scenarios of the inelastic behavior of the brick and mortar components. In this study, a concrete damage plasticity model which is available in ABAQUS FE analysis is used to describe the stress-strain relationship in each component of an unreinforced masonry wall under uniaxial compressive loads. Once the material parameters of all the components in the wall are calibrated, they can then be used to investigate the effect of spatial variations and material heterogeneities on the overall mechanical responses of unreinforced masonry walls. This study demonstrates the mechanical response using the probabilistic calibration approach to show the benefits of assessing the performance of model predictions, by taking into account all likely scenarios of material variations for mortar and brick when incorporated into an unrein-forced masonry wall.

Various combinations of cement, lime, sand, water and variations in brick strength due to material type, geometric effect, and manufacturing process may produce masonry walls with significant variance in their load bearing performance. Early studies investigated

brick and mortar samples in an effort to understand the distribution of stress through compression zones and general stress-strain relationship (C. S. Barbosa et al., 2010; Blackard et al., 2007; Blackard et al., 2009; Kaushik et al., 2007; Kaynia et al., 2008; Mohamad et al., 2017; Mosalam, 1996; Singh & Munjal, 2017; Stavridis, 2009; Yang et al., 2019). The Bayesian probabilistic calibration framework applied in the following studies (Gauer, Medina-Cetina, Lied, & Kristensen, 2009; Medina-Cetina, 2007; Ranalli, Gottardi, Medina-Cetina, & Nadim, 2010; Rechenmacher & Medina-Cetina, 2007) allowed for a deeper understanding of the overall mechanical responses of such wall systems, as expressed through the model parameters. This framework facilitated a systematic exploration of parametric space through a functional formulation that employed knowledge of governing parameters and the rheological behavior of masonry components. A Concrete Damaged Plasticity (CDP) constitutive model that described both plasticity models and damage behaviors was used to analyze the mechanical responses of masonry structures, J Lubliner et al. (1989). This CDP model included seven material parameters. The three more sensitive parameters (i.e., Young's modulus E , viscosity μ , and deviatoric out-of-roundness κ), as previously demonstrated in Chapter II , were used for the probabilistic brick and mortar calibration analysis, to illustrate the applicability of the probabilistic calibration methodology. This study used a mortar and brick model to present the results for Young's modulus E, viscosity μ, and deviatoric out-of-roundness κ, where κ, and μ are parameters controlling hardening and softening behavior in stress-strain curves, respectively. Abaqus2Matlab was used as an interface software for linking ABAQUS and MATLAB, which was used for optimization and for the probabilistic calibration of the CDP parameters of both the brick and the mortar (Papazafeiropoulos et al., 2017).

3.2. Probabilistic Calibration

3.2.1. Uncertainty Framework

The uncertainty quantification of an inverse problem identifies, characterizes, and simulates the various sources of uncertainty inherent in the physical process of interest. The expected output of the true process is represented by a set of random vectors $\boldsymbol{d}$ and experimental observations $\boldsymbol{d}_{obs}$. It can be retrieved from lab or field measurements and compared to predicting outcomes of the same process $\boldsymbol{d}_{pred}$. The uncertainty quantification framework in terms of $\boldsymbol{d}$, $\boldsymbol{d}_{obs}$, and $\boldsymbol{d}_{pred}$ can be summarized by Medina-Cetina (2007):

$$\begin{aligned} \boldsymbol{d} &= \boldsymbol{d}_{obs} + \Delta\boldsymbol{d}_{obs} \\ \boldsymbol{d} &= \boldsymbol{d}_{pred} + \Delta\boldsymbol{d}_{pred} \\ \boldsymbol{d}_{obs} - \boldsymbol{d}_{pred} &= \Delta\boldsymbol{d}_{obs} - \Delta\boldsymbol{d}_{pred} \end{aligned} \qquad (7)$$

The uncertainty involved in the present research was assumed both in the experimental observations and theoretical predictions. Eq. (7) illustrates the tradeoff between the scientific evidence $\boldsymbol{d}_{obs}$ and $\boldsymbol{d}_{pred}$ through the gradients $\Delta\boldsymbol{d}$. Herein, $\boldsymbol{d}_{obs}$ are comprised of mathematical predictions stemming from a forward model $g(\boldsymbol{\theta})$, which is governed or characterized by a set of parameters θ that represent geometric and material properties (i.e., the Young's modulus E, viscosity μ, and deviatoric out-of-roundness κ).

The proposed probabilistic calibration method follows a Bayesian approach that accounts for the full probabilistic description of the model's parameters through probability maps(Zhu, Cong, Hu, & Medina-Cetina, 2012). This starts with an expert's belief setting up to the prior $(\pi(\boldsymbol{\theta}))$ state for model parameter θ before the experimental evidence is

presented to the mathematical model (i.e., the forward model). This prior knowledge ideally facilitates calibration of the model parameters by limiting and defining plausible values in the form of the probability distribution, which later is updated systematically via quantifying the likelihood $\left(f\ \left(\boldsymbol{d}_{obs}\,|\,\boldsymbol{\theta}\right)\right)$between available observations $\boldsymbol{d}_{obs}$ and model parameters$\boldsymbol{\theta}$. From the basic definition of the Bayes theorem:

$$\pi(\boldsymbol{\theta}\,|\,\boldsymbol{d}_{obs}) = \frac{f(\mathbf{d}_{obs}\,|\,g(\boldsymbol{\theta}),\boldsymbol{\theta})\pi(\boldsymbol{\theta})}{\int_{\theta} f(\mathbf{d}_{obs}\,|\,g(\boldsymbol{\theta}),\boldsymbol{\theta})\pi(\boldsymbol{\theta})d\boldsymbol{\theta}} \alpha\, f(\boldsymbol{d}_{obs}\,|\,g(\boldsymbol{\theta}),\boldsymbol{\theta})\pi(\boldsymbol{\theta}) \qquad (8)$$

The posterior $\pi\ \left(\boldsymbol{\theta}\,|\,\boldsymbol{d}_{obs}\right)$ is the probability proportional to the prior $\pi\ \left(\boldsymbol{\theta}\right)$ and the likelihood$\left(f\ \left(\boldsymbol{d}_{obs}\,|\,\boldsymbol{\theta}\right)\right)$. This is because of the integral of the denominator is a normalizing constant over the parametric space $\boldsymbol{\theta}$, so that the integral of the posterior $\pi\ \left(\boldsymbol{\theta}\,|\,\boldsymbol{d}_{obs}\right)$ can be 1.

3.2.2. Probabilistic Calibration for Mortar and Brick

The probabilistic calibration method is used in this work to study the uncertainty quantification of the material parameters of the concrete damage plasticity model implemented in the FE model. Concrete mortar and brick unit was tested under an axial compression load with cylindrical dimensions of 4" x 8" and parallelepiped dimension 4.5" x 3.75" x 2.25", respectively (Blackard et al., 2007). A numerical model simulated in ABAQUS was used to optimize the material parameters E , μ , and κ via MATLAB using a nonlinear least square algorithm (Levenberg, 1944; Marquardt, 1963).The optimal vector of parameters $\hat{\boldsymbol{\theta}}$ was used as the starting point for the probabilistic calibration. The probabilistic calibration starts from the optimal set of parameters, where MCMC, coupled

with Metropolis-Hastings, is implemented. Table 2.2 in chapter two shows the optimal parameters compared to the numerical parameters obtained by Blackard et al. (2007) .

3.2.2.1. One-Parameter Calibration for Mortar and Brick Model

The likelihood measured from the trade-off between the experimental observation $\boldsymbol{d}_{obs}$ and the model prediction $\boldsymbol{d}_{pred}$, which is the variation around the experimental observation assumed as a Gaussian distribution, from the deterministic optimal parameters. The prior is probability function in which depends on the expert's judgment or previous prior distribution introduced by experimental data (Medina-Cetina & Arson, 2014). Therefore, the prior considered non-informative, which is relay on a lower and upper bond of previous experimental observation of the parameters Young's modulus E viscosity μ, and deviatoric out-of-roundness κ, to generate a uniform probability density function. The proposed distribution was the sampling of the posterior that is derives from the Markov Chain Monte Carlo approach coupled with Metropolis Hastings criteria (MCMC- MH) to infer the statistical results. The solution to the numerical integration of the posterior was certainly converging for single experimental study such as E, and κ after the number of iterations reaches to 1.5e+4 and for, μ, to 3e+4 with a coefficient of variation 0.03 to obtain the statistical results (see Figure 3.1-3.3). The coefficient of variation values (e.g., 0.01, 0.015, 0.02, 0.025, and 0.03) for mortar and brick unit were examined in prior in this study to investigate the effect of response behavior in CDP model. The burn-in iterations were varying based on the convergence of the parameters which are considered between 30% and 50% of the total number of iterations to ensure the statistical inference.

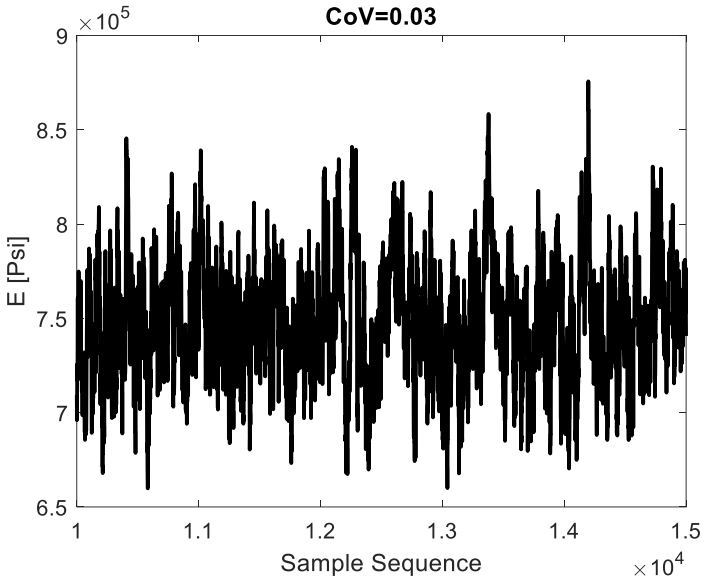

a)

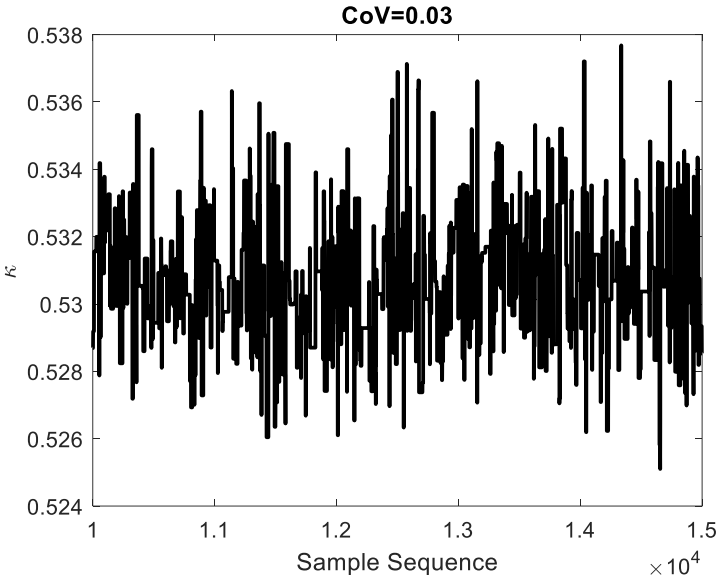

b)

Figure 3.1 Sample sequence a) Young's modulus E b) Deviatoric out-of-roundness κ c) Viscosity μ

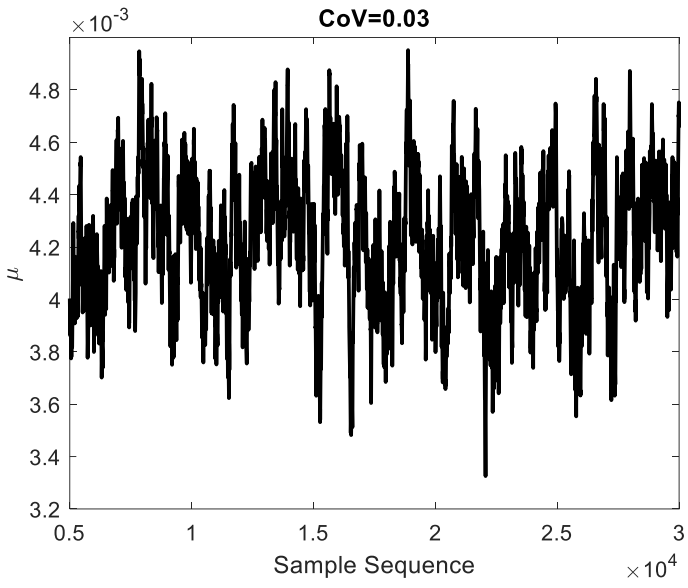

c)

Figure 3.1 Continued

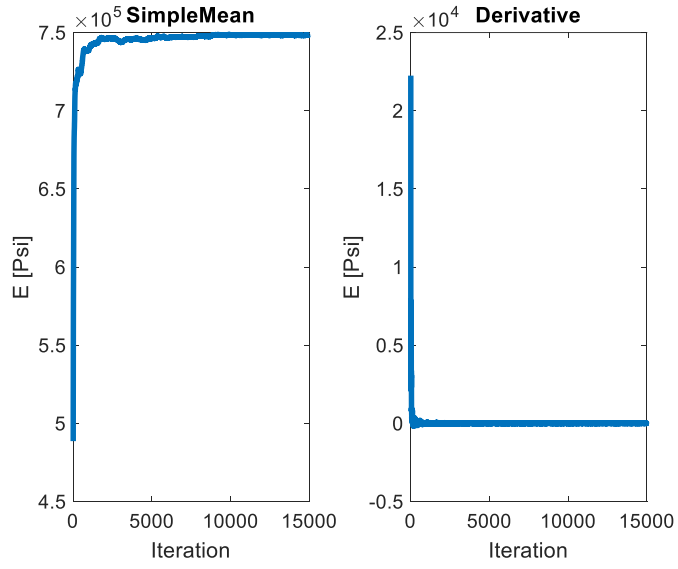

a)

Figure 3.2 Sample mean for mortar a) Young's modulus E b) Deviatoric out-of-roundness κ c) Viscosity μ

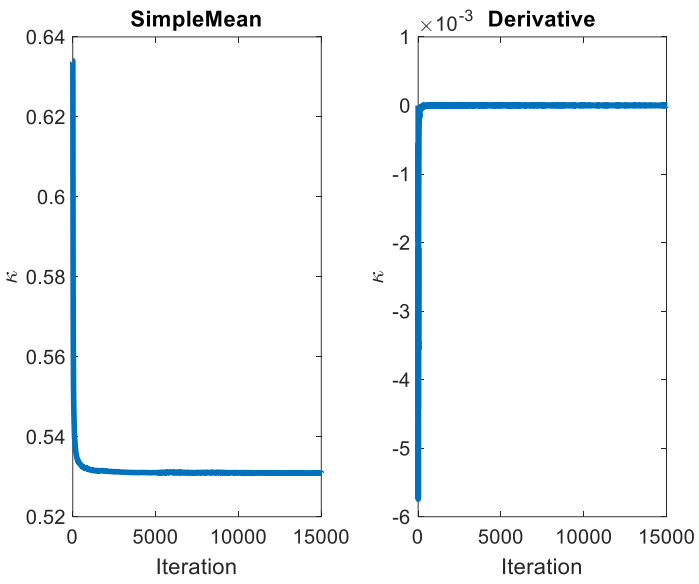

b)

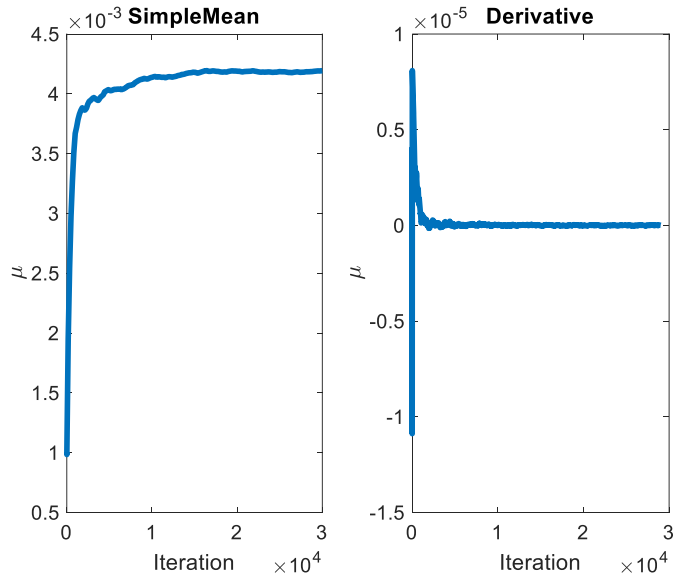

c)

Figure 3.2 Continued

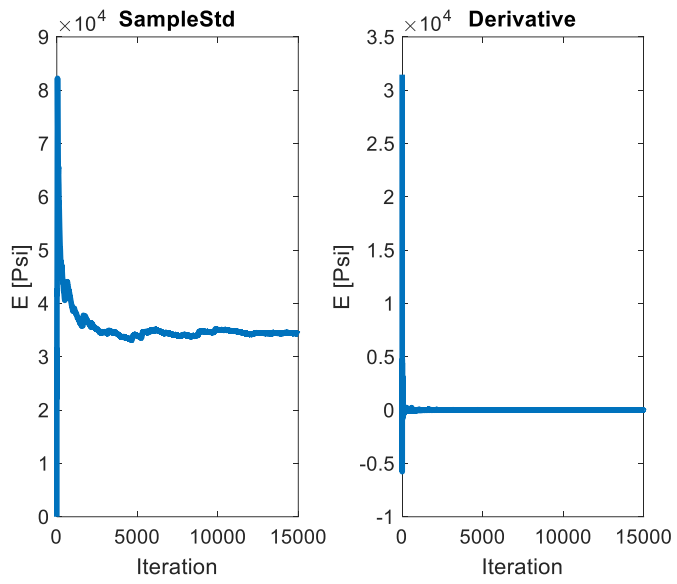

a)

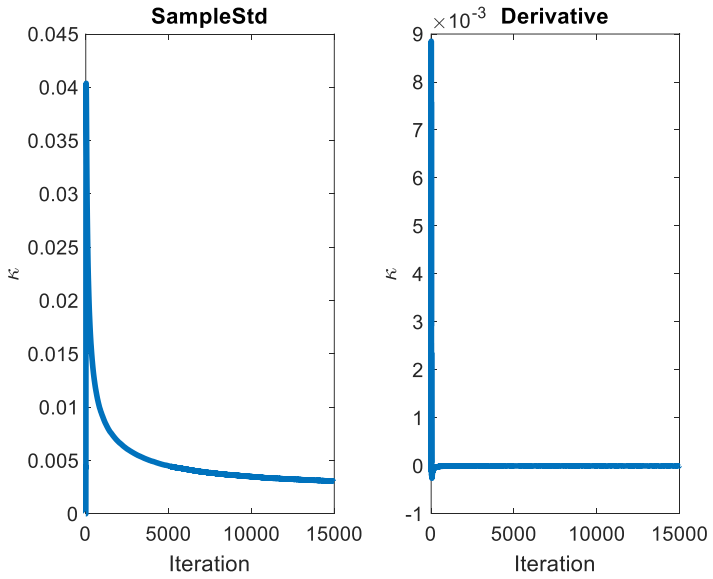

b)

Figure 3.3 Sample Std for mortar a) Young's modulus E b) Deviatoric out-of-roundness κ c) Viscosity μ

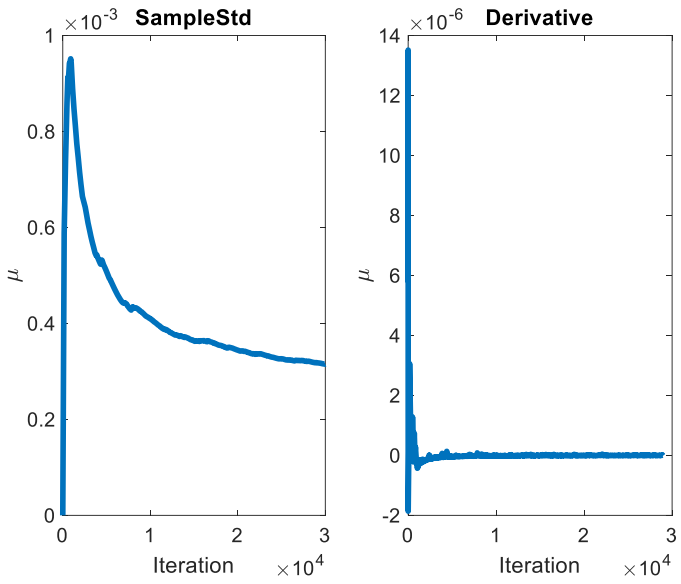

c)

Figure 3.3 Continued

In addition, the inverse problem solution can be used to simulate potential realizations of the model prediction in which the Figure 3.5 shows the empirical cumulative density functions of for each parameter of interest. From this figure is observed, that model showed an excellent agreement the mean of the observations. Figure 3.4 illustrates the frequency histogram for the parameter models for the Young's modulus E, viscosity μ and deviatoric out-of-roundness κ, respectively. Similarly, the analysis for the brick model has been shown (Figure 3.6-3.10).

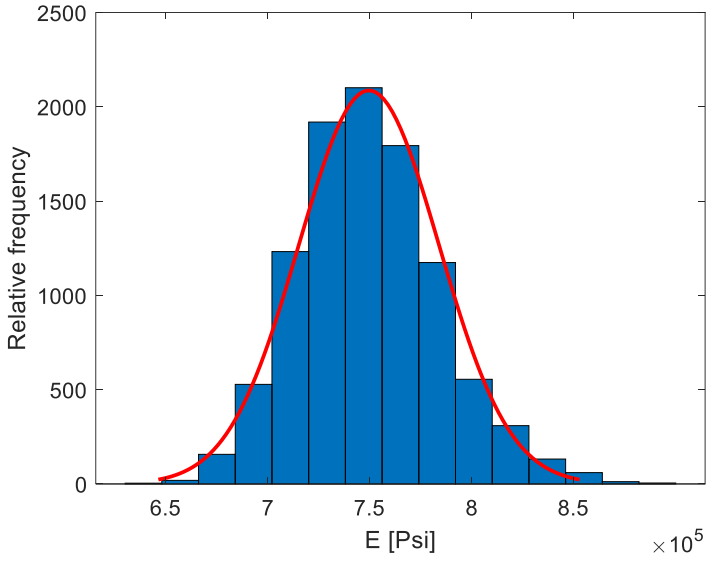

a)

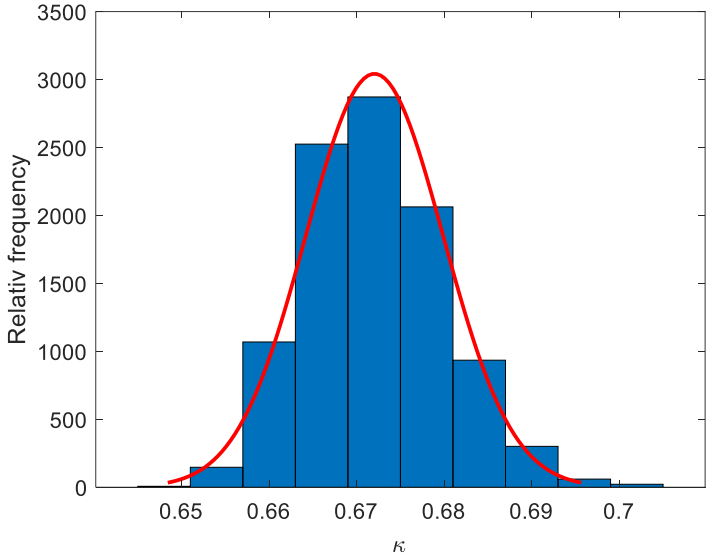

b)

Figure 3.4 Frequency histogram for mortar a) Young's modulus E b) Deviatoric out-of-roundness κ c) Viscosity μ

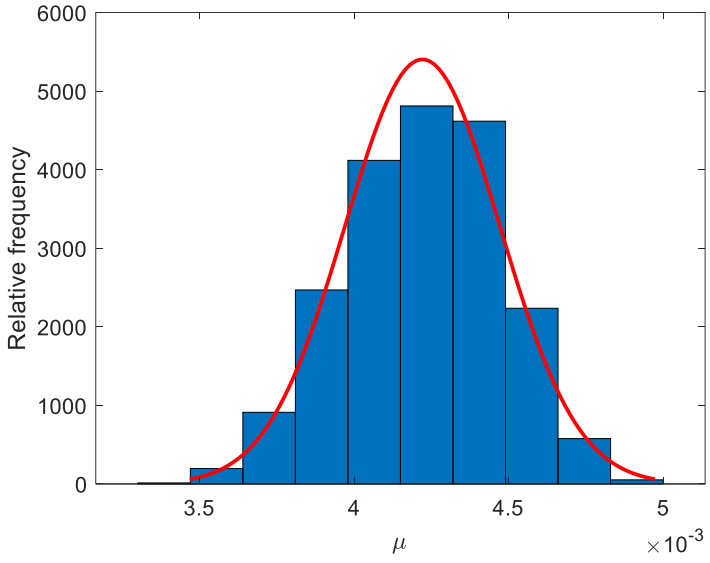

c)

Figure 3.4 Continued

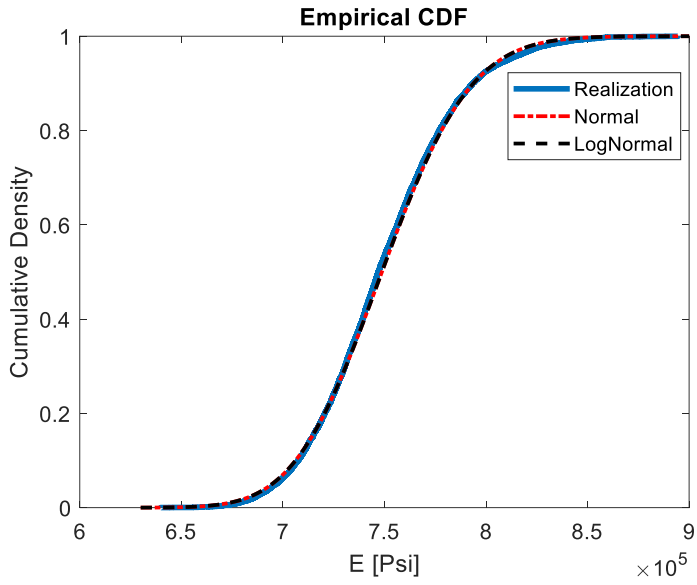

a)

Figure 3.5 Empirical cumulative density function for mortar a) Young's modulus E b) Deviatoric out-of-roundness κ c) Viscosity μ

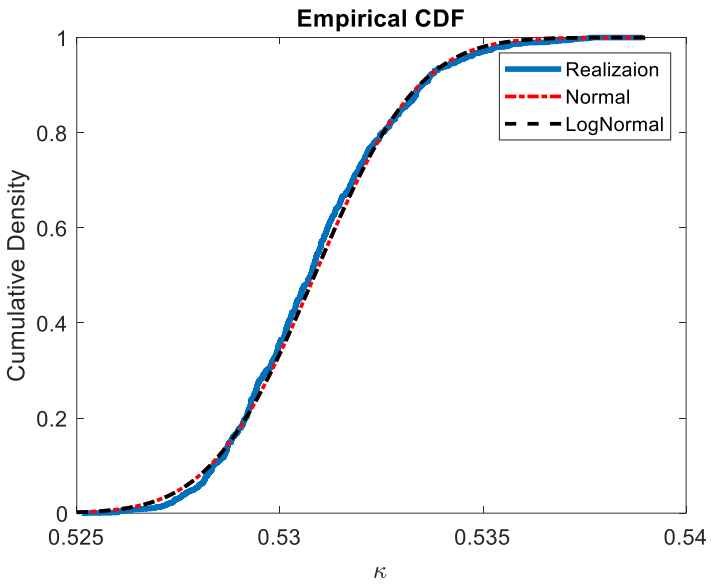

b)

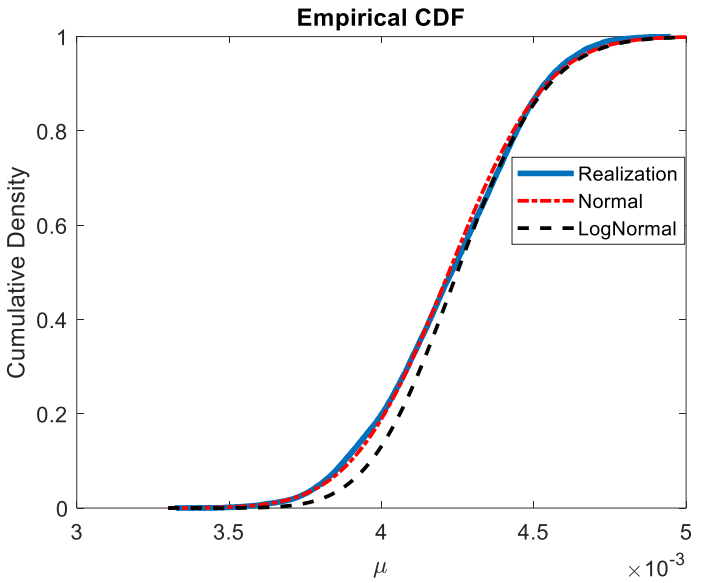

c)

Figure 3.5 Continued

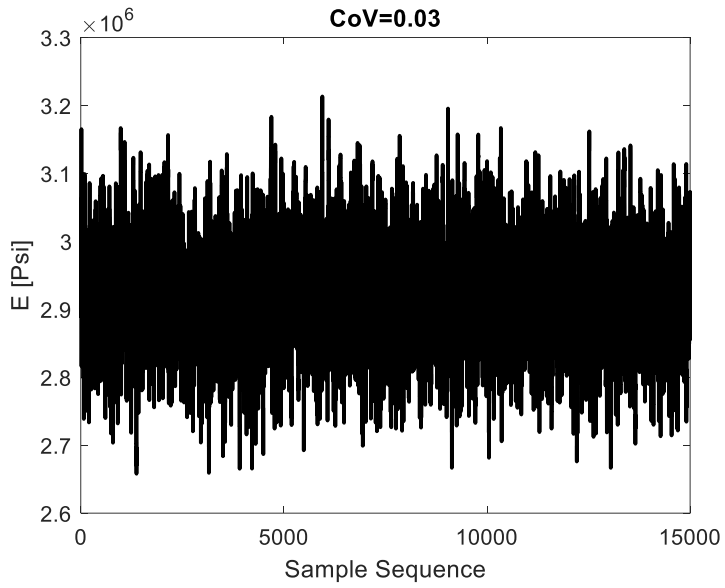

a)

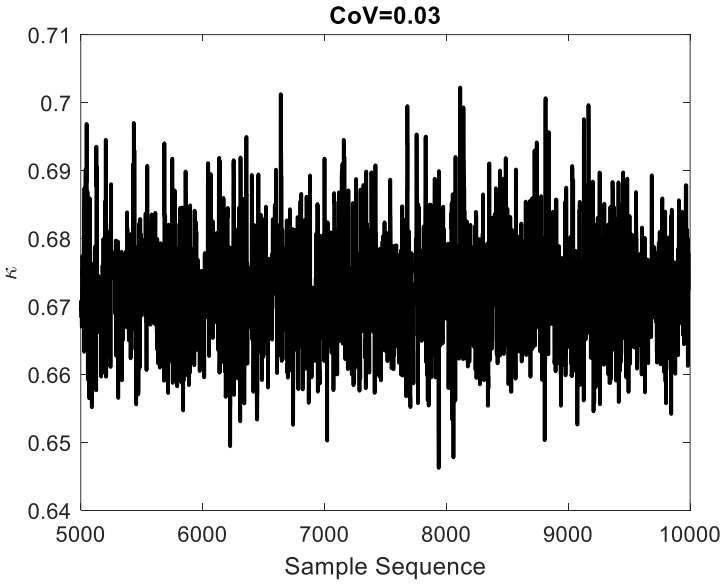

b)

Figure 3.6 Sample sequence for brick a) Young's modulus E b) Deviatoric out-of-roundness κ c) Viscosity μ

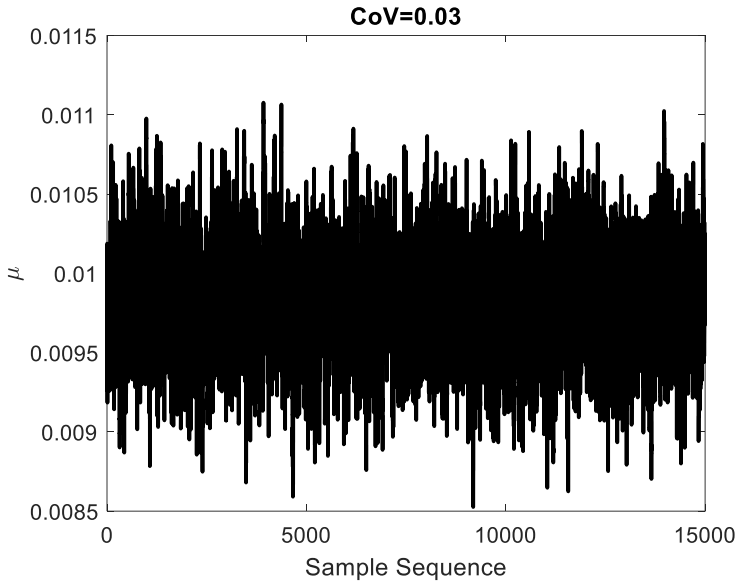

c)

Figure 3.6 Continued

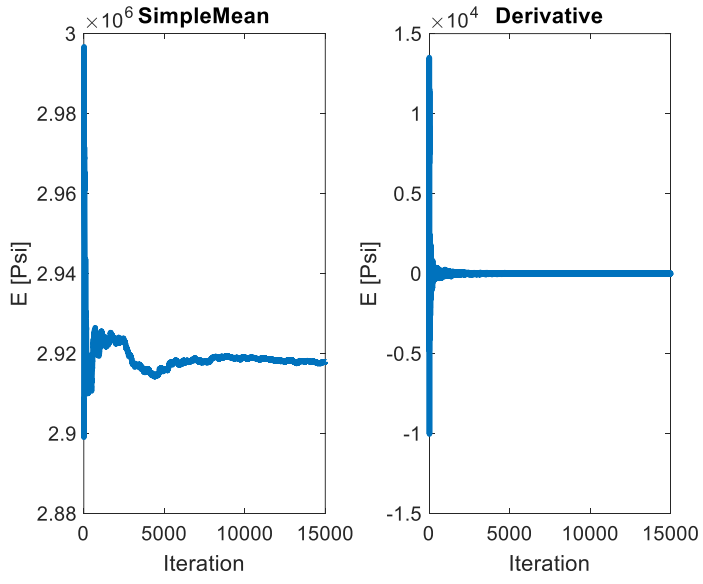

a)

Figure 3.7 Sample mean for brick a) Young's modulus E b) Deviatoric out-of-roundness κ c) Viscosity μ

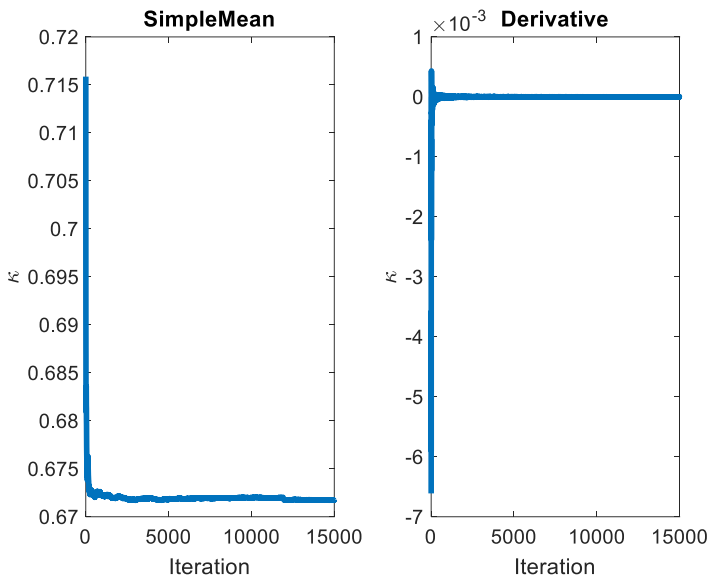

b)

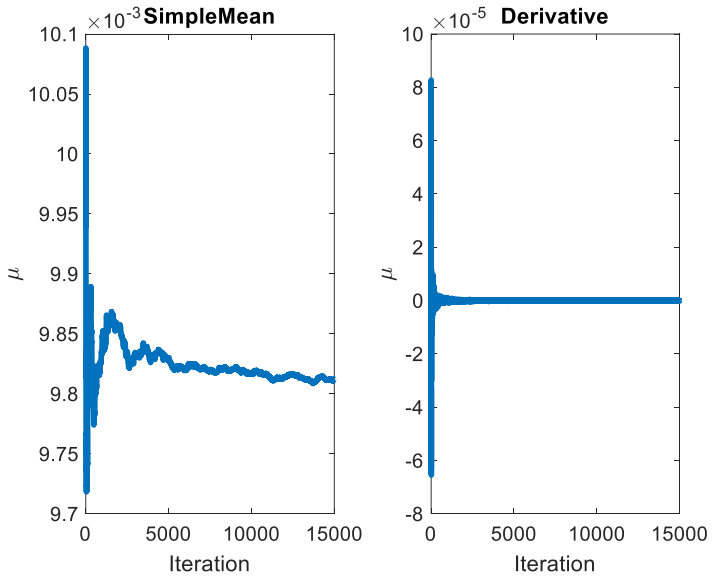

c)

Figure 3.7 Continued

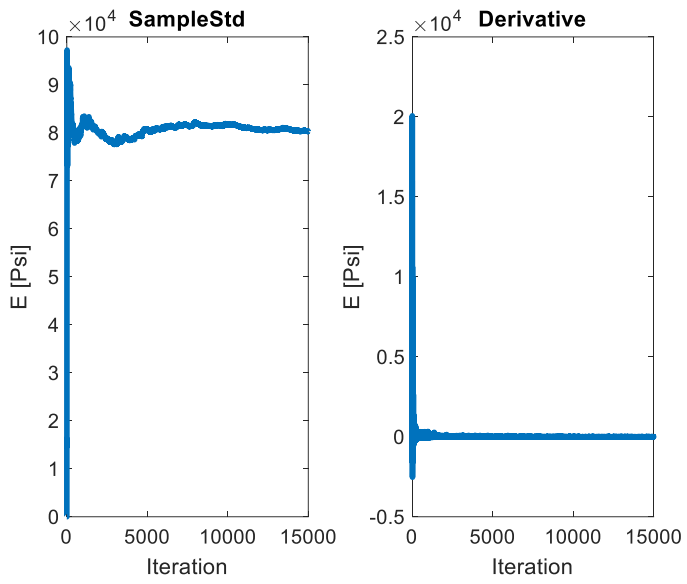

a)

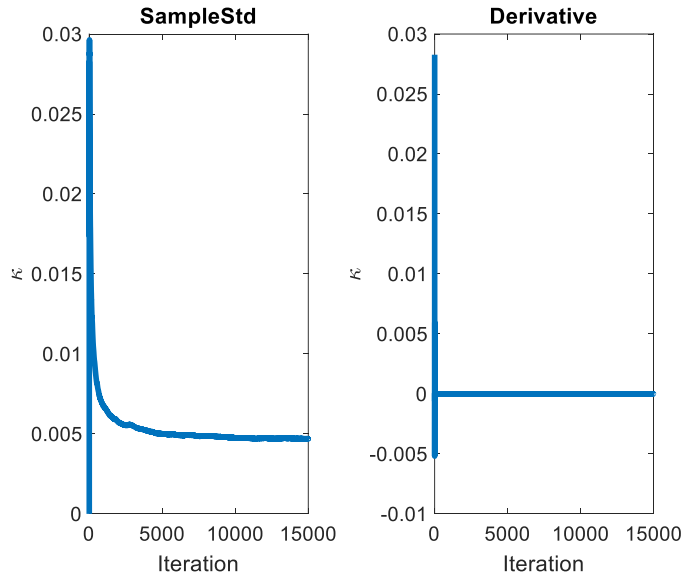

b)

Figure 3.8 Sample Std for brick a) Young's modulus E b) Deviatoric out-of-roundness κ c) Viscosity μ

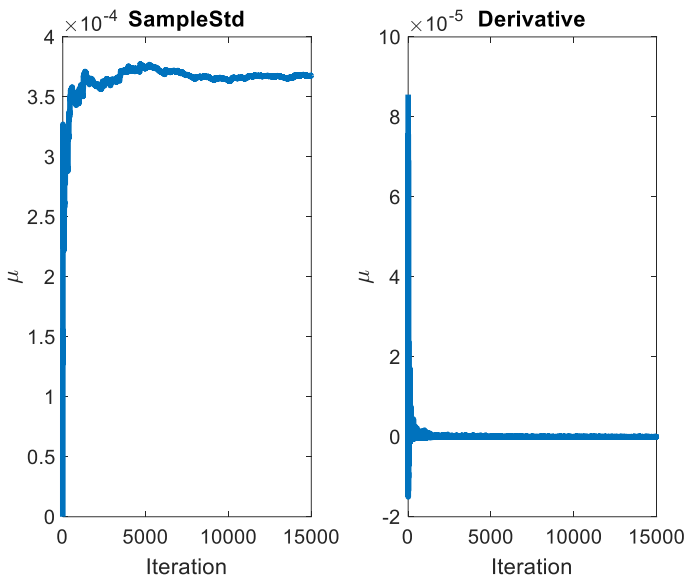

c)

Figure 3.8 Continued

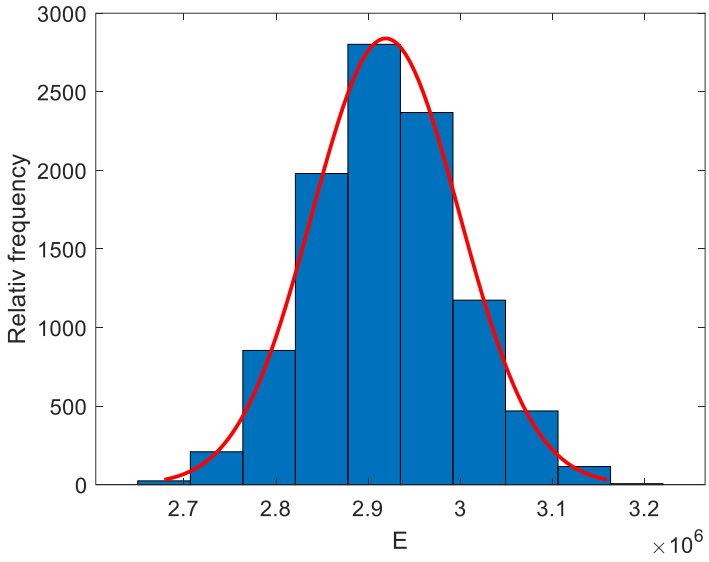

a)

Figure 3.9 Frequency histogram for brick a) Young's modulus E b) Deviatoric out-of-roundness κ c) Viscosity μ

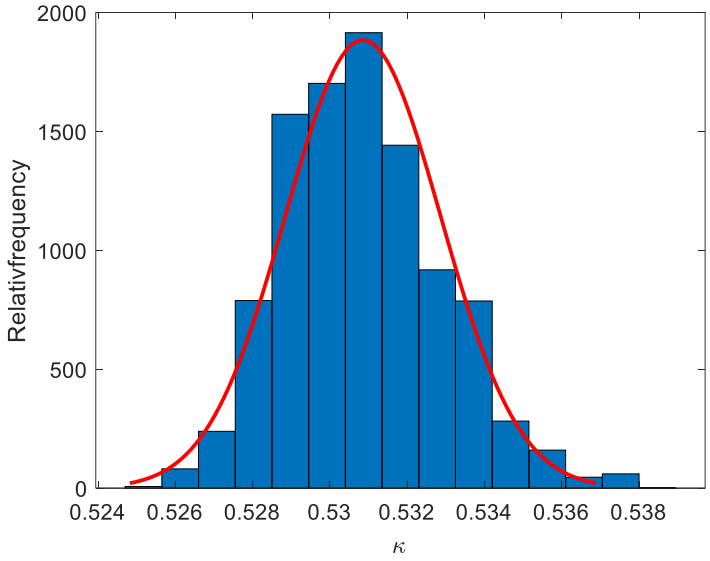

b)

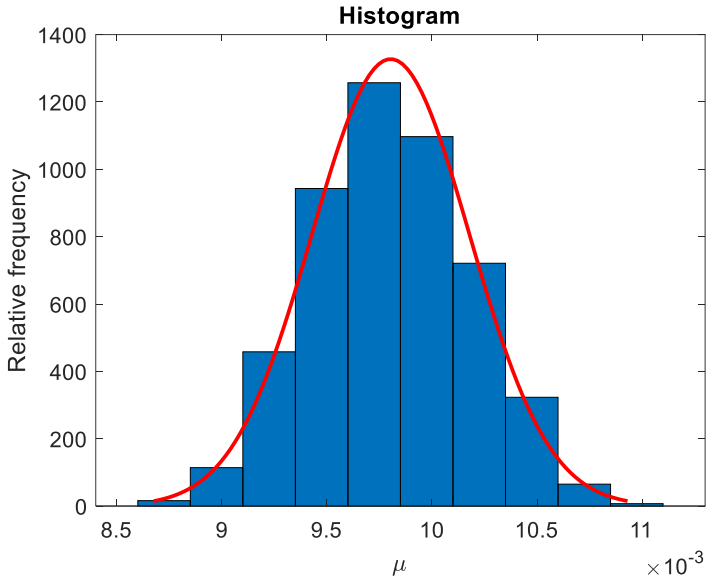

c)

Figure 3.9 Continued

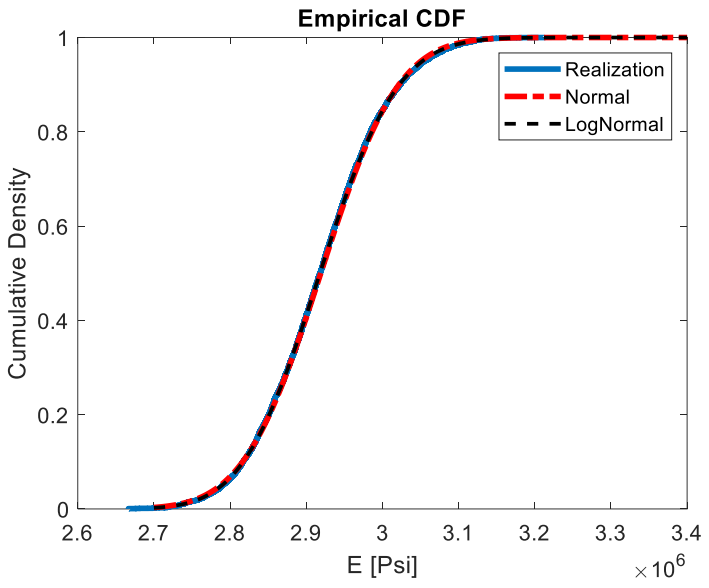

a)

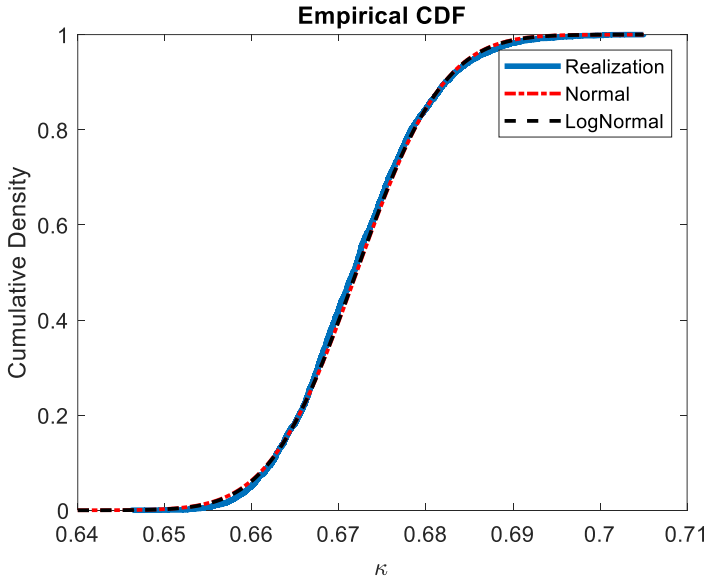

b)

Figure 3.10 Empirical cumulative density function for brick a) Young's modulus E b) Deviatoric out-of-roundness κ c) Viscosity μ

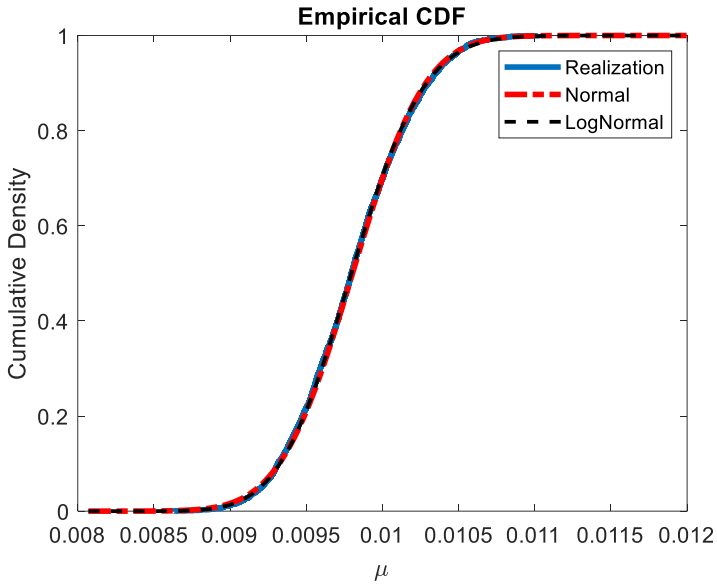

c)
Figure 3.10 Continued

Table 3.1 Statistical Parameters for Mortar Young's modulus E Deviatoric out-of-Roundness κ and Viscosity μ

Mortar	$E(psi)$	κ	μ
Mean	748427.905	0.530	0.0042
Std	34294.613	0.00307	0.000315

Table 3.2 Statistical Parameters for Brick Young's modulus E Deviatoric out-of-Roundness κ and Viscosity μ

Brick	$E(psi)$	κ	μ
Mean	2917957.265	0.671	0.00981
Std	80310.394	0.00850	0.000367

According to the MCMC simulations, the realization of the model predictions can be constructed by sampling random parameter combinations after the burn-in point. In order to

estimate their mean and standard deviation and second moments (correlation structure) (see Table 3.1-2). Consequently, the probabilistic calibrations of the model parameters are assessing the confidence of the model prediction (see Figure 3.11 and 3.12).

After the stationary condition of the parameters is grasped on the MCMC- MH, the first order statistics of model response is formulated from the statistical inferences of the parameters. The mean and standard deviation of the burn-in points plotted with respect to the axial stress for each data point for brick unit and mortar are shown in Figure 3.13 and 3.14. The mean reveals a good fitting with the experimental observation. Also, the standard deviation of Young's modulus E mortar reflects the variability on the model predictions that start with a steep growth and a sudden drop at about strain equal to 0.0016 in which coincides approximately with strain equal to 0.0012 of the stress-strain curves while κ and μ gradually increase to reach the maximum values of standard deviation at 0.0035 in which did not match with strain of stress-stress curves. However, the brick unit shows that the parameters κ and μ gradually increase to reach the maximum values at about strain equal to 0.0035 in which coincides approximately with strain equal to 0.0035 of the stress-strain curves while the Young's modulus E is differentiate with maximum strain in which the value of maximum the standard deviation at about 0.0013 (see Figures 3.13 and 3.14).

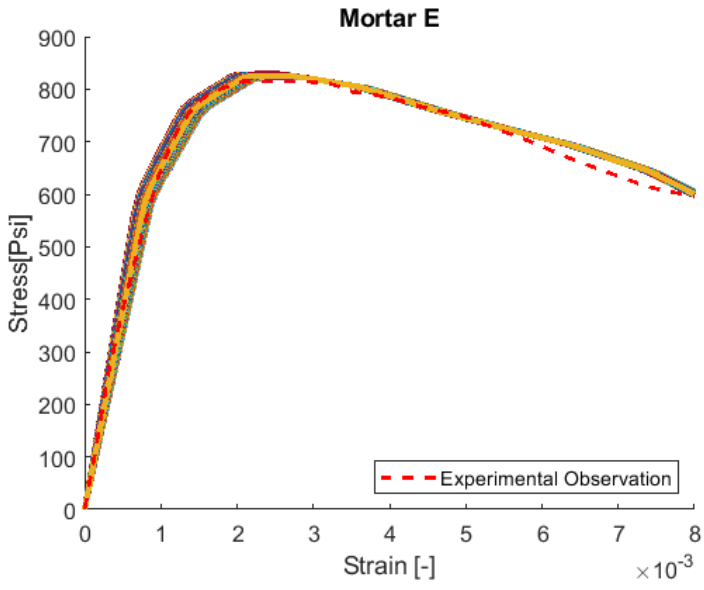

a)

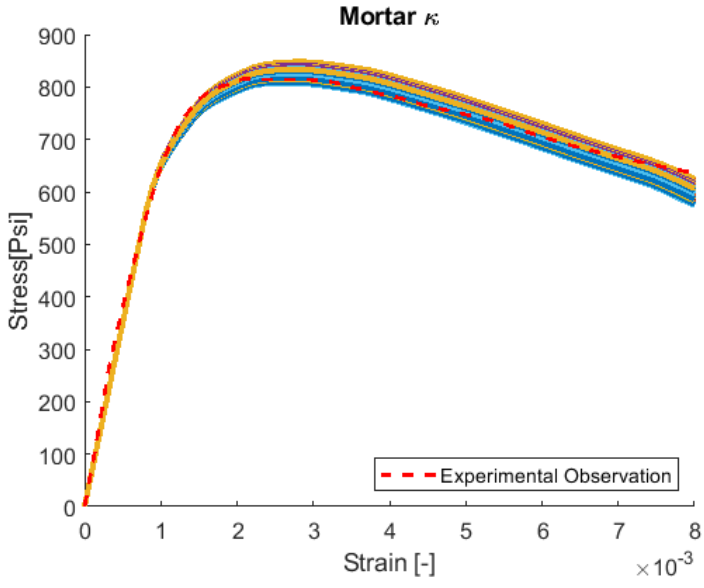

b)

Figure 3.11 Model realization for mortar a) Young's modulus E b) Deviatoric out-of-roundness κ c) Viscosity μ (Blackard et al., 2007)

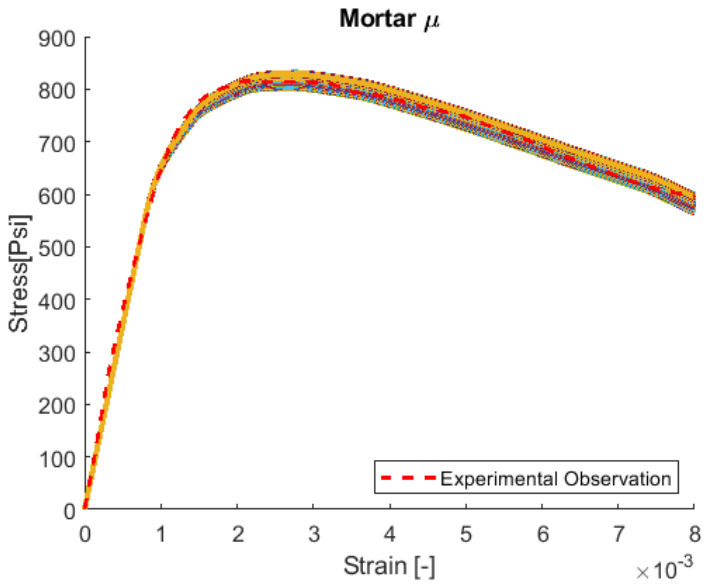

c)

Figure 3.11 Continued

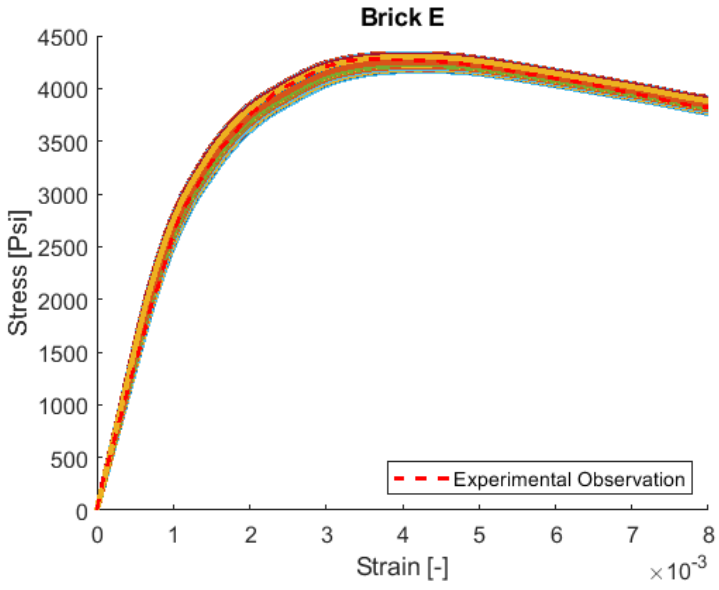

a)

Figure 3.12 Model realization for brick a) Young's modulus E b) Deviatoric out-of-roundness κ c) Viscosity μ (Blackard et al., 2007)

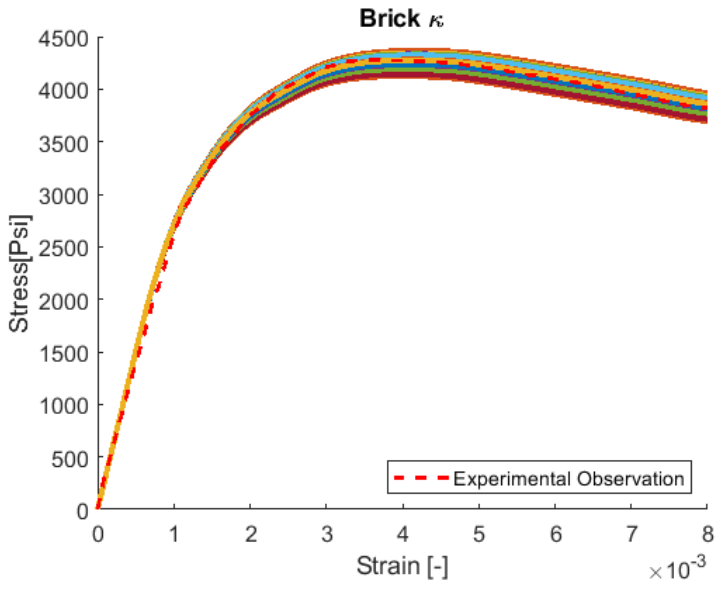

b)

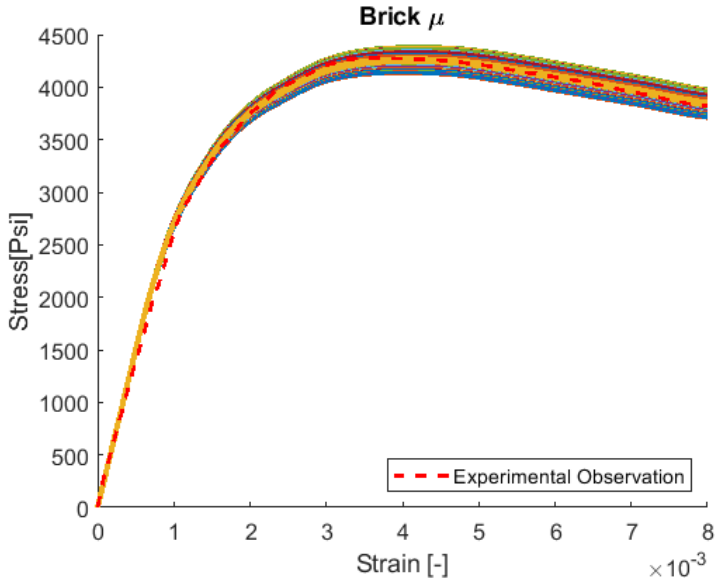

c)

Figure 3.12 Continued

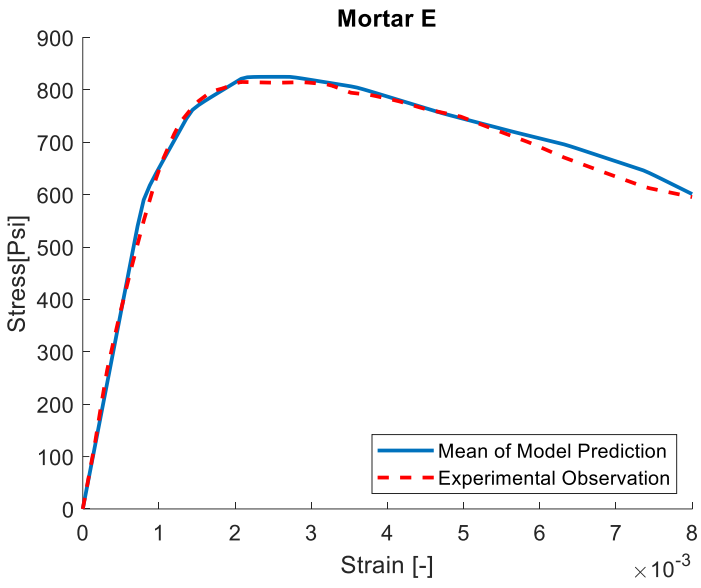

a)

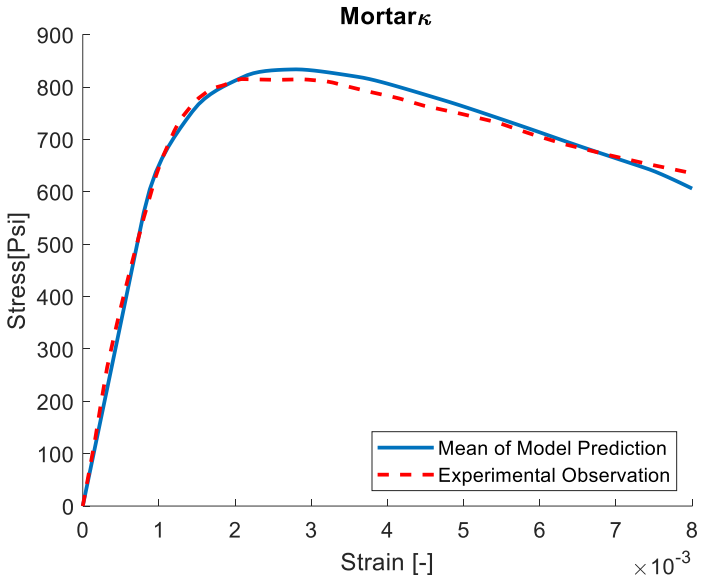

b)

Figure 3.13 Mean of model predictions E for mortar b) Mean of model predictions κ for mortar c) Mean of model predictions μ for mortar d) Standard deviations of model predictions E for mortar e) Standard deviations of model predictions κ f) Standard deviations of model predictions μ for mortar (Blackard et al., 2007)

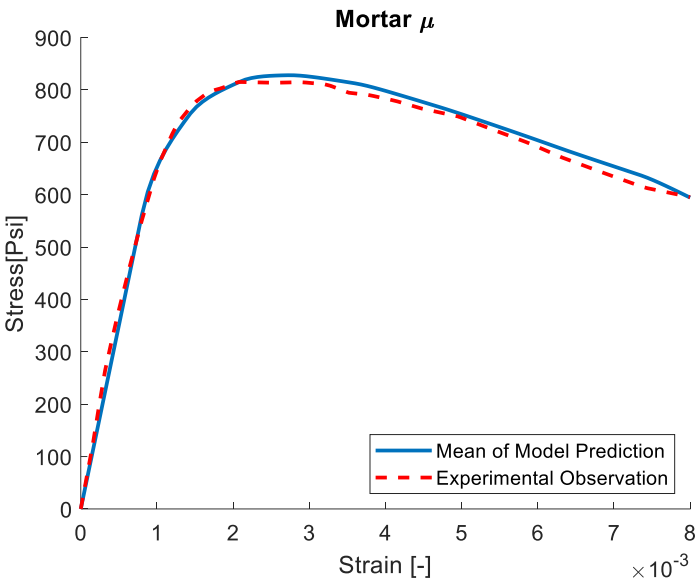

c)

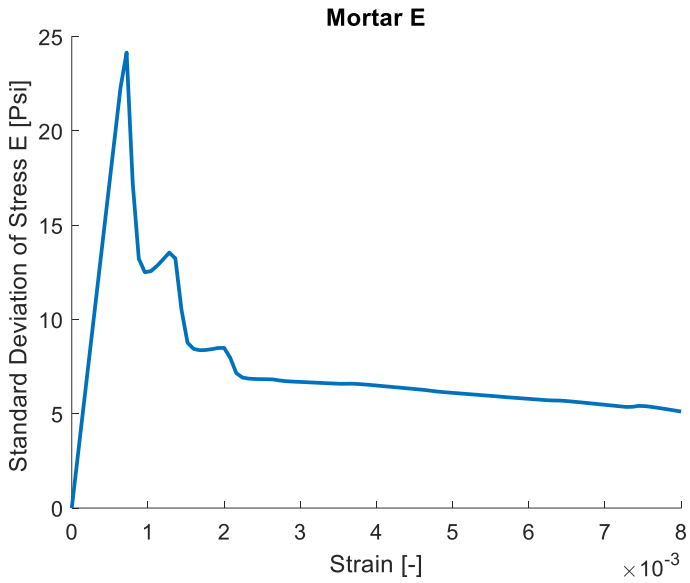

d)

Figure 3.13 Continued

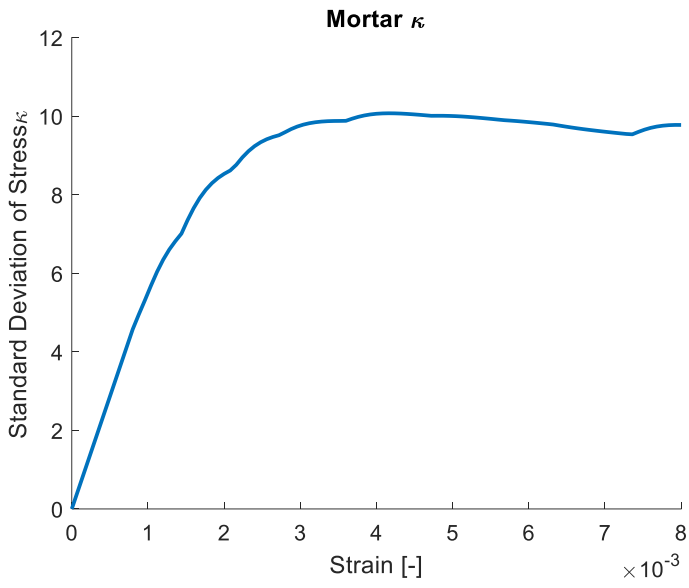

e)

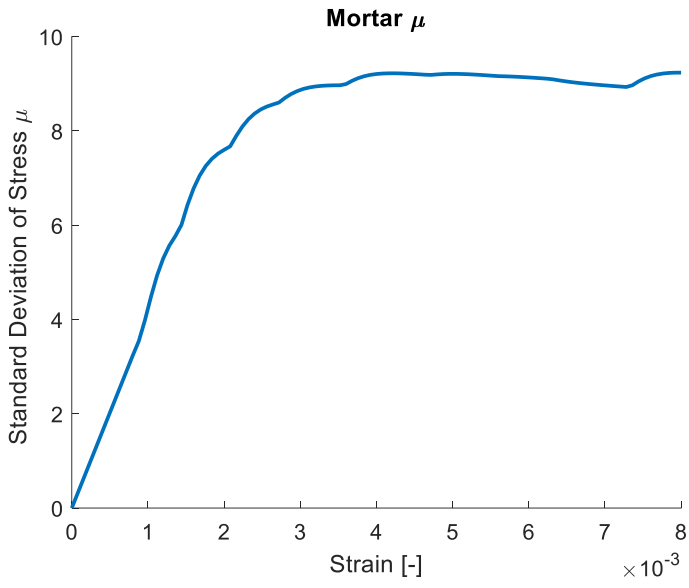

f)

Figure 3.13 Continued

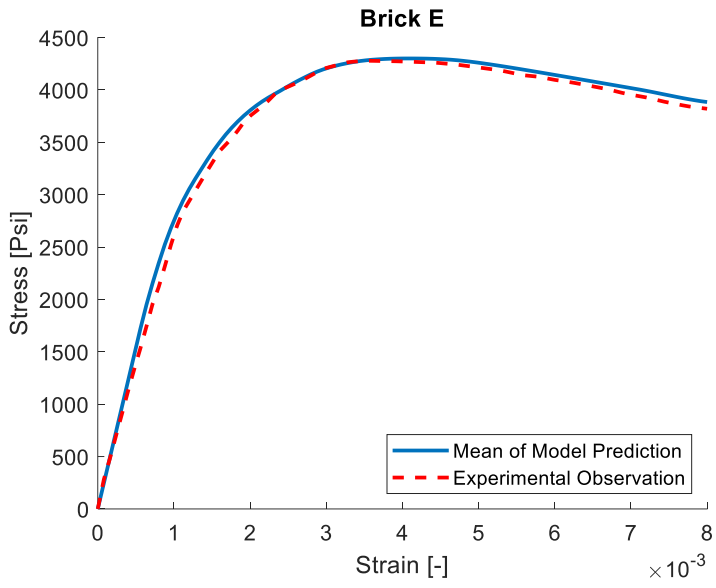

a)

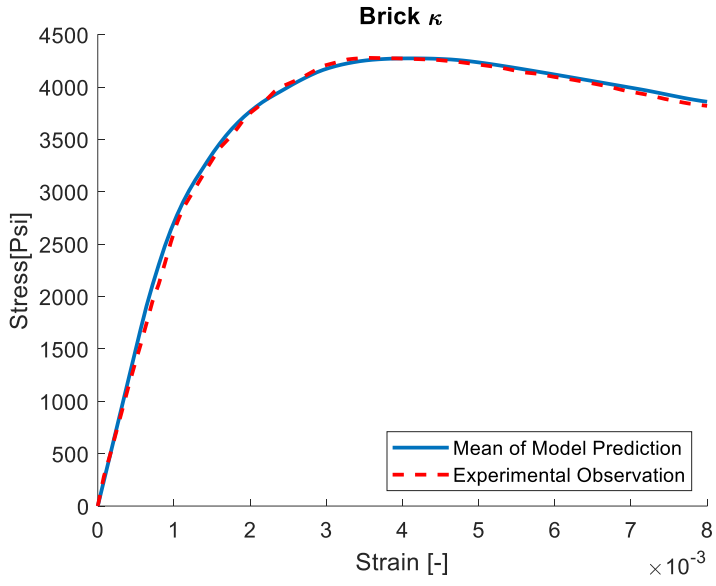

b)

Figure 3.14 a) Mean of model predictions E for brick b) Mean of model predictions κ for brick c) Mean of model predictions μ for brick d) Standard deviations of model predictions E for brick e) Standard deviations of model predictions κ f) Standard deviations of model predictions μ for brick (Blackard et al., 2007)

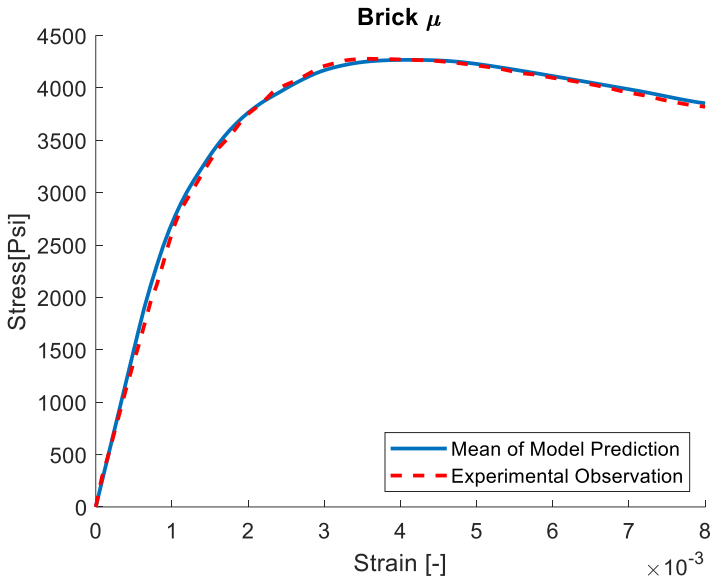

c)

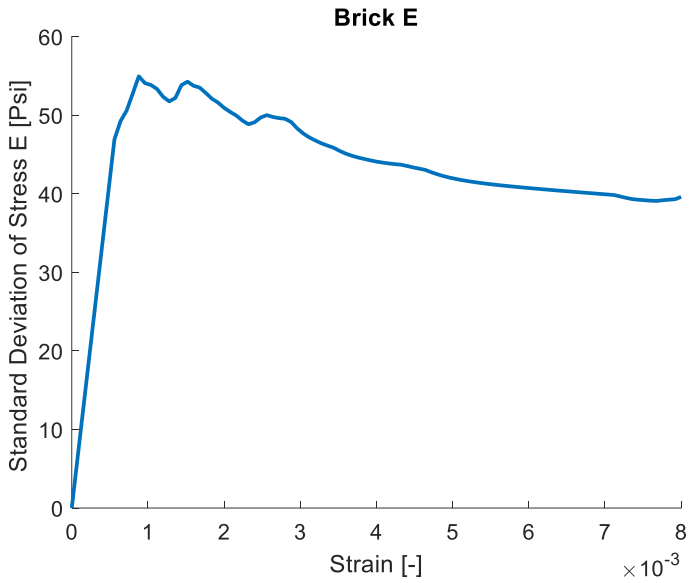

d)

Figure 3.14 Continued

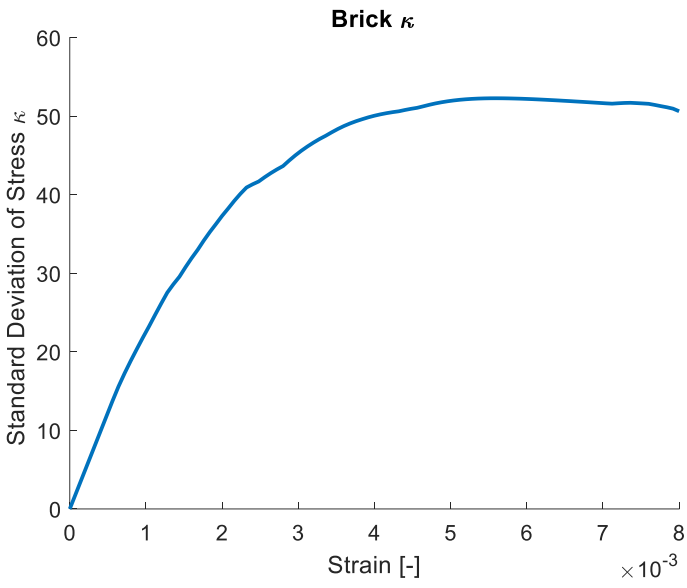

e)

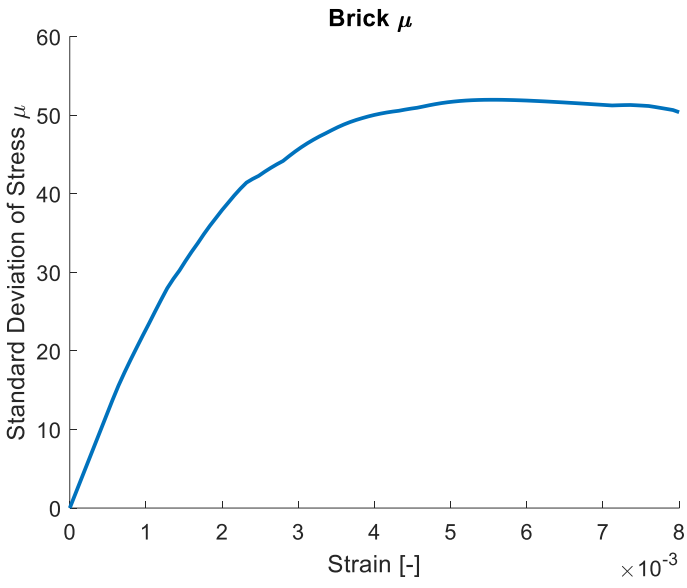

f)

Figure 3.14 Continued

3.2.2.2. Two-Parameters Calibration for Mortar and Brick Model

The probabilistic calibration method introduced in the preceding sections is now applied for two parameters at the time for brick unit and mortar. A bimodal distribution with non-linear relationships is investigated for the parameters the Young's modulus E with viscosity μ , and Young's modulus E with deviatoric out-of-roundness κ . These types of inferences are very engaging characteristics of the probabilistic calibration as compared to typical optimization approaches, which predict identify uncertainty associations with two parameters. The solution of the numerical was converging at 1e+5 in which the statistical inference can be obtained for the mortar (see Figure 3-15-3.17). However, the brick unit model converges faster in which was guaranteed at 5e+4, and the *burn-in* points started at 50% to infer the statistical results (see Figure 3-18-3.20).

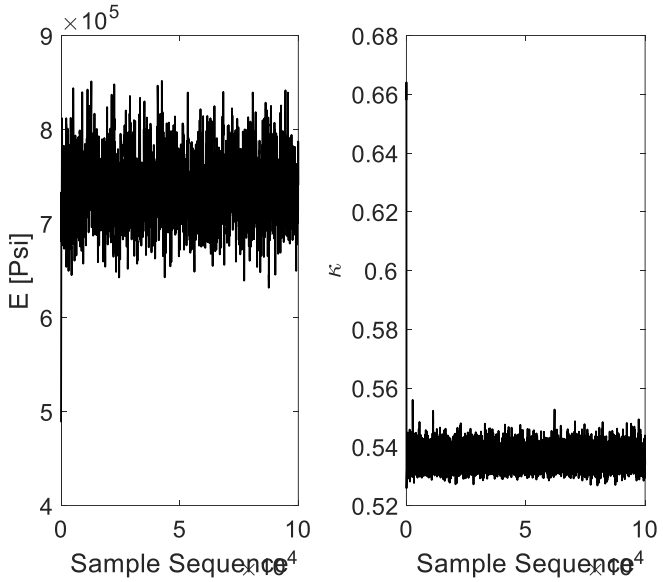

a)

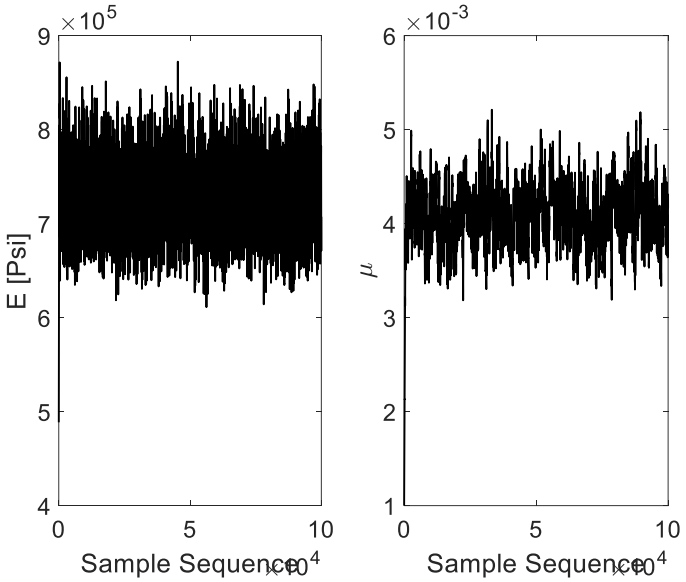

b)

Figure 3.15 Sample Sequence for Mortar a) Young's modulus E and deviatoric out-of-roundness κ b) Young's modulus E and viscosity μ

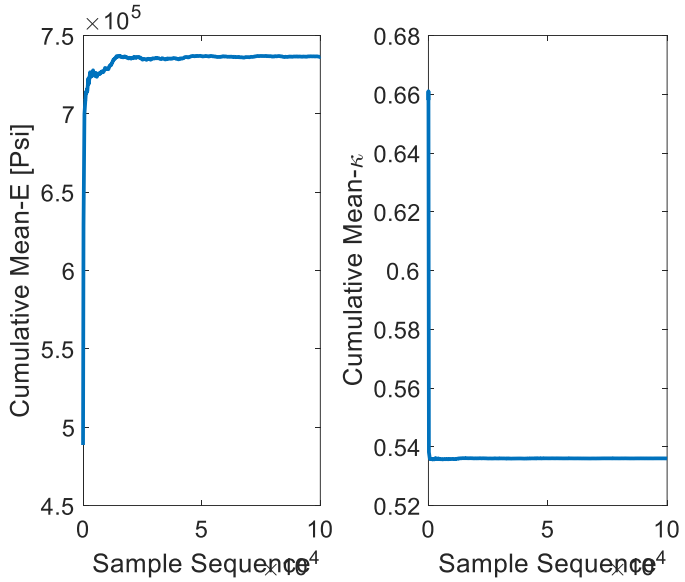

a)

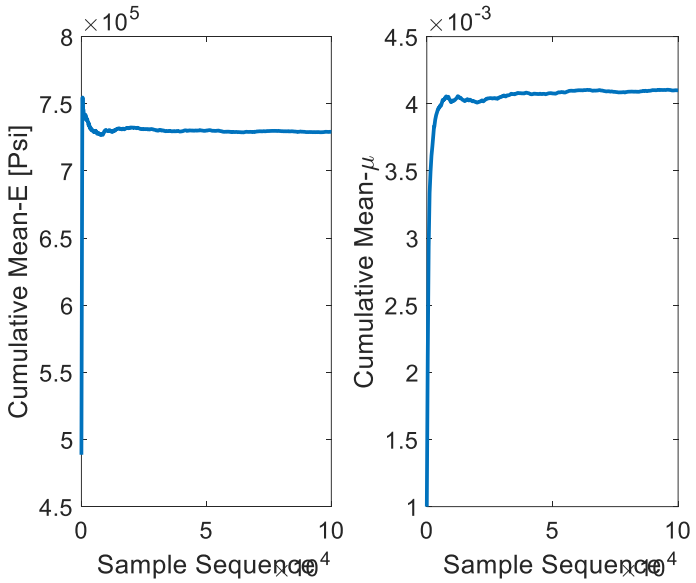

b)

Figure 3.16 Cumulative Mean for Mortar a) Young's modulus E and deviatoric out-of-roundness κ b) Young's modulus E and viscosity μ

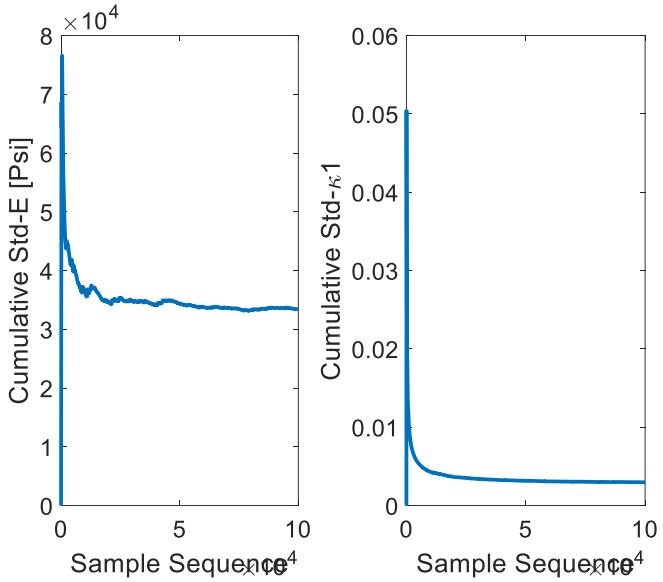

b)

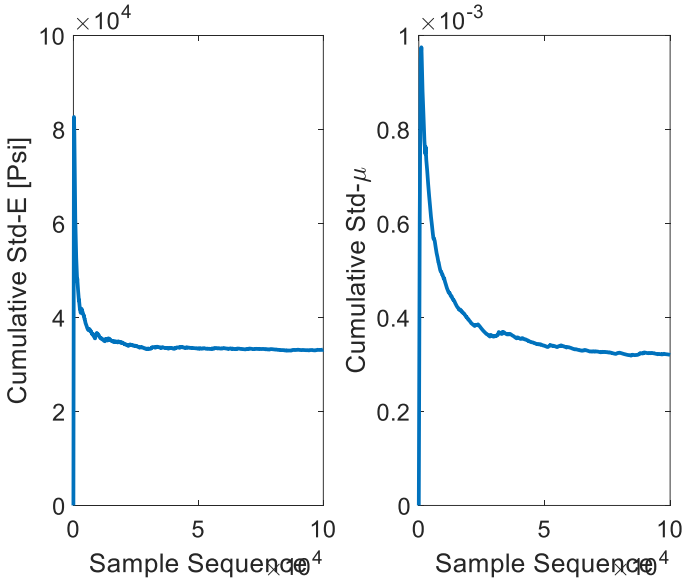

b)

Figure 3.17 Cumulative Std for Mortar a) Young's modulus E and deviatoric out-of-roundness κ b) Young's modulus E and viscosity μ

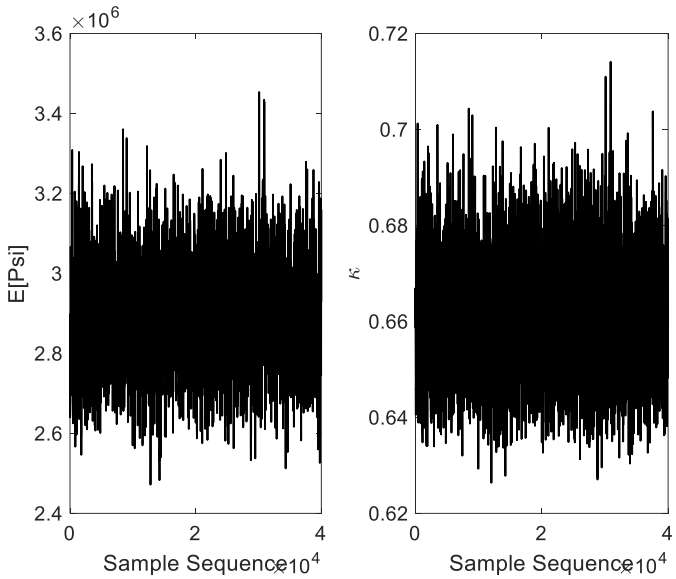

a)

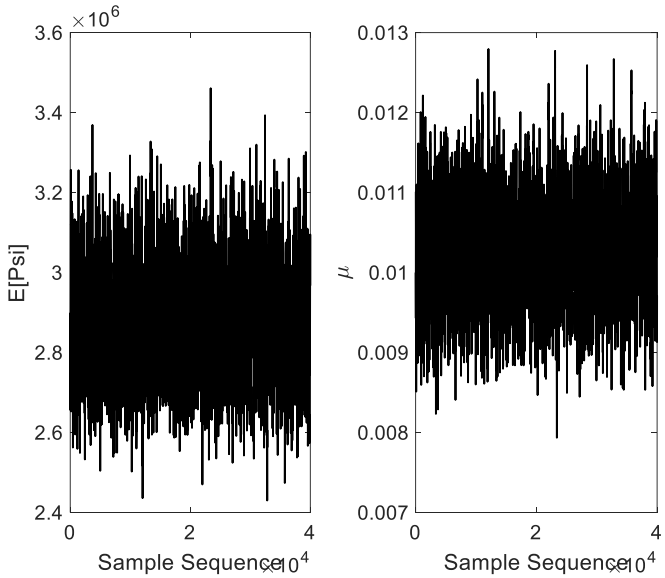

b)

Figure 3.18 Sample Sequence for Brick a) Young's modulus E and deviatoric out-of-roundness κ b) Young's modulus E and viscosity μ

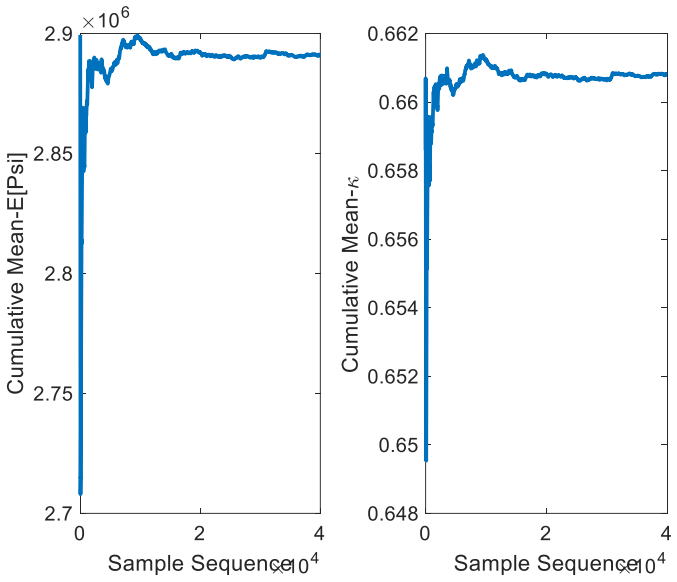

a)

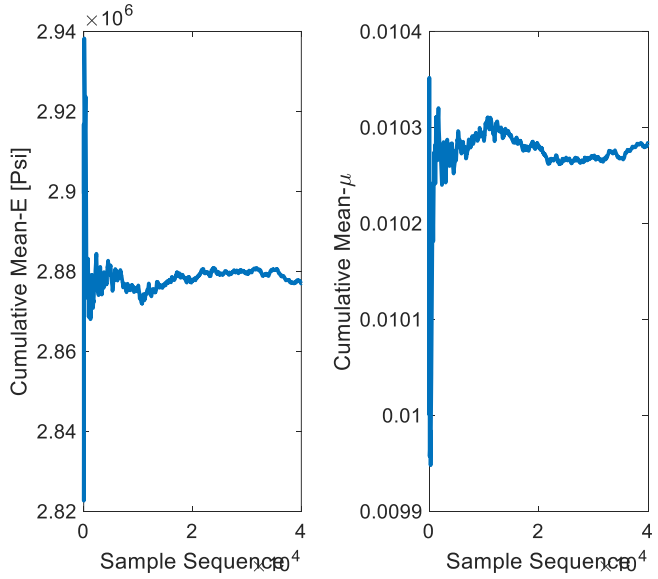

b)

Figure 3.19 Cumulative Mean for Brick a) Young's modulus E and deviatoric out-of-roundness κ b) Young's modulus E and viscosity μ

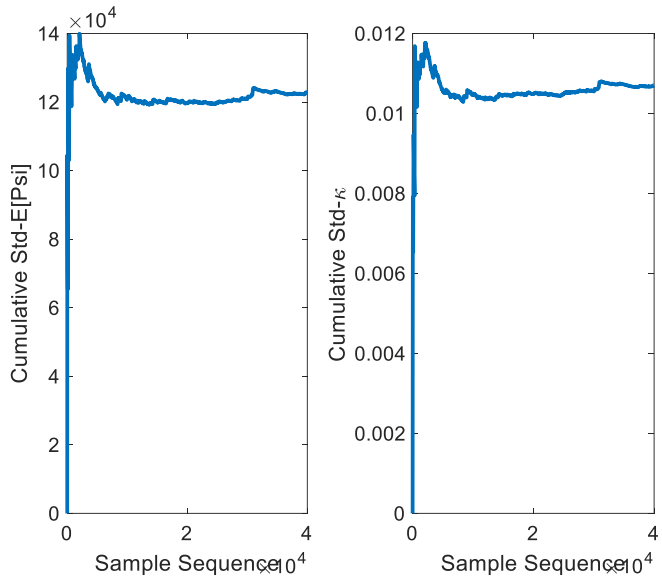

a)

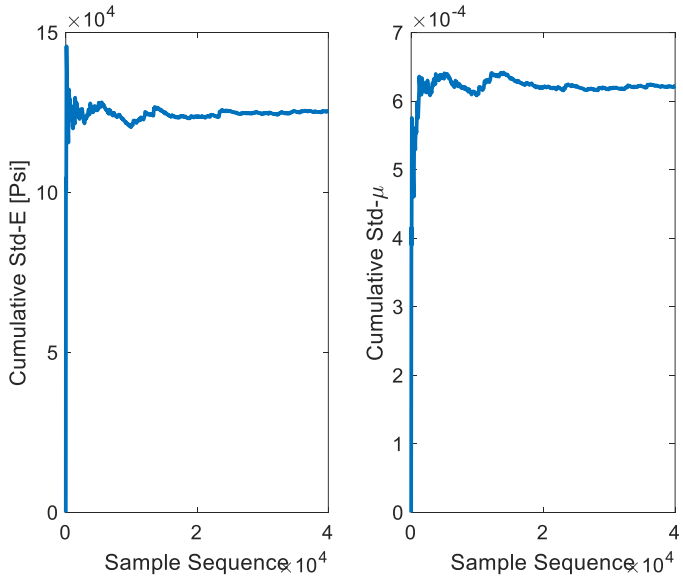

b)

Figure 3.20 Cumulative Std for Brick a) Young's modulus E and deviatoric out-of-roundness κ b) Young's modulus E and viscosity μ

The objective of the probabilistic calibration is to populate a joint probability distribution of the model parameters of interest for Young's modulus E with deviatoric out-of-Roundness κ and Young's modulus E and viscosity μ. Figures 3-21 and 3.22 show the joint relative frequency histograms (JRFH) of E with κ, and E with μ that quantifies the marginal probability distributions of each parameter in order to estimate their mean and standard deviation and second moments (correlation structure) (see Table 3.3-4). These figures show bimodal distribution with non-linear relationships between parameters for instance, and κ in which the higher values of Young's modulus E, the higher values for deviatoric out-of-Roundness κ increase. Frankly, the higher values of Young's modulus E, the viscosity μ intents to decrease. The viscosity μ is controlling the softening part of the stress-strain curve while deviatoric out-of-Roundness κ depends on hardening part of stress-strain curves. Consequently, the probabilistic calibrations of the model parameters are assessing the confidence of the model prediction in which can infer the statistical results.

Table 3.3 Statistical Parameters for Mortar of Young's modulus E and deviatoric out-of-roundness κ b) Young's modulus E and viscosity μ

Mortar	$E(psi)$	κ	$E(psi)$	μ
Mean	736440.483	0.536	729076.941	0.0041
Std	33401.476	0.0023	33100.650	0.00032

Table 3.4 Statistical Parameters for Brick of Young's modulus E and deviatoric out-of-roundness κ b) Young's modulus E and viscosity μ

Brick	$E(psi)$	κ	$E(psi)$	μ

Table 3.4 Continued

Mean	**2893077.56**	**0.662**	**2875354.256**	**0.01029**
Std	121014.48	0.0152	127212.711	0.00063

According to the MCMC simulations, the realization of the model predictions can be constructed by sampling random parameter combinations after the burn-in point (see Figure 3.23 and 3.24).

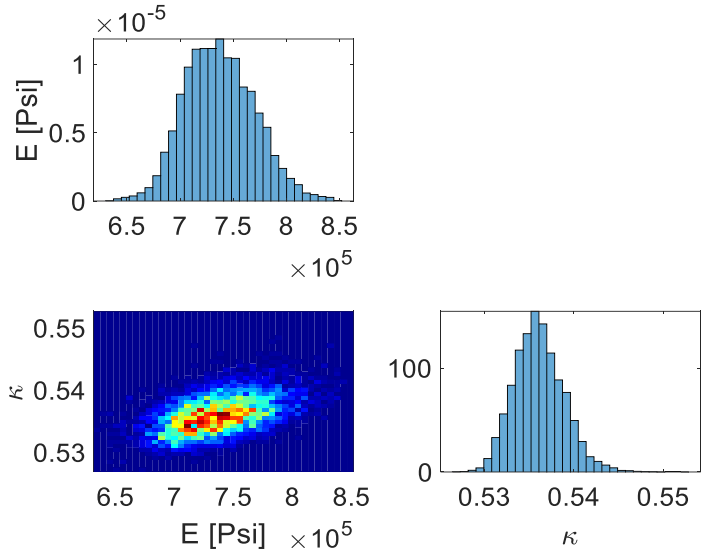

a)

Figure 3.21 Joint relative frequency histograms (JRFH) of mortar a) Young's modulus E and deviatoric out-of-roundness κ b) Young's modulus E and viscosity μ

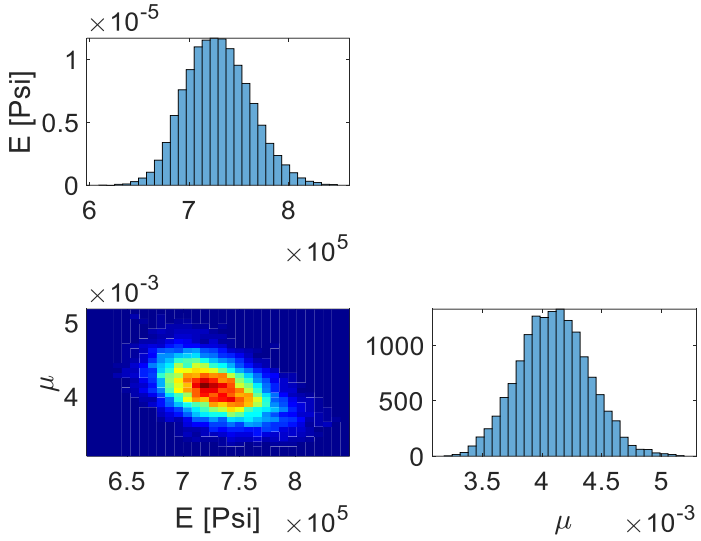

b)

Figure 3.21 Continued

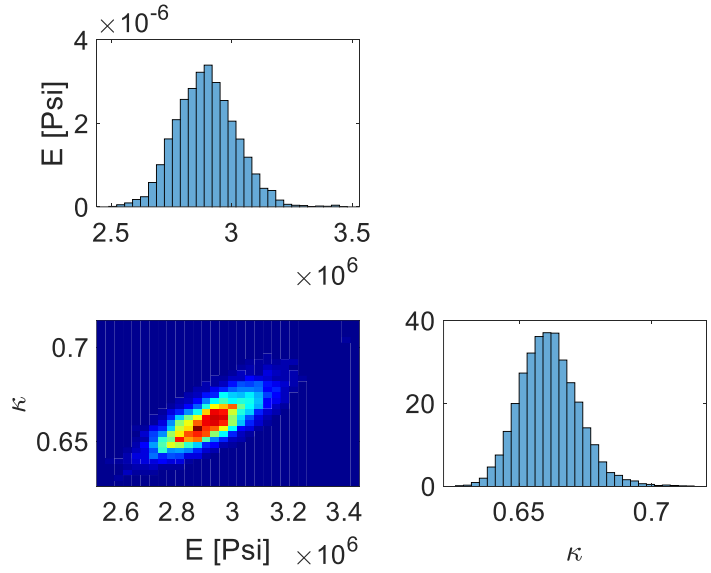

a)

Figure 3.22 Joint relative frequency histograms (JRFH) of brick a) Young's modulus E and deviatoric out-of-roundness κ b) Young's modulus E and viscosity μ

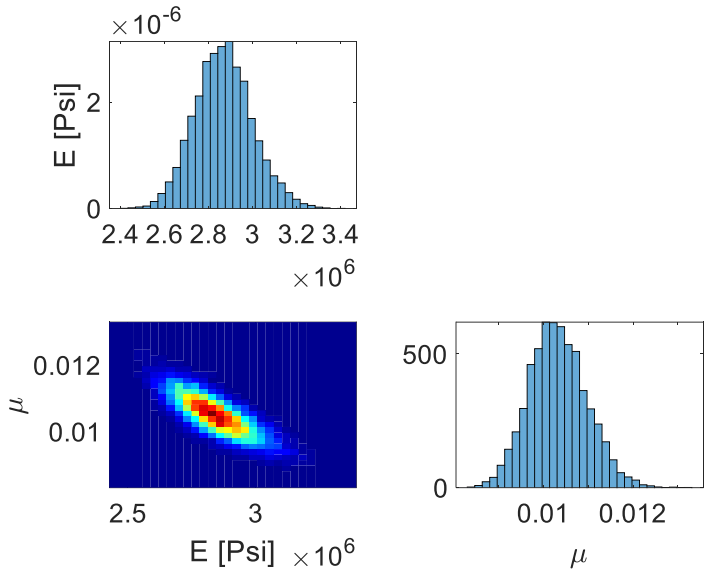

b)

Figure 3.22 Continued

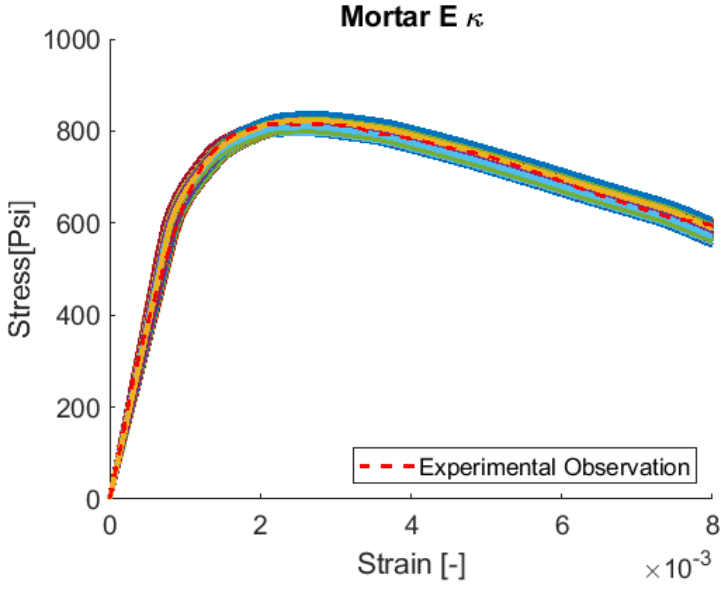

a)

Figure 3.23 Model realization of mortar a) Young's modulus E and deviatoric out-of-roundness κ b) Young's modulus E and viscosity μ (Blackard et al., 2007)

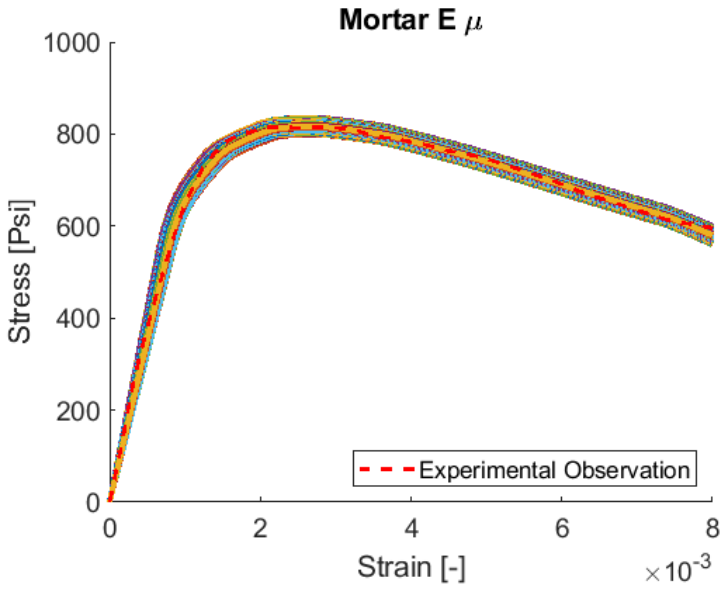

b)

Figure 3.23 Continued

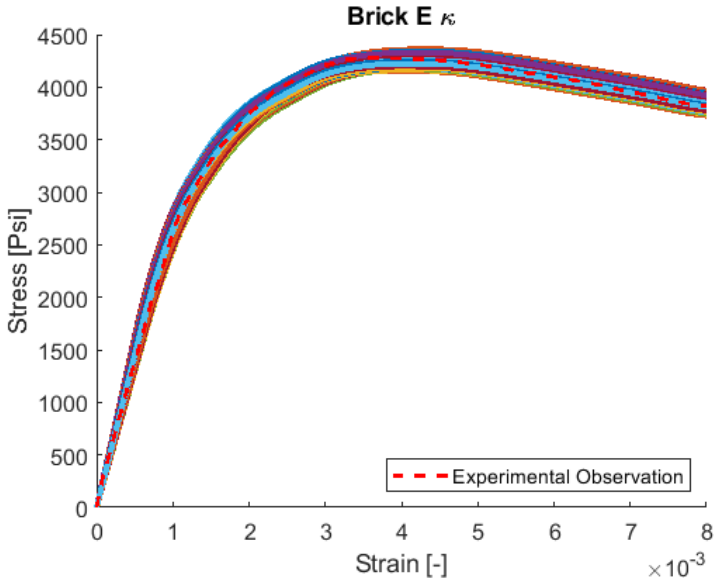

a)

Figure 3.24 Model realization of brick a) Young's modulus E and deviatoric out-of-roundness κ b) Young's modulus E and viscosity μ (Blackard et al., 2007)

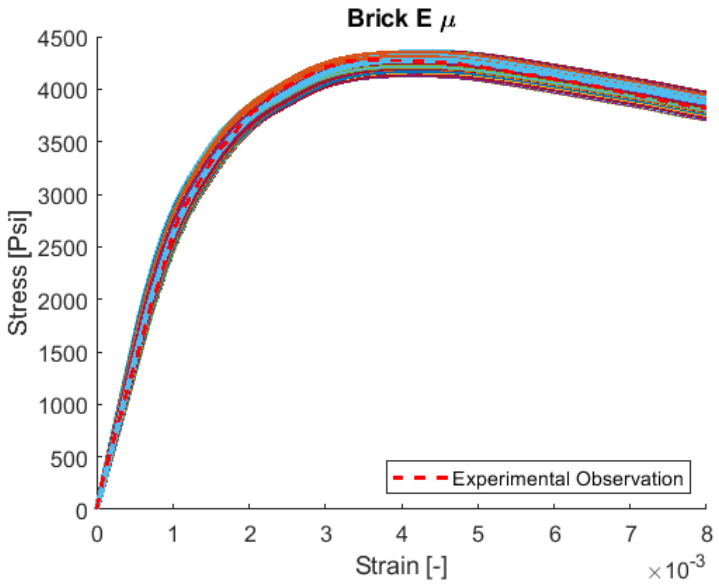

b)
Figure 3.24 Continued

After the convergence condition of the parameters is reached on the MCMC- MH, the first order statistics of model response is formulated from the statistical inferences of the parameters. The mean and standard deviation of the burn-in points plotted with respect to the axial stress for each data point for mortar and brick unit are shown in Figure 3.25 and Figures 3.26, respectively. The mean shows a good fitting with the experimental observation compared to single parameters calibration in section 3.2.2.1. Also, the standard deviation reflects of E with κ and E with μ for mortar the variability on the model predictions that start with a steep growth and a sudden drop at about strain equal to 0.0016 in which coincides approximately with strain equal to 0.0012 of the stress-strain curves. However for the brick unit the parameters of E with κ and E with μ show that maximum strain of

the standard division curve did not match with in the stress-strain curve (see Figure 3.25 and 2.26).

Table 3.5-6 illustrates the statistical results of the mean and standard deviation for the individual constitutive CDP parameters of the brick for one parameter and two parameters calibrations. The results the uncertainty associated with two parameters calibration are reduced compared to one parameter calibration. Besides this, the result proves the existence of a unique range of material parameters that are closed with parameter values obtain from literatures.

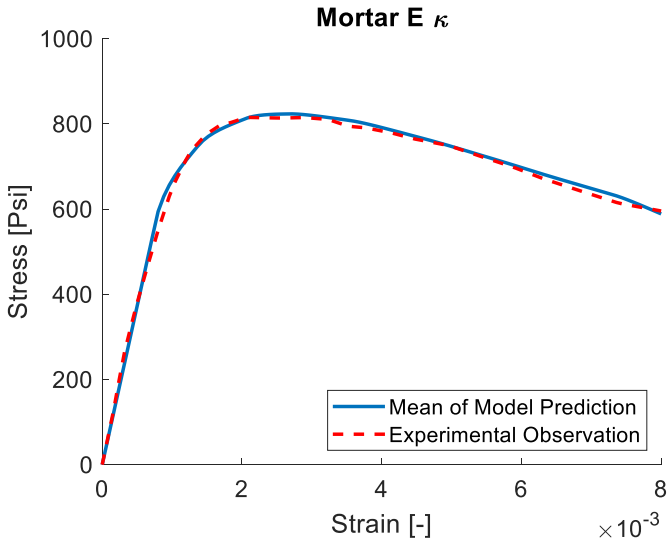

a)

Figure 3.25. a) Mean of model predictions young's modulus E and deviatoric out-of-roundness κ for mortar b) Mean of model predictions young's modulus E and viscosity μ for mortar c) Standard deviations of model predictions E with κ for mortar d) Standard deviations of model predictions E with μ for mortar (Blackard et al., 2007).

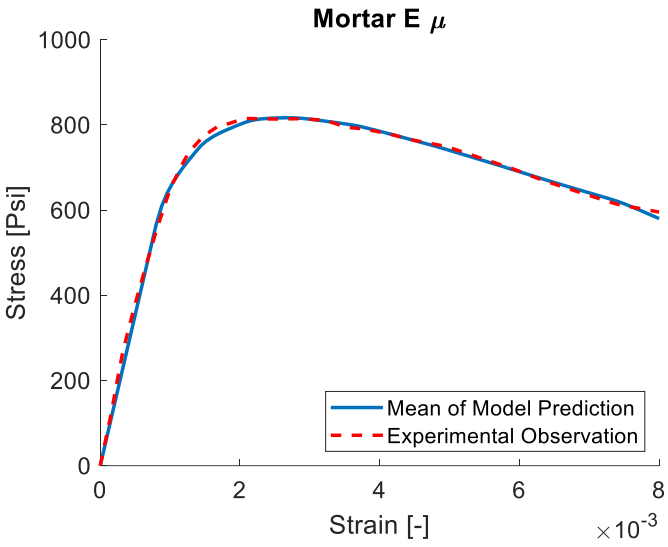

b)

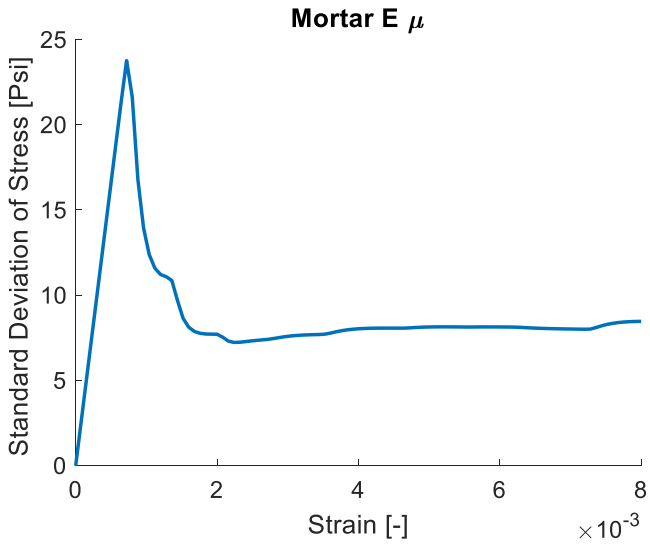

c)

Figure 3.25 Continued

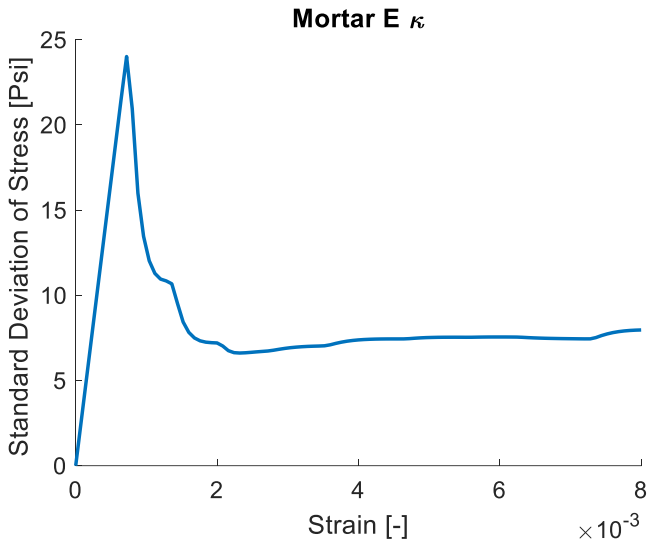

d)

Figure 3.25 Continued

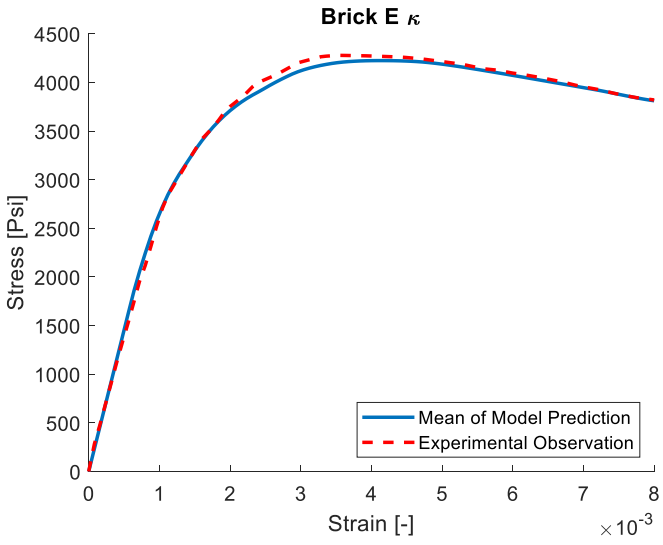

a)

Figure 3.26. a) Mean of model predictions young's modulus E and deviatoric out-of-roundness κ for brick b) Mean of model predictions young's modulus E and viscosity μ for brick c) Standard deviations of model predictions E with κ for brick d) Standard deviations of model predictions E with μ for brick (Blackard et al., 2007).

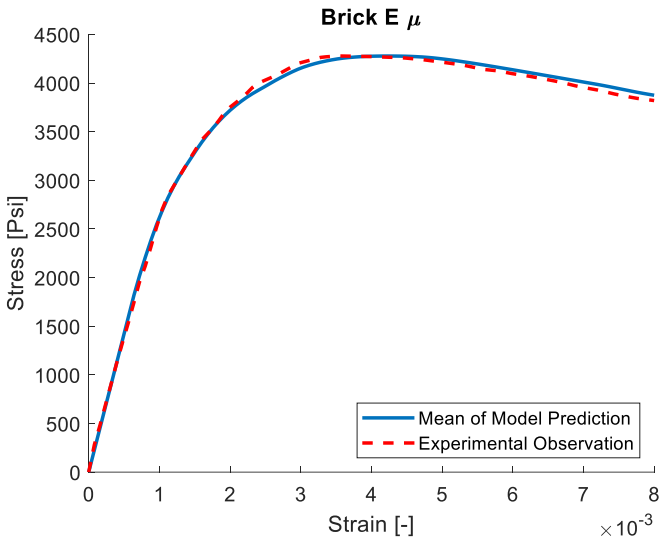

b)

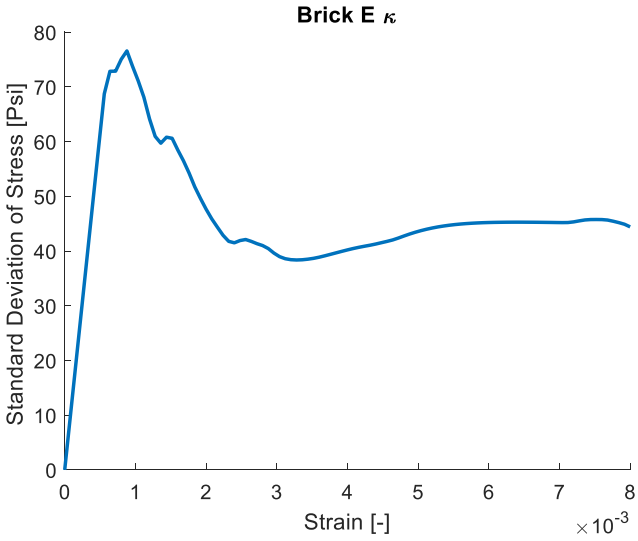

c)

Figure 3.25 Continued

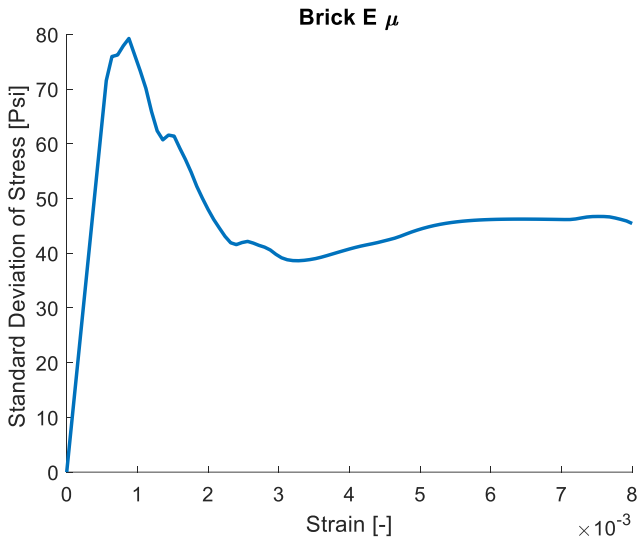

d)

Figure 3.25 Continued

Table 3.5 Statistical Results for One and Two Parameters for Mortar.

	Two-parameters Calibration				One-parameter Calibration		
Mortar	$E(psi)$	κ	$E(psi)$	μ	$E(psi)$	κ	μ
Mean	736440.483	0.536	729076.941	0.0041	748427.905	0.530	0.0042
Std	33401.476	0.0023	33100.650	0.00032	34294.613	0.00307	0.000315

Table 3.6 Statistical Results for One and Two Parameters for Brick.

	Two-parameters Calibration				One-parameter Calibration		
Brick	$E(psi)$	κ	$E(psi)$	μ	$E(psi)$	κ	μ
Mean	2893077.56	0.662	2875354.256	0.01029	2917957.265	0.671	0.00981
Std	121014.48	0.0152	127212.711	0.00063	80310.394	0.00850	0.000367

3.3. Conclusion

A Bayesian probabilistic calibration was conducted to investigate the effects of the uncertainty of concrete damage plasticity model parameters in URM walls. The main objective of this work was to identify the uncertainty and correlation structure of the model parameters, capturing the mechanical responses of brick and mortar in masonry walls. Furthermore, by assessing the model's responses and related statistics, the model was validated in terms of its ability to capture the trend in mechanical response behavior for the brick unit and mortar. In addition, the CDP model presented higher flexibility for capturing nonlinear behavior throughout the time relaxation of the viscosity parameters μ and the hardening of deviatoric out-of-Roundness κ with respect to the linear elastic response of the Young's modulus E. The JRFH show ability to retrieve the correlation structure that is defining the degree of association between the parameter of interest and capture the true mechanical response. Consequently, the final results of the stress-strain behavior show a good agreement with the experimental observations. Further investigation should be based on the influence of masonry walls under different load combinations (e.g., wind load, seismic loading) to understand the overall response.

3.4. References

Abrams, D. P., & Shah, N. (1992). Cyclic load testing of unreinforced masonry walls. Retrieved from

Broyden, C. G. (1970). The convergence of a class of double-rank minimization algorithms general considerations. IMA Journal of Applied Mathematics, 6(1), 76-90.

Byrd, R. H., Gilbert, J. C., & Nocedal, J. (2000). A trust region method based on interior point techniques for nonlinear programming. Mathematical programming, 89(1), 149-185.

Byrd, R. H., Hribar, M. E., & Nocedal, J. (1999). An interior point algorithm for large-scale nonlinear programming. SIAM Journal on Optimization, 9(4), 877-900.

Carmeliet, J. (1999). Optimal estimation of gradient damage parameters from localization phenomena in quasi-brittle materials. Mechanics of Cohesive-frictional Materials: An International Journal on Experiments, Modelling and Computation of Materials and Structures, 4(1), 1-16.

Chisari, C. (2015). Inverse techniques for model identification of masonry structures.

Chisari, C. (2019). Tolerance-based Pareto optimality for structural identification accounting for uncertainty. Engineering with Computers, 35(2), 381-395.

Chisari, C., Macorini, L., Amadio, C., & Izzuddin, B. (2015). An inverse analysis procedure for material parameter identification of mortar joints in unreinforced masonry. Computers & Structures, 155, 97-105.

Chisari, C., Macorini, L., Amadio, C., & Izzuddin, B. A. (2018). Identification of mesoscale model parameters for brick-masonry. International journal of solids and structures, 146, 224-240.

Epperson, G. S., & Abrams, D. P. (1990). Nondestructive evaluation of masonry buildings (Vol. 89): University of Illinois at Urbana-Champaign.

Fadale, T. D., Nenarokomov, A. V., & Emery, A. F. (1995). Uncertainties in parameter estimation: the inverse problem. International Journal of Heat and Mass Transfer, 38(3), 511-518.

Fletcher, R. (1970). A new approach to variable metric algorithms. The computer journal, 13(3), 317-322.

Foresee, F. D., & Hagan, M. T. (1997). Gauss-Newton approximation to Bayesian learning. Paper presented at the Proceedings of International Conference on Neural Networks (ICNN'97).

Gambarotta, L., & Lagomarsino, S. (1997). Damage models for the seismic response of brick masonry shear walls. Part I: the mortar joint model and its applications. Earthquake engineering & structural dynamics, 26(4), 423-439.

Goldfarb, D. (1970). A family of variable-metric methods derived by variational means. Mathematics of computation, 24(109), 23-26.

Grassl, P., & Jirásek, M. (2006). Damage-plastic model for concrete failure. International journal of solids and structures, 43(22-23), 7166-7196.

Jankowiak, T., & Lodygowski, T. (2005). Identification of parameters of concrete damage plasticity constitutive model. Foundations of civil and environmental engineering, 6(1), 53-69.

Karush, W. (1939). Minima of functions of several variables with inequalities as side constraints. M. Sc. Dissertation. Dept. of Mathematics, Univ. of Chicago.

Kmiecik, P., & Kamiński, M. (2011). Modelling of reinforced concrete structures and composite structures with concrete strength degradation taken into consideration. Archives of civil and mechanical engineering, 11(3), 623-636.

Kuhn, H., & Tucker, A. (1951). Proc. Second Berkeley Symp. on Math. Stats. and Prob.

Lee, J., & Fenves, G. L. (1998). Plastic-damage model for cyclic loading of concrete structures. Journal of Engineering Mechanics, 124(8), 892-900.

Levenberg, K. (1944). A method for the solution of certain non-linear problems in least squares. Quarterly of applied mathematics, 2(2), 164-168.

Lotfi, H., & Shing, P. (1991). An appraisal of smeared crack models for masonry shear wall analysis. Computers & Structures, 41(3), 413-425.

Lubliner, J. (1991). A simple model of generalized plasticity. International journal of solids and structures, 28(6), 769-778.

Lubliner, J., Oliver, J., Oller, S., & Oñate, E. (1989). A plastic-damage model for concrete. International journal of solids and structures, 25(3), 299-326.

MacKay, D. J. (1992). Bayesian interpolation. Neural computation, 4(3), 415-447.

Marquardt, D. W. (1963). An algorithm for least-squares estimation of nonlinear parameters. Journal of the society for Industrial and Applied Mathematics, 11(2), 431-441.

MATLAB, V. (2016). 9.0. 0.341360 (R2016a). Natick, Massachusetts: The MathWorks Inc.

Muñoz-Rojas, P., Cardoso, E., & Vaz, M. (2010). Parameter identification of damage models using genetic algorithms. Experimental Mechanics, 50(5), 627-634.

Nazari, A., & Sanjayan, J. G. (2015). Modelling of compressive strength of geopolymer paste, mortar and concrete by optimized support vector machine. Ceramics International, 41(9), 12164-12177.

Papazafeiropoulos, G., Muñiz-Calvente, M., & Martínez-Pañeda, E. (2017). Abaqus2Matlab: a suitable tool for finite element post-processing. Advances in Engineering Software, 105, 9-16.

Rechea, C., Levasseur, S., & Finno, R. (2008). Inverse analysis techniques for parameter identification in simulation of excavation support systems. Computers and Geotechnics, 35(3), 331-345.

Sarhosis, V., & Sheng, Y. (2014). Identification of material parameters for low bond strength masonry. Engineering Structures, 60, 100-110.

Shanno, D. F. (1970). Conditioning of quasi-Newton methods for function minimization. Mathematics of computation, 24(111), 647-656.

Simulia, D. (2016). Abaqus Version 2016 Documentation USA. In: Dassault Systems Simulia Corp, Johnston, RI, USA.

Toropov, V. V., & van der Giessen, E. (1993). Parameter identification for nonlinear constitutive models: Finite Element simulation—Optimization—Nontrivial experiments. In Optimal design with advanced materials (pp. 113-130): Elsevier.

Waltz, R. A., Morales, J. L., Nocedal, J., & Orban, D. (2006). An interior algorithm for nonlinear optimization that combines line search and trust region steps. Mathematical programming, 107(3), 391-408.

Xu, W., & Abrams, D. P. (1992). Evaluation of Lateral Strength and Deflection for Cracked Unreinforced Masonry Walls. Illinois University at Urbana Advanced Construction Technology Center.

4. A NEURAL NETWORK OPTIMIZATION ALGORITHM FOR THE CALIBRATION OF MATERIAL PROPERTIES OF URM WALL PRISMS

4.1. Introduction

A Neural Network Optimization (NNO) algorithm is presented to calibrate the material constitutive parameters in masonry prisms for describing the mechanical response of the Unreinforced Masonry (URM) walls. The goal herein is to demonstrate that the optimal values of the material properties of conventional small-scale (prism) experiments can be directly used for validation of large-scale (wall) experiments, implying thus that the proposed inverse algorithm is sufficiently robust and efficient. The Concrete Damaged Plasticity (CDP) constitutive model in ABAQUS commercial finite element software is being used for the calibration of the material parameters. The optimal material parameters for the prism showed a good agreement between the experimental curve and the model prediction. The general procedure of the material parameter identification method and the numerical results are presented. The interface behavior is described by considering a Coulomb-type friction criterion on the mortar bed joints.

Unreinforced masonry (URM) walls are structural elements, which generally show brittle and nonlinear inelastic mechanical response. Formulating constitutive models and calibrating material parameters in the constitutive models is essential in order to provide reliable predictions of the response of structures comprised of these materials. A concrete damage plasticity (CDP) constitutive model that describes both stages of plasticity modes and of damage behavior was used to analyze the mechanical response of masonry structures (Lee & Fenves, 1998; Jacob Lubliner, 1991; J Lubliner et al., 1989). The CDP model

includes eight material parameter $(i.e., E, \nu, f'c, \psi, f_b / f_c, \grave{o}, \kappa, \mu)$; however, among these, the four most sensitive parameters Young's modulus E, viscosity, deviatoric out-of-roundness κ, and dilation angle ψ) were used for the prism calibration analysis, to demonstrate the applicability of the proposed Neural Network Optimization (NNO) methodology. The numerical implementation of the NNO requires an interface to establish communication between ABAQUS and MATLAB. Abaqus2Matlab (A2M) was used for this purpose, which allowed to run the NNO algorithms developed in MATLAB (Papazafeiropoulos et al., 2017).

Extensive laboratory tests have been carried out in the past decades at the University of Illinois-Urbana-Champaign to evaluate the behavior of masonry structures (Abrams & Shah, 1992; Epperson & Abrams, 1990; Xu & Abrams, 1992). On the other hand, many studies have used various constitutive models that have been formulated for masonry walls and their constituents. Representative studies have been presented and developed for concrete constitutive models such as concrete damage plasticity CDP and smeared crack model and validated their material parameters through experimental tests (Gambarotta & Lagomarsino, 1997; Grassl & Jirásek, 2006; Lee & Fenves, 1998; Lotfi & Shing, 1991; Jacob Lubliner, 1991; J Lubliner et al., 1989; Sarhosis & Sheng, 2014), et al.

To minimize errors between the observation-based datasets and model parameters, inverse methods have been applied to identify and characterize the material properties in the constitutive models (Carmeliet, 1999; Chisari, 2015, 2019; Chisari et al., 2015; Chisari et al., 2018; Fadale et al., 1995; Muñoz-Rojas et al., 2010; Nazari & Sanjayan, 2015; Rechea et al., 2008; Sarhosis & Sheng, 2014; V. V. Toropov & van der Giessen, 1993). Several studies have discussed a wide variety of material parameters calibrated from experimental

data and provided typical ranges for the different parameters, e.g., the dilatancy angle (ψ) (0-36°), biaxial strength ratio (f_b / f_c) (1.10-1.16) and deviatoric plane in the yield surfaces (κ), (0.5-1) (Jankowiak & Lodygowski, 2005; Kmiecik & Kamiński, 2011; J Lubliner et al., 1989). In this paper, the objective function was applied using the least-squares technique which minimizes the sum of the squares of the differences between experiment-based measurements and the calculated response of the model (Levenberg, 1944; Marquardt, 1963).

In this chapter, calibration of the material properties of the Abaqus CDP model with reference to an experimental stress – strain curve is performed. The experimental stress – strain curve is obtained from a uniaxial compression test of a wall prism. The material properties that correspond to the optimum fit between the numerical and experimental curves are found using a novel NNO algorithm.

4.2. Description of the Prism Model

The model is comprised of 5 bricks and 4 layers of mortar between the former. The cross-section dimensions of the prism are 3.75” x 8” x 12.65” and the mortar thickness between the bricks is 0.375” (Epperson & Abrams, 1990). The prism is fixed at its bottom and at the top a uniform displacement is imposed. The ABAQUS model of the prism is discretized in 530 3D solid elements (C3D8R), defined by 1073 nodes (see Figure 4.1). The constitutive behavior of both the bricks and the mortar is defined by the CDP model, the parameters of which are the design variables of the NNO problem. The Poisson ratio of the brick is equal to 0.1 whereas the Poisson ratio of the mortar is 0.2. In addition, the flow potential eccentricity (ò) is equal to 0.1 for both the bricks and the mortar layers, and the

ratio of initial equibiaxial compressive yield stress to initial uniaxial compressive yield stress (f_b / f_c) is set equal to 1.16 for both the brick and mortar materials. The bricks and the mortar layers are considered to be tied across their interfaces. A static analysis is performed to obtain the response of the prism due to the imposed displacement. An appropriate mesh sensitivity analysis has been performed in order to ensure that the mesh refinement does not affect significantly the final results.

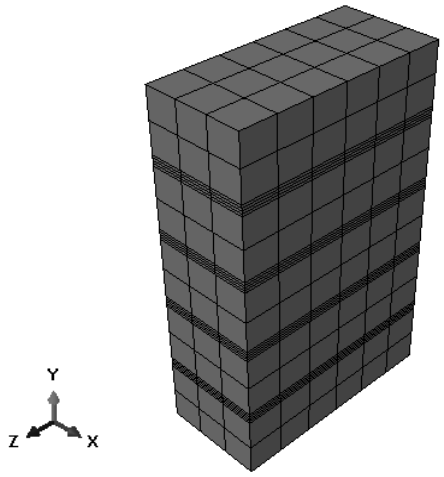

Figure 4.1 3D FE prism model (Epperson & Abrams, 1990)

More specifically, there are 8 design variables in this optimization problem:

- The moduli of elasticity $(\mathrm{E}_C, \mathrm{E}_M)$ of the brick and the mortar respectively
- The dilation angles in the p–q plane of the brick and the mortar (ψ_C, ψ_M)
- The ratios of the second stress invariant on the tensile meridian to that on the compressive meridian of the brick and the mortar (κ_C, κ_M)

- The viscosity parameters $\boldsymbol{\mu}$ of the brick and the mortar (μ_C, μ_M)
- The upper and lower limits are set for the design variables based on the literature and are shown in Table 4.1.

Table 4.1 Description and Bounds of The Design Variables Considered for Fitting the Experimental Stress Strain Curve Of The Prism.

Design variable	Description	Lower bound	Upper bound
E_C	Modulus of elasticity of the brick material	800000	4000000
ψ_C	Dilation angle in the p–q plane of the brick material	0.1	36
κ_C	Ratio of the second stress invariant on the tensile meridian to that on the compressive meridian for the brick material	0.51	1
μ_C	Viscosity parameter of the brick material	0.0001	0.1
E_M	Modulus of elasticity of the mortar	100000	900000
ψ_M	Dilation angle in the p–q plane of the mortar	0.1	36
κ_M	Ratio of the second stress invariant on the tensile meridian to that on the compressive meridian for the mortar	0.51	1
μ_M	Viscosity parameter of the mortar	0.0001	0.1

4.3. Proposed Method for Material Parameter Identification

The NNO algorithm that has been used for the optimization process employs a novel technique that combines inverse analysis and neural network optimization. The essential steps are illustrated in the flowchart presented in Figure 4.2.

4.3.1. General

The constitutive properties of the ABAQUS Concrete Damaged Plasticity (CDP) model were calibrated so that the numerical stress-strain curve (SSnum) fits the corresponding experimental curve (SSexp). This is done through the implementation of an inverse analysis, whereby an optimization procedure is implemented which minimizes the least square error between the numerical and experimental data. ABAQUS Simulia (2016) was used for purposes of Finite Element (FE) simulation and MATLAB (2016) was used for the implementation of the optimization procedure. MATLAB was appropriately coupled with ABAQUS by using Abaqus2Matlab (Papazafeiropoulos et al., 2017), a novel software that can transfer model data and results between ABAQUS with MATLAB and vice versa, leading thus in a user-friendly integrated simulation and programming environment.

4.3.2. Initial Sets of Values Assigned to the Design Variables

Initially, a set of initial values is assigned to the design variables, let's say M sets of values for the design variables. The values of the design variables can be selected randomly, or according to a given distribution which can be different among the various design variables. Each one of the M design variable combinations corresponds to a single ABAQUS simulation case. The initial sets of design variable values should be chosen so that they span a range which is large enough, so that it includes the optimal solution. Generally, the more initial points that are specified, the higher the performance of the neural network. However, care should be taken so that the number of initial points is neither too small nor too large with respect to the capacity of the neural network. In the first case of low number of training data, the Artificial Neural Network (ANN) could learn the initial data too "well" and over fit the initial dataset, which prevents the ANN from performing well on new training data

that are generated as the neural optimization algorithm proceeds. The opposite happens in the case of under fitting, i.e. when the ANN has capacity too high to learn from the initial training data. In this case, the ANN cannot learn neither from the initial training data, nor from the new training data generated during the neural optimization procedure. As a result, there is an optimum size of the initial training data that needs to be considered, to avoid both of the above negative situations. Currently, there is not any standard methodology of selecting the initial data size; this depends on the nature of the algorithm, the ABAQUS model(s) involved and also the hyperparameters of the ANN and the optimizer function.

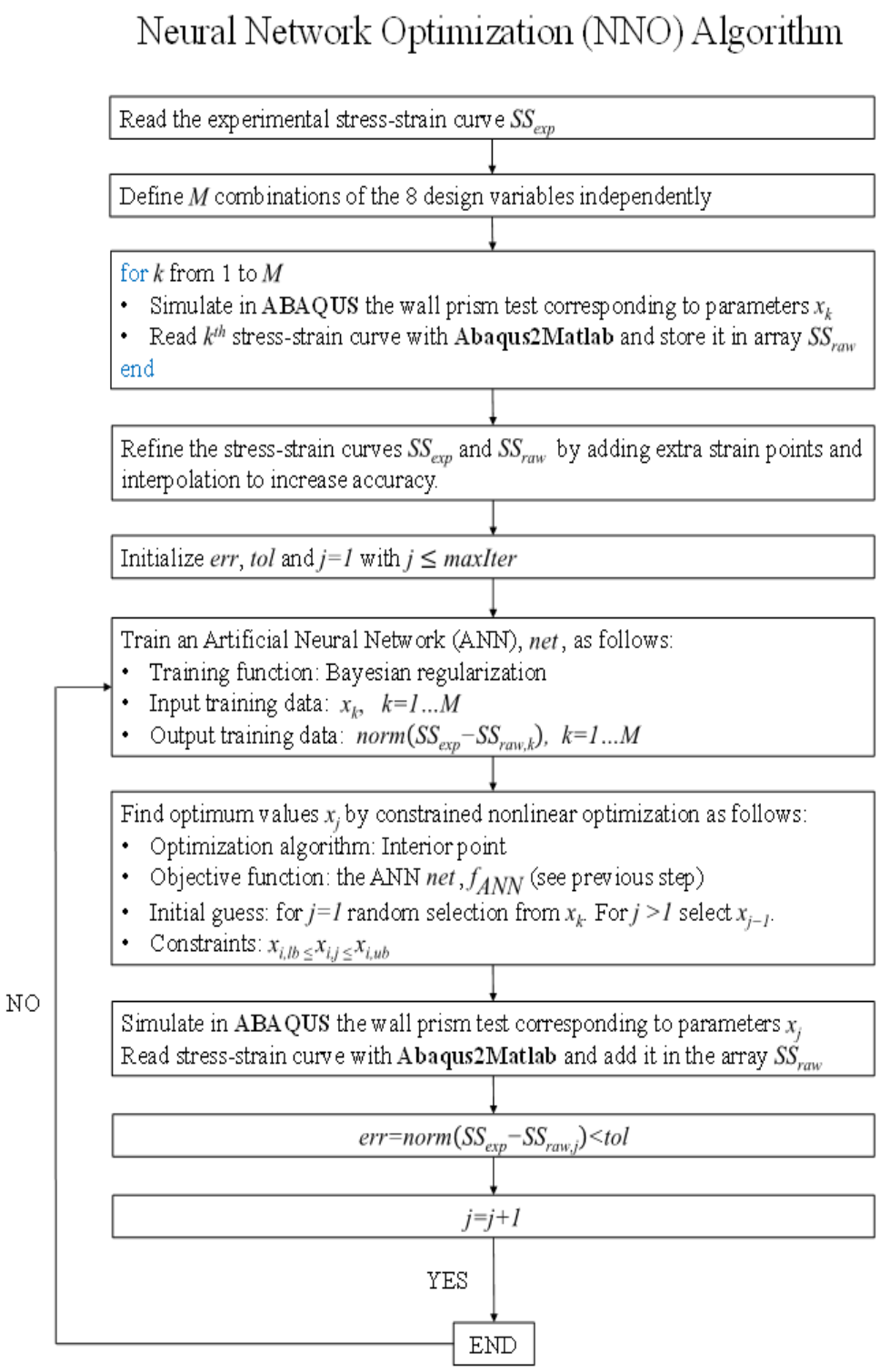

Figure 4.2 General flowchart of the neural network optimization algorithm used in this study.

4.3.3. Calculation of Initial Stress Strain Curves

The M ABAQUS models that correspond to the M design variable value combinations generated in the previous step are analyzed using the ABAQUS software, the stress – strain curve of the prism model is obtained using Abaqus2Matlab after the ABAQUS analysis terminates, and is stored in an array so that after the loop finishes, all stress-strain curves of the various cases are accessible. During this step, the ABAQUS capabilities are exploited, a practice which eliminates the difficulty of developing the FE simulation method of the model analyzed in MATLAB.

The stress strain curve is obtained in Abaqus2Matlab by reading the stresses at the upper surface of the prism and summing them appropriately to obtain the stress averaged over the loading area. The strain is obtained by reading the imposed displacement at the upper surface of the prism, and then dividing it by the prism length. Furthermore, the computations are efficiently carried out by using a for loop which scans all the M sets of the initial design variable values by taking advantage of Abaqus2Matlab capabilities to read and modify ABAQUS input files automatically.

4.3.4. Discretization of Stress-Strain Curves

The stress – strain curves that are extracted from the ABAQUS simulations are further discretized in a larger number of points via linear interpolation and extrapolation, in order to render the calculation of the error between the numerical and experimental curves more accurate. These data points are generated from the lower and upper bounds of the material parameters to simulate the stress-strain curves of the masonry prism. This operation, apart from making the estimation of the error more accurate, it can enable the application of weighting factors that depend on strain values that are specified a priori. For example, if for

some reason emphasis is placed on the error between the experimental and numerical stress strain curves in their elastic branch, then this part of the curve should be highly discretized and/or appropriately weighted.

4.3.5. Training of the ANN

The ANN is set up and trained with the initial data. The training function that is specified for the ANN is Bayesian Regularization ('trainbr'). This function uses the Levenberg-Marquardt optimization algorithm to update the weight and bias values of the ANN, and then determines a combination of squared errors and weights so as to produce a network that generalizes well. MATLAB's 'trainbr' function can train any network as long as its weight, net input, and transfer functions have derivative functions.

The procedure of neural network training can be viewed as a function optimization problem, where the weights and biases are considered as design variables and the network error is considered as the objective function to be minimized. The neural network can be considered as an arbitrary function of the input vector x and the weights of the network w as follows:

$$F(x,w)=y \tag{9}$$

where y is the corresponding output vector approximated or predicted by the network. The Levenberg-Marquardt algorithm approximates the function F by solving in each iteration the equation:

$$\left(J^T J+\lambda I\right)\delta = J^T E \tag{10}$$

where:

- J is the Jacobian n_t – by – n_w matrix, where n_t is the number of entries in the training set and n_w is the number of number of the design variables (weights and biases), containing all the first-order partial derivatives of F with respect to w ($J = \partial F / \partial w$).
- λ is the damping factor which is adjusted at each iteration according to the convergence rate of the optimization process. If the reduction in the error is rapid, then λ can be reduced, which gradually makes the algorithm behave in a way similar to that of Gauss-Newton algorithm. In the opposite case of insufficient reduction in the residual, then λ can be increased, which makes the algorithm resemble to the gradient descent algorithm.
- E is the error vector containing the residual for each input vector that is used for training the network.
- δ is the update of the weights.

Bayesian regularization minimizes a linear combination of squared errors and weights (cost function), mainly to overcome the problem in interpolating noisy data (Foresee & Hagan, 1997; MacKay, 1992). Two Bayesian hyperparameters α and β are used in the cost function, which determine the direction that the learning process must seek, in order not only to minimize the errors, but the weights as well. These parameters are updated after each training cycle. The cost function is given by the following equation:

$$C = \beta E_e + \alpha E_w \tag{11}$$

where E_e is the sum of squared errors and E_w is the sum of squared weights. The Bayesian parameters are updated using MacKay's formulae as follows:

$$\gamma = n_w - \left[\alpha \cdot tr\left(H^{-1}\right)\right] \tag{12}$$

$$\beta = \frac{n_t - \gamma}{2E_e} \tag{13}$$

$$\alpha = \frac{\gamma}{2E_w} \tag{14}$$

Typically, the flowchart of the Levenberg-Marquardt algorithm expanded with Bayesian regularization is similar to that shown in Figure 4.3.

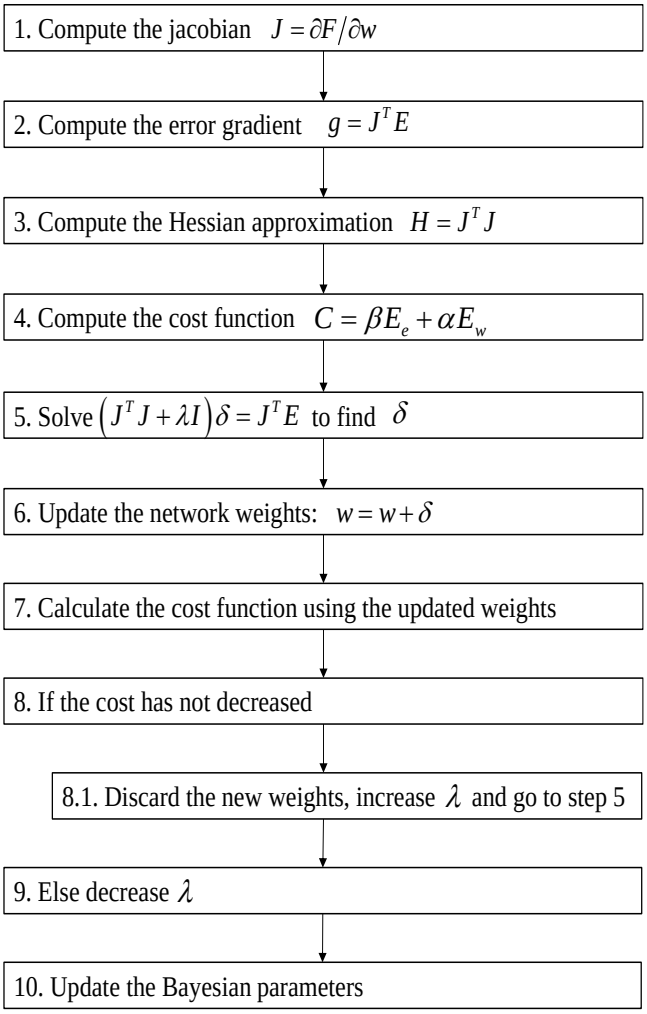

Figure 4.3 Flowchart of the Levenberg-Marquardt algorithm expanded with Bayesian regularization.

The ANN has three hidden layers, each of which has size 10. One of the objectives of the proposed NNO algorithm is that it should approach the optimum solution by using a minimum amount of training data, which saves ABAQUS simulation time. To achieve this goal, the target data are fully exploited to train the ANN and no target data are used for either its validation or testing. The maximum number of epochs of the ANN training process is specified equal to 50.

4.3.6. Optimization Procedure

An optimization procedure is carried out in order to minimize the error between the experimental and the numerical stress – strain curve, f_{ANN}, subject to the following constraints:

$$\begin{gathered} 800000 \le E_C \le 4000000 \\ 0.1 \le \psi_C \le 56 \\ 0.51 \le k_C \le 1 \\ 0.005 \le \mu_C \le 0.05 \\ 100000 \le E_M \le 900000 \\ 0.1 \le \psi_M \le 56 \\ 0.51 \le k_M \le 1 \\ 0.005 \le \mu_M \le 0.05 \end{gathered} \qquad (15)$$

The objective function f_{ANN} is a function that accepts any set of design variable values (input data of the ANN) and gives as output the error (output data of the ANN). It is important to note here that as the algorithm proceeds, the training data increases, the trained ANN becomes "better", and the objective function that is based on this ANN becomes better as well. This means that the objective function changes continuously as the algorithm proceeds. Consequently, the optimum values of the design variables and the objective value change as well (see Figure 4.4).

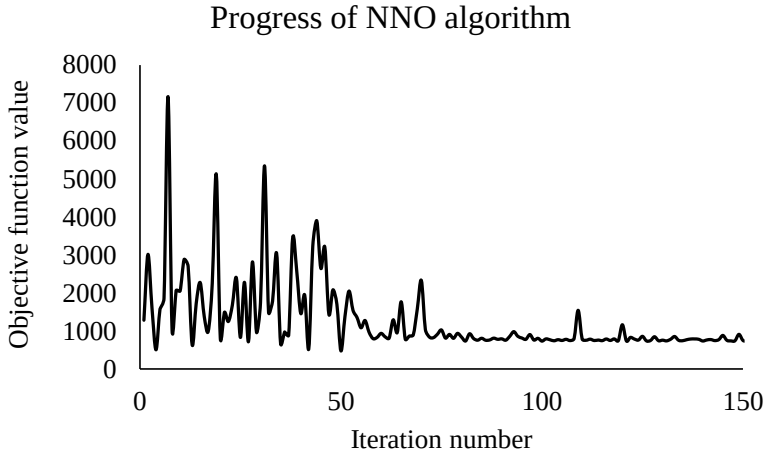

Figure 4.4 Evolution of the objective function during the NNO process.

The gradient-based interior point algorithm (IPA) approach is used for the solution of the optimization problem (Byrd, Gilbert, & Nocedal, 2000; Byrd, Hribar, & Nocedal, 1999; Waltz, Morales, Nocedal, & Orban, 2006). According to this algorithm, the original inequality-constrained minimization problem is stated as follows:

$$\min_{X}\left\{ f_{ANN}\left(X\right)\right\} \quad \text{Subject to} \quad g\left(X\right)=\begin{bmatrix} LB-X \\ X-UB \end{bmatrix} \leq \begin{bmatrix} 0 \\ 0 \end{bmatrix} \qquad (16)$$

where X is a vector containing the 8 design variables and LB, UB are also vectors containing the lower and upper bounds of the design variables respectively. Eq. (16) is solved as a sequence of the following approximate equality-constrained minimization problems for μ >0:

$$\min_{X,s}\left\{ f_{ANN}\left(X,s\right)\right\} = \min_{X,s}\left\{ f_{ANN}\left(X\right)\right\} - \mu\sum_{i}\ln\left(s_i\right) \quad \text{Subject to} \quad g\left(X\right)+s=0 \qquad (17)$$

There are two slack variables ($s_i \geq 0$) for each inequality and each design variable, namely the optimization problem at hand has 16 slack variables. For two stiffeners there will be a total of 4 slack variables. As μ decreases to zero, the minimum of [f_{ANN} , μ] and the minimum of f_{ANN} should coincide.

To solve the approximate problem, the algorithm uses one of the following two main types of steps at each iteration:

N Step. A direct (Newton) step in (X, s). This step attempts to solve the Karush-Kuhn-Tucker (KKT) equations (Karush, 1939; Kuhn & Tucker, 1951) for the approximate problem using a linearized Lagrangian as follows:

$$\begin{bmatrix} H & 0 & J_g^T \\ 0 & S\Lambda & -S \\ J_g & -S & I \end{bmatrix} \begin{bmatrix} \Delta X \\ \Delta s \\ -\Delta\lambda \end{bmatrix} = -\begin{bmatrix} -\nabla k_b - J_g^T \lambda \\ S\lambda - \mu e \\ g + s \end{bmatrix} \qquad (18)$$

where H is the Hessian of the Lagrangian of the approximate equality-constrained minimization problem, calculated according to the BFGS formula (Broyden, 1970; Fletcher, 1970; Goldfarb, 1970; Shanno, 1970), J_g is the Jacobian of the inequality-constraint function $g(X)$, S is a diagonal matrix with entries s_i , λ denotes the Lagrange multiplier vector associated with constraints $g(X)$, Λ is a diagonal matrix with entries λ_i , and e is a vector of ones the same size as $g(X)$. Eq. (10) defines the direct step $(\Delta X, \Delta s)$:

CG Step. A CG (Conjugate Gradient) step, using a trust region. The conjugate gradient approach to solve the approximate problem, Eq. (17) adjusts both X and S ,

keeping the slacks s positive. The algorithm obtains Lagrange multipliers by approximately solving the KKT equations:

$$\nabla_X L = -\nabla_X k_b + \sum_i \lambda_i \nabla g_i(X) = 0 \qquad (19)$$

subject to $\lambda > 0$. The following quadratic approximation to eq. (9) is minimized in a trust region of radius R:

$$\min_{\Delta X, \Delta s} \left\{ -\nabla k_b{}^T \Delta X + \frac{1}{2} \Delta X^T \nabla^2_{XX} L \Delta X + \mu e^T S^{-1} \Delta s + \frac{1}{2} \Delta s^T S^{-1} \Lambda \Delta s \right\} \qquad (20)$$

subject to the linearized constraints:

$$g(X) + J_g \Delta X + \Delta s = 0 \qquad (21)$$

From Eq. (24) the step $(\Delta X, \Delta s)$ is obtained.

By default, the algorithm first attempts to take a direct N step. If it cannot, it attempts a CG step. The algorithm takes a CG step either if the approximate problem is not locally convex near the current iterate, or if the Hessian is not positive definite at the current iteration.

For the first iteration, the initial guess that is supplied to the optimization function corresponds to the best case (i.e. that has the minimum error) among the initial design variable value combinations. For subsequent iterations the initial guess corresponds to the optimum values that have been obtained in the last iteration of the NNO algorithm.

4.3.7. Evaluation of Stress Strain Curves of the Optimal Points

An ABAQUS analysis is performed in which the material constitutive properties of the prism model are set equal to the optimum solution obtained in the optimization procedure that is described in section 4.2.3.5 From the ABAQUS analysis the stress – strain curve is

obtained in the same way as outlined in section4.2.3.2 At this step it is checked if any one of the termination conditions is satisfied. Two termination conditions have been included in the neural optimization algorithm:

$$j > \max Iter \quad (22)$$

$$err < tol \quad (23)$$

If any of these two conditions is satisfied, the algorithm terminates and returns as output the best design that is achieved so far (i.e. the design that corresponds to minimum error). If no one of the above conditions is satisfied, the last optimum solution is treated as an additional input – output training data and is added into the pool of the initial training data. The procedure continues to step 4.2.3.4 where the ANN is re-trained based on the enriched training data.

4.4. Calibration results

The stress strain curve is showing a good fitting with experimental observations (see Figure 4.5). The deterministic optimal parameters of the masonry prism implemented in the numerical simulations of walls are summarized in Table 4.2.

Table 4.2 Optimal Parameters for Prism.

Mortar Test	**E (psi)**	**ψ**	**κ**	**μ**
NNO algorithm	647361.223	27.1953	0.9894	0.010221
Brick Test	**E (psi)**	**ψ**	**κ**	**μ**
NNO algorithm	424382.869	35.3803	0.5025	0.099214

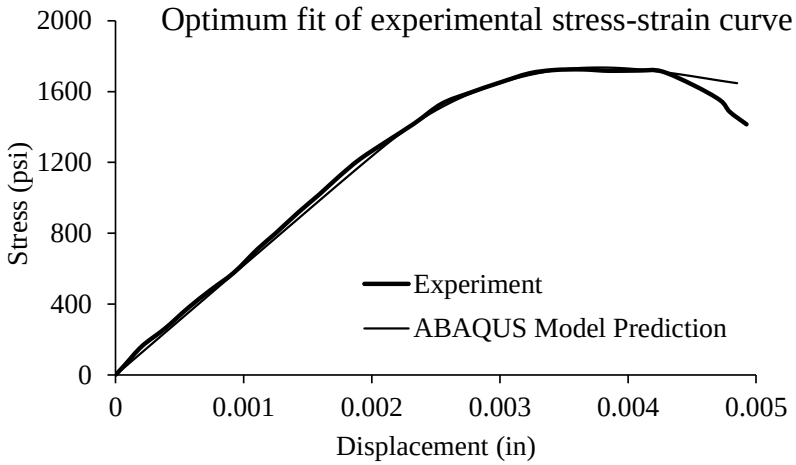

Figure 4.5 Stress-strain experimental Observation Vs FE model prediction(Epperson & Abrams, 1990).

4.5. Conclusion

A novel Neural Network Optimization (NNO) algorithm has been proposed for the calibration of the material properties of URM walls based on experimental stress – strain curves taken from compression tests of a wall prism. It is shown that the proposed NNO algorithm is sufficiently robust and accurate for calibration of constitutive material properties based on experimental data. In addition, an appealing characteristic of the NNO is its ability to fit numerical model with minimal computational effort. Consequently, the concrete damaged plasticity (CDP) showed high flexibility to fit the experimental observation as well as all parameters verified within a proper range.

4.6. References:

Abrams, D. P., & Shah, N. (1992). Cyclic load testing of unreinforced masonry walls. Retrieved from

Carmeliet, J. (1999). Optimal estimation of gradient damage parameters from localization phenomena in quasi-brittle materials. Mechanics of Cohesive-frictional Materials: An International Journal on Experiments, Modelling and Computation of Materials and Structures, 4(1), 1-16.

Chisari, C. (2015). Inverse techniques for model identification of masonry structures.

Chisari, C. (2019). Tolerance-based Pareto optimality for structural identification accounting for uncertainty. Engineering with Computers, 35(2), 381-395.

Chisari, C., Macorini, L., Amadio, C., & Izzuddin, B. (2015). An inverse analysis procedure for material parameter identification of mortar joints in unreinforced masonry. Computers & Structures, 155, 97-105.

Chisari, C., Macorini, L., Amadio, C., & Izzuddin, B. A. (2018). Identification of mesoscale model parameters for brick-masonry. International journal of solids and structures, 146, 224-240.

Epperson, G. S., & Abrams, D. P. (1990). Nondestructive evaluation of masonry buildings (Vol. 89): University of Illinois at Urbana-Champaign.

Fadale, T. D., Nenarokomov, A. V., & Emery, A. F. (1995). Uncertainties in parameter estimation: the inverse problem. International Journal of Heat and Mass Transfer, 38(3), 511-518.

Gambarotta, L., & Lagomarsino, S. (1997). Damage models for the seismic response of brick masonry shear walls. Part I: the mortar joint model and its applications. Earthquake engineering & structural dynamics, 26(4), 423-439.

Grassl, P., & Jirásek, M. (2006). Damage-plastic model for concrete failure. International journal of solids and structures, 43(22-23), 7166-7196.

Jankowiak, T., & Lodygowski, T. (2005). Identification of parameters of concrete damage plasticity constitutive model. Foundations of civil and environmental engineering, 6(1), 53-69.

Kmiecik, P., & Kamiński, M. (2011). Modelling of reinforced concrete structures and composite structures with concrete strength degradation taken into consideration. Archives of civil and mechanical engineering, 11(3), 623-636.

Lee, J., & Fenves, G. L. (1998). Plastic-damage model for cyclic loading of concrete structures. Journal of Engineering Mechanics, 124(8), 892-900.

Levenberg, K. (1944). A method for the solution of certain non-linear problems in least squares. Quarterly of applied mathematics, 2(2), 164-168.

Lotfi, H., & Shing, P. (1991). An appraisal of smeared crack models for masonry shear wall analysis. Computers & Structures, 41(3), 413-425.

Lubliner, J. (1991). A simple model of generalized plasticity. International journal of solids and structures, 28(6), 769-778.

Lubliner, J., Oliver, J., Oller, S., & Oñate, E. (1989). A plastic-damage model for concrete. International journal of solids and structures, 25(3), 299-326.

Marquardt, D. W. (1963). An algorithm for least-squares estimation of nonlinear parameters. Journal of the society for Industrial and Applied Mathematics, 11(2), 431-441.

Muñoz-Rojas, P., Cardoso, E., & Vaz, M. (2010). Parameter identification of damage models using genetic algorithms. Experimental Mechanics, 50(5), 627-634.

Nazari, A., & Sanjayan, J. G. (2015). Modelling of compressive strength of geopolymer paste, mortar and concrete by optimized support vector machine. Ceramics International, 41(9), 12164-12177.

Papazafeiropoulos, G., Muñiz-Calvente, M., & Martínez-Pañeda, E. (2017). Abaqus2Matlab: a suitable tool for finite element post-processing. Advances in Engineering Software, 105, 9-16.

Rechea, C., Levasseur, S., & Finno, R. (2008). Inverse analysis techniques for parameter identification in simulation of excavation support systems. Computers and Geotechnics, 35(3), 331-345.

Sarhosis, V., & Sheng, Y. (2014). Identification of material parameters for low bond strength masonry. Engineering Structures, 60, 100-110.

Toropov, V., & Garrity, S. (1998). Material parameter identification for masonry constitutive models. Paper presented at the Proceedings of the Eighth Canadian Masonry Symposium.

Toropov, V. V., & van der Giessen, E. (1993). Parameter identification for nonlinear constitutive models: Finite Element simulation—Optimization—Nontrivial experiments. In Optimal design with advanced materials (pp. 113-130): Elsevier.

Xu, W., & Abrams, D. P. (1992). Evaluation of Lateral Strength and Deflection for Cracked Unreinforced Masonry Walls. Illinois University at Urbana Advanced Construction Technology Center.

5. EVALUATION OF THE EFFECT OF THE HETEROGENEITY OF THE PRISM ON ITS STRESS STRAIN RESPONSE USING THE NEURAL NETWORK OPTIMIZATION ALGORITHM.

5.1. Introduction

This study examines the influence of a constitutive model and its parameters on the predictions of the stress-strain relationship with the correlated random variable field. The prism model simulation in ABAQUS involves constitutive model parameters that are optimized to validate ABAQUS URM models against laboratory experiments. The validated model was used as a baseline to generate four individual simulations, where each simulation examined the heterogeneity of different material parameter combinations. The concrete damage plasticity (CDP) constitutive model consisting of plasticity modes and damage indices was used to analyze the mechanical response of masonry prism (J Lubliner et al., 1989). Abaqus2Matlab was used as an interface platform for linking ABAQUS and MATLAB, which was used for deterministic calculation of material parameters by using random variables (Papazafeiropoulos et al., 2017). It is well known that the response of masonry walls (and consequently of the prism) is highly nonlinear, which is attributed to the material nonlinearities inherent to the bricks and the mortar, microstructural topology, and interfacial responses between the various structural components of the masonry wall (bricks, mortar, etc.). Therefore, it is expected that the FEA of masonry walls is generally computationally demanding. Given this fact, and also taking into account the relatively large number of simulations that are required for performing an optimization procedure, it is generally attempted to minimize the required number of simulations for reaching the

optimum fit between model and experiment, so that the computational effort and running time are minimized. The suitability of an optimization algorithm for addressing the aforementioned issues usually depends on the model that is analyzed. In the case of the URM walls considered in this thesis, a novel Neural Network Optimization (NNO) algorithm is being presented to calibrate the material parameters of a masonry prism. The Neural Network that is incorporated in this algorithm is expected to accelerate the optimization procedure through the more effective use of the optimization history (i.e. the history of the unsuccessful points from which the algorithm has passed so far), which is used for training an Artificial Neural Network (ANN). This in turn gives better directions for the algorithm to proceed, compared to the gradient information alone. The masonry prism that is considered for calibration has been tested by Blackard et al. (2007). Esmailzadeh, Medina-Cetina, Kang, and Kallivokas (2015) introduce a methodology to infer the spatial variation of model parameters and their corresponding mechanical characteristics by using random variables. Another study introduces by Medina-Cetina, Kang, Esmailzadeh, and Kallivokas (2013) to investigate the spatial correlation across the parameters using Bayesian inversion of 1D heterogeneity media. In this study, correlation between four parameters of CDP model $(i.e., E, \psi, \kappa, \mu)$ are being investigated using as random variable throughout a masonry prism in which consist of five brick units and four mortar layers.

5.2. Calibration of Masonry Prism

5.2.1. Model Description

The model consists of 5 bricks and 4 layers of mortar between the brick units. The cross-section dimensions of the prism are 3.75” x 4.5” x 12.75” and the mortar thickness between the bricks is 0.375” (Blackard et al., 2007). The prism is fixed on its bottom and on

the top surface a uniform displacement is imposed. The ABAQUS model of the prism is discretized in 5120 3D solid elements (C3D8R), defined by 7337 nodes (see Figure 5.1). The model parameters of each brick unit and mortar layers have been defined using the CDP model. The optimal parameters of individual components (brick and mortar) obtained in Table 2.2 of Chapter II are used as initial guess to validate the stress-strain relationship against the experiment tests. According to the parametric sensitivity analysis that was conducted in chapter 2, the parameters $(i.e., E, \psi, \kappa, \mu)$ seem to be more sensitive compared to other parameters $(i.e., \nu,\ f_b / f_c, \delta)$. Therefore, the Poisson ratio of the brick is taken as 0.1 whereas the Poisson ratio of the mortar is 0.2 which remain constant during the simulation as well as the flow potential eccentricity (δ) and the ratio of initial equibiaxial compressive yield stress to initial uniaxial compressive yield stress (f_b / f_c) are equal to 0.1 and 1.16 for both the bricks and the mortar layers, respectively. The interface elements between the bricks and the mortar layers are considered to be tied across the intact area. A static analysis has been performed to obtain the response of the prism under vertical imposed load-displacement. An appropriate mesh sensitivity analysis has been performed in order to ensure that the mesh refinement provides sufficiently accurate results.

5.2.2. Material Parameters Identification

The constitutive parameters that were considered in this study for the brick and the mortar materials have been designated as the parameters with the highest influence on the stress –strain response according to the sensitivity study that has been carried out in Chapter 2.

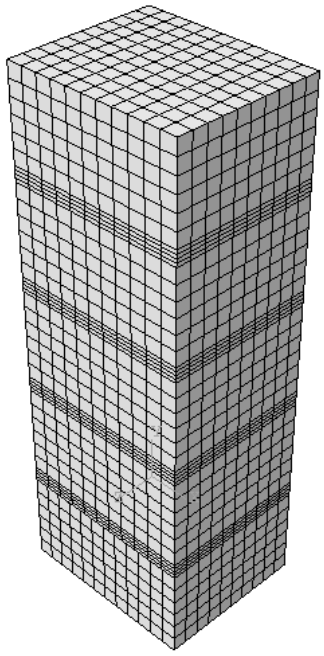

Figure 5.1. 3D Model Prism (Blackard et al., 2007)

Therefore, there are four material parameters for each brick layer and mortar layer that will be investigated using random variables in which the dilation angle has been found sensitive when two parameters are varying randomly. The purpose of this study is to examine the influence of material heterogeneity on these eight parameters that can be randomly varying in a masonry prism. More specifically, there are 8 design variables in this optimization in CDP model namely the moduli of elasticity $(\mathrm{E}_C, \mathrm{E}_M)$ of the brick and the mortar respectively, the dilation angles in the p–q plane of the brick and the mortar (ψ_C, ψ_M), the ratios of the second stress invariant on the tensile meridian to that on the compressive meridian of the brick and the mortar (κ_C, κ_M), and the viscosity parameters μ of the brick

Table 5.1 Description and Bounds of the Design Variables of the Prism

Design variable	Description	Lower bound	Upper bound
E_C	Modulus of elasticity of the brick material	100000	5000000
ψ_C	Dilation angle in the p–q plane of the brick material	0.1	36
κ_C	Ratio of the second stress invariant on the tensile meridian to that on the compressive meridian for the brick material	0.51	1
μ_C	Viscosity parameter of the brick material	0.0001	0.1
E_M	Modulus of elasticity of the mortar	100000	900000
ψ_M	Dilation angle in the p–q plane of the mortar	0.1	36
κ_M	Ratio of the second stress invariant on the tensile meridian to that on the compressive meridian for the mortar	0.51	1
μ_M	Viscosity parameter of the mortar	0.0001	0.1

and the mortar (μ_C, μ_M). The upper and lower limits are set for the design variables based on the available experimental results in literature and are shown in Table 5.1.

More specifically, there are 4 cases of the prism model which will be assigned a combination of material parameters as random variables in order to investigate the effect of material heterogeneity in five brick units and four mortar layers:

- 8 random variables (8RV): Four parameters assigned as dependent random variables for five brick units as well as for four mortar layers in which the prism will consist of eight design variables for all bricks and mortar layers $(e.g., E_{C1}, \psi_{C1}, \kappa_{C1}, \mu_{C,1} E_{M1}, \psi_{M1}, \kappa_{M1}, \mu_{M1})$.

- 16 random variables (16RV): sixteen parameters assigned as independent random variables for four mortar layers only in which the prism consists of sixteen design variables varying independently for only mortar layers (e.g., $(e.g., \mathrm{E}_{Mq}, \psi_{Mq}, \kappa_{Mq}, \mu_{Mq})$, where q starts from 1 to 4. The parameters in the brick units are fixed (see Table 4.2).

- 20 random variables (20RV): twenty parameters assigned as independent random variables for five brick units only in which the prism consists of twenty design variables varying independently for only brick units $(e.g., \mathrm{E}_{Cn}, \psi_{Cn}, \kappa_{Cn}, \mu_{Cn})$ where n starts from 1 to 4. The parameters in the mortal layers are fixed (see Table 4.2).

- 36 random variables (36RV): thirty six parameters assigned as independent random variables for five brick units and four mortar layers in which the prism consists of thirty six design variables varying independently for both brick units and mortar layers (e.g., $\mathrm{E}_{C1}, \psi_{C1}, \kappa_{C1}, \mu_{C1}.....\mathrm{E}_{Cn}, \psi_{Cn}, \kappa_{Cn}, \mu_{Cn}$) and (e.g., $\mathrm{E}_{M1}, \psi_{M1}, \kappa_{M1}, \mu_{M1}.....\mathrm{E}_{Mq}, \psi_{Mq}, \kappa_{Mq}, \mu_{Mq}$) where n starts from 1 to 4 and q is from 1 to 4, respectively (see Table 5.3).

5.2.3. Neural Optimization Algorithm

In this thesis a new algorithm has been used for the calibration of the material properties, which combines neural network and optimization techniques. More specifically, it involves a Neural Network and an interior point optimization algorithm, both of them implemented in MATLAB programming language. In Figure 5.2 the flowchart of the calculation procedure is shown. The main steps of the algorithm are described below:

Table 5.2 Fixed Material Parameters for the Prism

Fixed All Brick Parameters & All Mortar Parameters									
	Brick1	**Mortar1**	**Brick2**	**Mortar2**	**Brick3**	**Mortar3**	**Brick4**	**Mortar4**	**Brick5**
E	2.89E+06	7.36E+05	2.89E+06	7.36E+05	2.89E+06	7.36E+05	2.89E+06	7.36E+05	2.89E+06
Ψ	19.69E+00	18.81E+00	19.69E+00	18.81E+00	19.69E+00	18.81E+00	19.69E+00	18.81E+00	19.69E+00
K	0.662	0.536	0.662	0.536	0.662	0.536	0.662	0.536	0.662
μ	0.01029	0.0041	0.01029	0.0041	0.01029	0.0041	0.01029	0.0041	0.01029

- Step 1: Initial sets of values assigned to the constitutive parameters

An initial set of values (initial points) are generated for the unknown constitutive parameters of the material in question. The initial points can be specified at random or according to a specified distribution. Each combination of these values of the constitutive properties corresponds to an ABAQUS simulation. It has to be noted that the selection of the initial points must span an adequately large interval, ensuring that the optimum values of the constitutive properties lie within this interval. The number of the initial points must lie within acceptable limits, namely it must not be too low or too high with respect to the capacity of the neural network. Generally, as this number increases, the performance of the ANN increases as well. However, large size of training data can lead to overfitting in premature stages of the optimization process which prevents the ANN from performing well on new training data that are generated as the neural optimization algorithm proceeds.

Table 5.3 Illustrate the Material Parameters Distribution of Random Variables for the Prism

Prism	Brick & Mortar	Mortar Layers	Brick Units	All Parameters
Brick1	E1	2.89E+06	E1	E1
	Ψ1	19.69E+00	Ψ1	Ψ1
	K1	0.662	K1	K1
	μ1	0.01029	μ1	μ1
Mortar1	E2	E1	7.36E+05	E2
	Ψ2	Ψ1	18.81E+00	Ψ2
	K2	K1	0.536	K2
	μ2	μ1	0.0041	μ2
Brick2	E1	2.89E+06	E2	E3
	Ψ1	19.69E+00	Ψ2	Ψ3
	K1	0.662	K2	K3
	μ1	0.01029	μ2	μ3
Mortar2	E2	E2	7.36E+05	E4
	Ψ2	Ψ2	18.81E+00	Ψ4
	K2	K2	0.536	K4
	μ2	μ2	0.0041	μ4
Brick3	E1	2.89E+06	E3	E5
	Ψ1	19.69E+00	Ψ3	Ψ5
	K1	0.662	K3	K5
	μ1	0.01029	μ3	μ5
Mortar3	E2	E3	7.36E+05	E6
	Ψ2	Ψ3	18.81E+00	Ψ6
	K2	K3	0.536	K6
	μ2	μ3	0.0041	μ6
Brick4	E1	2.89E+06	E4	E7
	Ψ1	19.69E+00	Ψ4	Ψ7
	K1	0.662	K4	K7
	μ1	0.01029	μ4	μ7
Mortar4	E2	E4	7.36E+05	E8
	Ψ2	Ψ4	18.81E+00	Ψ8
	K2	K4	0.536	K8
	μ2	μ4	0.0041	μ8
Brick5	E1	2.89E+06	E5	E9
	Ψ1	19.69E+00	Ψ5	Ψ9
	K1	0.662	K5	K9
	μ1	0.01029	μ5	μ9
R.V	**8**	**16**	**20**	**36**

In addition, when the training data is too low with respect to the ANN's capacity, the performance of the latter deteriorates, losing its ability to evaluate the objective value correctly. The selection of the size of the initial data depends on the nature of the algorithm, the ABAQUS model(s) involved and also the hyperparameters of the ANN and the optimizer function.

- Step 2: Calculation of initial stress strain curves

The ABAQUS simulation cases that correspond to the initial training data are executed and then post-processed by Abaqus2Matlab (Papazafeiropoulos et al., 2017)in order to calculate the corresponding stress – strain curves for the various values of the constitutive parameters. Hence, the ABAQUS capabilities are exploited, eliminating the need for MATLAB code development in order to carry out the FE analysis.

- Step 3: Discretization of stress strain curves

The stress – strain curves that are calculated in the previous step are discretized in an increased number of strain values, in order to calculate the error between the numerical and experimental curves more accurately. This discretization is made through linear interpolation and extrapolation. Another advantage of this operation is that weighting factors can be imposed in selected values of strains. For example, if for some reason emphasis is placed on the error between the experimental and numerical stress strain curves in their elastic branch, then this part of the curve should be highly discretized and scaled with increased weighting factors.

- Step 4: Training of the ANN

The ANN is set up and trained with the initial data. The training function that is specified for the ANN is Bayesian Regularization ('trainbr'). In this function the Levenberg-

Marquardt optimization algorithm is used to update the weight and bias values of the ANN, minimizing a linear combination of squared errors and weights so as to overcome the problem in interpolating noisy data(Foresee & Hagan, 1997; MacKay, 1992) and thus allow for proper generalization of the ANN. MATLAB's 'trainbr' function can train any network as long as its weight, net input, and transfer functions are differentiable. The ANN has three hidden layers, each of which has size 10. The maximum number of epochs of the ANN training process is specified equal to 50.

- Step 5: Optimization procedure

In each repetition of the main loop of the NNO algorithm an optimization procedure is carried out in order to minimize the error between the experimental and the numerical stress – strain curves, f_{ANN}, subject to the constraints shown in eq. (24) below. It is noted that the values of the lower and upper limits of these constraints are specified so that a realistic formulation of the involved constitutive models is ensured. For the selection of these values the data collection that is presented in Chapter 2 was used.

$$\begin{gathered} 800000 \le E_C \le 4000000 \\ 0.1 \le \psi_C \le 56 \\ 0.51 \le k_C \le 1 \\ 0.005 \le \mu_C \le 0.05 \\ 100000 \le E_M \le 900000 \\ 0.1 \le \psi_M \le 56 \\ 0.51 \le k_M \le 1 \\ 0.005 \le \mu_M \le 0.05 \end{gathered} \qquad (24)$$

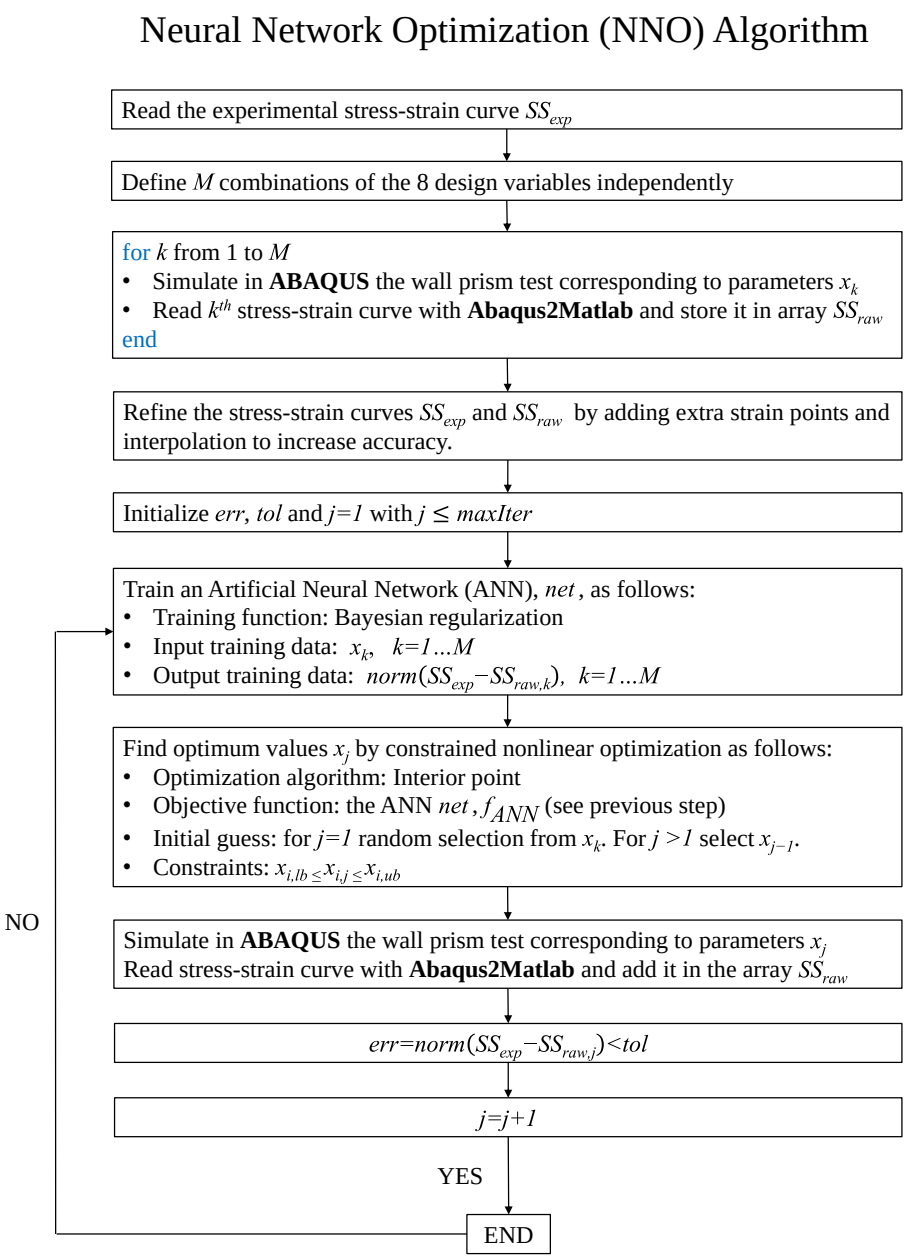

Figure 5.2. General flowchart of the neural network optimization algorithm used in this study.

The objective function f_{ANN} is a function that accepts any set of constitutive material parameter values (input data of the ANN) and gives the error between simulation and

experiment as output (output data of the ANN). The same job is done from the ANN which is continuously trained as the number of the available ABAQUS simulation data increases. Therefore, the main idea here is to use the ANN as the objective function of the optimization process. As the algorithm proceeds, the size of the training data increases and consequently the ANN becomes "better". This means that as the NNO algorithm proceeds, the quality of the objective function increases as well. Thus, the optimum values of the constitutive parameters and the objective value change as well (see Figure 5.3).

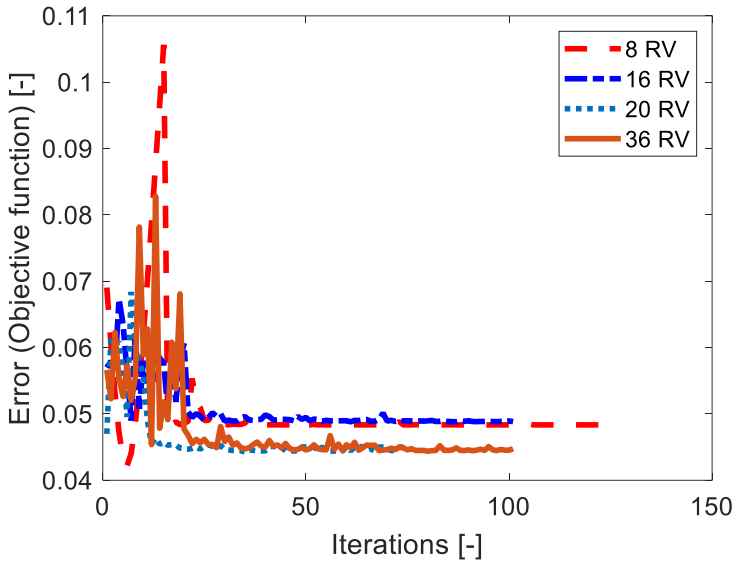

Figure 5.3. Evolution of the objective function during the NNO process

The gradient-based interior point algorithm (IPA) approach is used for the solution of the optimization problem ((Byrd et al., 2000; Byrd et al., 1999; Waltz et al., 2006).

According to this algorithm, the original inequality-constrained minimization problem is stated as follows:

$$\min_{X}\left\{ f_{ANN}\left(X\right)\right\} \text{ Subject to } g\left(X\right)=\begin{bmatrix} LB-X \\ X-UB \end{bmatrix}\leq\begin{bmatrix} 0 \\ 0 \end{bmatrix} \qquad (25)$$

where X is a vector containing the 8 constitutive parameters and LB, UB are also vectors containing the lower and upper bounds of the constitutive parameters respectively. The algorithm attempts to take a direct Newton step in each iteration, or, if this is impossible, it attempts a CG step. For the first iteration, the initial guess that is supplied to the optimization function corresponds to the best case (i.e. that has the minimum error) among the initial constitutive parameter value combinations. For subsequent iterations the initial guess corresponds to the optimum values that have been obtained in the last iteration of the NNO algorithm.

- Step 6: Evaluation of the stress strain curve of the optimal point

After the optimization algorithm of each repetition of the main loop completes, an ABAQUS analysis that corresponds to the optimum values is performed and the stress – strain curve is obtained, in a way similar to that described in steps 2 & 3 above. After this, it is checked if any one of the termination conditions is satisfied. Two termination conditions have been included in the neural optimization algorithm:

$$j > \max Iter \qquad (26)$$

$$err < tol \qquad (27)$$

If any of these two conditions is satisfied, the algorithm terminates and returns as output the best design that is achieved so far (i.e. the design that corresponds to minimum error). If no one of the above conditions is satisfied, the last optimum solution is treated as

an additional input – output training data and is added into the pool of the initial training data. The procedure continues to step 4 above where the ANN is re-trained based on the enriched training data.

5.2.3.1. 8 Parameters Optimization

In order to investigate the material properties of masonry prisms, a relationship between the 8 material parameters, $(e.g., \mathrm{E}_{C1}, \psi_{C1}, \kappa_{C1}, \mu_{C,1} \mathrm{E}_{M1}, \psi_{M1}, \kappa_{M1}, \mu_{M1})$ and experimental observation is investigated. These parameters are varying dependently as random variables for instance, E_{C1} is varying with same value in five brick units each iteration as well as for the other seven parameters. The objective function for the 8RV case converges faster compared to other cases. However, the 8RV started with highest errors 0.105 and end with 0.05. Figure 5.4 show a good agreement between the experimental observation and FE model prediction. Table 5.4 lists the 8 parameters that are converging with same values for example E_{C1} in brick1 is equal to E_{C1} for brick 2.

Table 5.4 Material Parameters Distribution of 8 Random Variables for the Prism

8 Random Variable All Brick Parameters & All Mortar Parameters									
	Brick1	**Mortar1**	**Brick2**	**Mortar2**	**Brick3**	**Mortar3**	**Brick4**	**Mortar4**	**Brick5**
E	2.29E+06	2.80E+05	2.29E+06	2.80E+05	2.29E+06	2.80E+05	2.29E+06	2.80E+05	2.29E+06
Ψ	9.84E+00	3.59E+01	9.84E+00	3.59E+01	9.84E+00	3.59E+01	9.84E+00	3.59E+01	9.84E+00
K	1.02E+00	6.12E-01	1.02E+00	6.12E-01	1.02E+00	6.12E-01	1.02E+00	6.12E-01	1.02E+00
μ	1.37E-02	1.00E-02	1.37E-02	1.00E-02	1.37E-02	1.00E-02	1.37E-02	1.00E-02	1.37E-02

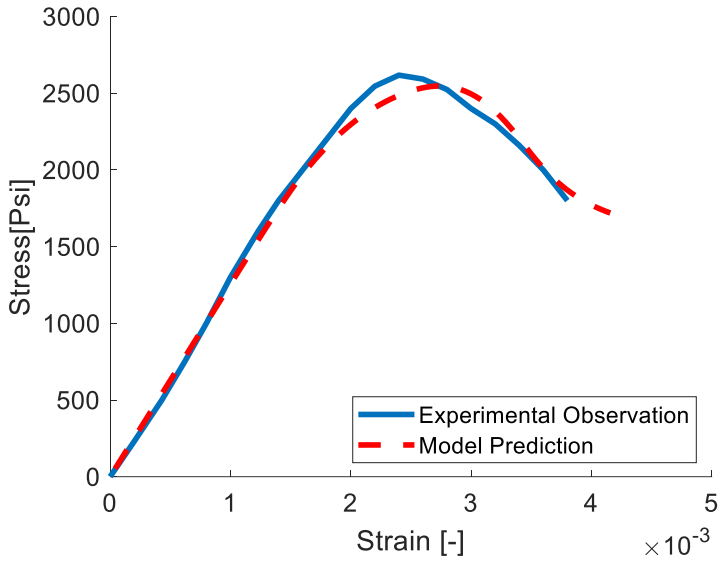

Figure 5.4. Stress-strain experimental observation vs model prediction for Case 8RV (Blackard et al., 2007).

5.2.3.2. 16 Parameters Optimization

The sixteen parameters are designated only for mortar layers in which each layer assigned of the four parameters $(e.g., \mathrm{E}_{Mq}, \psi_{Mq}, \kappa_{Mq}, \mu_{Mq})$, where q ranges from 1 to 4, varying independently. For example, young's modulus E_{M1} for mortar layers 1 is assigned a different value in mortar layer 2, layers 3 and layer 4, and the same applies for the other parameters. Figure 5.3 shows the objective function for the 16RV convergence which may take longer to reach a smooth convergence than for the 8RV. However, the final error appears to be slightly less than the case of 8RV. Figure 5.5 illustrates the stress strain curves from the analysis and experimental observation, which show a good agreement. Table 5.5 presents 16 parameters that have converged with same range of variation with respect to that presumed in the literature.

Table 5.5 Material parameters distribution of 16 random variables for the prism

16 Random Variable Mortar Parameters									
	Brick1	**Mortar1**	**Brick2**	**Mortar2**	**Brick3**	**Mortar3**	**Brick4**	**Mortar4**	**Brick5**
E	**2.89E+06**	2.67E+05	**2.89E+06**	2.71E+05	**2.89E+06**	2.63E+05	**2.89E+06**	2.89E+05	**2.89E+06**
Ψ	**19.69E+00**	5.27E+01	**19.69E+00**	5.56E+01	**19.69E+00**	5.55E+01	**19.69E+00**	5.04E+01	**19.69E+00**
K	**0.662**	0.59992	**0.662**	0.66160	**0.662**	0.66236	**0.662**	0.59676	**0.662**
μ	**0.01029**	0.01063	**0.01029**	0.01101	**0.01029**	0.01050	**0.01029**	0.01079	**0.01029**

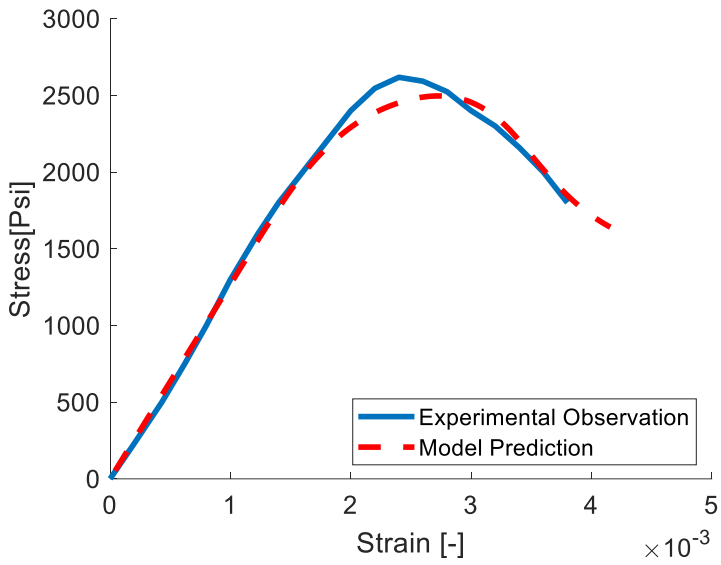

Figure 5.5. Stress-strain experimental observation vs model prediction for Case 16RV (Blackard et al., 2007).

5.2.3.3. 20 Parameters Optimization

This section presents the parameter optimization for the five brick units in the prism. The values of the four parameters $(e.g., \mathrm{E}_{Cn}, \psi_{Cn}, \kappa_{Cn}, \mu_{Cn})$, where n ranges from 1 to 4, are

varying independently. Similarly, in case 16RV the brick parameters' values are different for each brick unit in the prism. The objective function is obviously dropping in terms of the error compared to the 8RV and 16RV cases (see Figure 5.3). Although the analysis may take longer to converge the procedure yields better results compared to 8RV and 16RV cases (see Figure 5.6). Table 5.6 presents the values of parameters that have converged in the final iterations in which lie on the same range of the material parameters from the literature.

Table 5.6 Material parameters distribution of 20 random variables for the prism

20 Random Variable Brick Parameters									
	Brick1	**Mortar1**	**Brick2**	**Mortar2**	**Brick3**	**Mortar3**	**Brick4**	**Mortar4**	**Brick5**
E	2.34E+06	**7.36E+05**	2.15E+06	**7.36E+05**	2.07E+06	**7.36E+05**	2.18E+06	**7.36E+05**	2.15E+06
Ψ	9.36E+00	**18.81E+00**	9.29E+00	**18.81E+00**	9.18E+00	**18.81E+00**	9.23E+00	**18.81E+00**	9.36E+00
K	0.9500	**0.536**	0.9597	**0.536**	0.9745	**0.536**	0.9602	**0.536**	0.9494
μ	0.0146	**0.0041**	0.0139	**0.0041**	0.0130	**0.0041**	0.0140	**0.0041**	0.0146

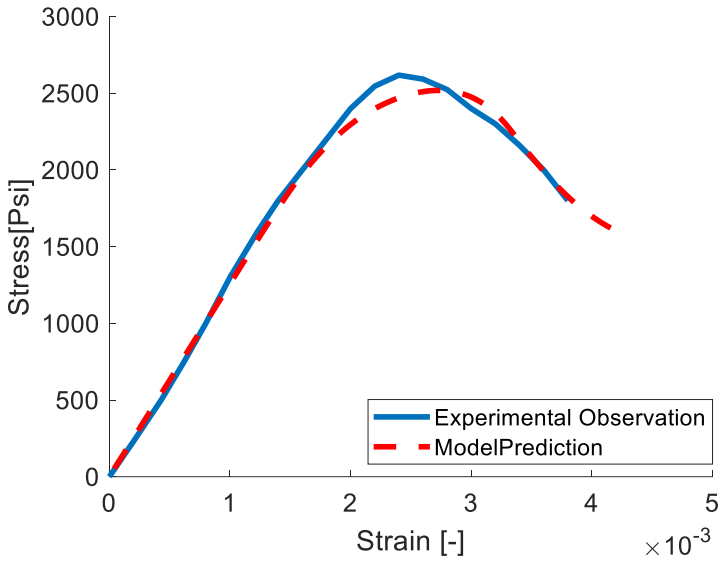

Figure 5.6. Stress-strain experimental observation vs model prediction for case 20RV (Blackard et al., 2007).

5.2.3.4. 36 Parameters Optimization

This is the most extreme case in which thirty-six parameters are varying independently. In other words, the prism consists of five brick units and four mortar layers are randomly assigned to the prism model. Figure 5.3 shows that the objective function of 36RV has the least error compared to other cases while the convergence took the longest running time to reach a steady state condition. The relationship between the experimental observation and the prediction model shows better fitting compared to other cases (see Figures 5.7). Table 5.7 presents the 36 parameters that are varying in independent intervals, and all parameters are converged within the same range.

Table 5.7 Material parameters distribution of 36 random variables for the prism

36 Random Variable All Brick Parameters & All Mortar Parameters									
	Brick1	**Mortar1**	**Brick2**	**Mortar2**	**Brick3**	**Mortar3**	**Brick4**	**Mortar4**	**Brick5**
E	2.38E+06	2.56E+05	2.08E+06	2.55E+05	2.08E+06	2.90E+05	2.44E+06	3.03E+05	2.13E+06
Ψ	9.08E+00	5.30E+01	9.12E+00	5.29E+01	9.14E+00	5.29E+01	9.38E+00	5.29E+01	9.35E+00
K	0.95054	0.611673	0.954089	0.621056	0.957345	0.643381	0.942894	0.606075	0.948019
μ	0.014686	0.010874	0.013289	0.010673	0.013259	0.011214	0.01496	0.010649	0.014404

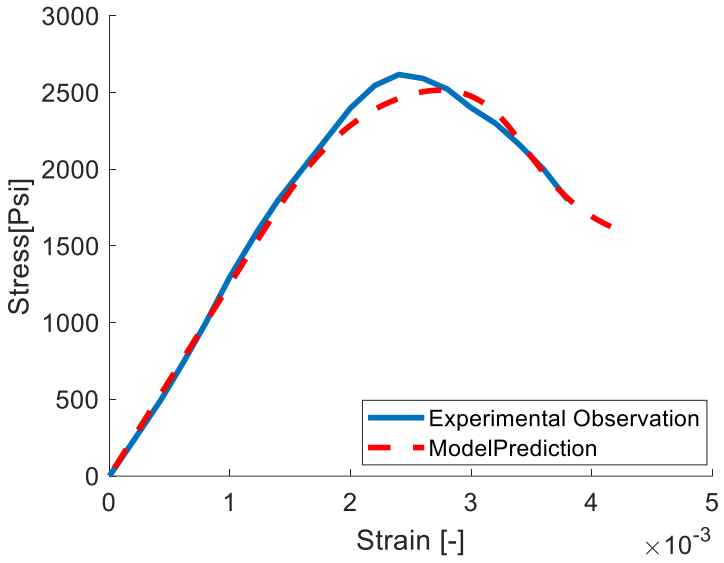

Figure 5.7. Stress-strain experimental observation vs model prediction for case 36RV (Blackard et al., 2007).

Table 5.8 presents the statistical results of the mean and standard deviation for the individual constitutive CDP parameters of the brick and the mortar of a masonry prism

obtained from NNO algorithm. Apart from the mean and standard deviation, the coefficient of variation is calculated. It is obvious that the CoV is sufficiently small, which verifies the convergence of the optimization algorithm. Besides this, the low value of CoV proves the existence of a unique combination of optimum CDP models for brick and mortar, regardless of the number of random design variables considered for fitting the numerical and the experimental curves.

Table 5.8 Statistical parameters *E*, κ, ψ and μ for the prism.

Mortar	$E(psi)$	ψ	κ	μ
Mean	2.74E+05	5.32E+01	0.62535	0.01079
Std	17669.5865	1.6664226	0.02686	0.00023
CoV	0.0645	0.0313	0.0430	0.0213
Brick	$E(psi)$	ψ	κ	μ
Mean	2.20E+06	9.25E+00	0.95467	0.01407
Std	135646.6	0.1134754	0.00886	0.00069
CoV	0.0617	0.0123	0.0093	0.0490

5.3. Conclusion

The results obtained from the NNO algorithm that is formulated in this study show very good agreement with the corresponding experimental observations. The concrete damage plasticity model has the capability to predict of the stress-strain relationship with the correlated random variable field. The converged values of the design variables (constitutive properties) show consistence for all cases and lie within the range of the lower and upper bounds. The Concrete Damaged Plasticity (CDP) showed high flexibility to fit the experimental observation as well as all parameters verified within a proper range. The prism

with thirty-six random variables shows the least error compared to the other cases while the convergence took longer to obtain steady state. Brick units have more influence on the mechanical response of the prism compared to mortar layers. The convergence of model simulation is faster for fewer number of parameters. The higher the number of parameters that are independently varying, the more accuracy there is in the prediction of the experimental observation of stress-strain relationship.

5.4. References

Blackard, B., Kim, B., Citto, C., Willam, K., & Mettupalayam, S. (2007). Failure issues of brick masonry. Paper presented at the Proceedings of the Sixth International Conference on Fracture Mechanics of Concrete and Concrete Structures.

Byrd, R. H., Gilbert, J. C., & Nocedal, J. (2000). A trust region method based on interior point techniques for nonlinear programming. Mathematical programming, 89(1), 149-185.

Byrd, R. H., Hribar, M. E., & Nocedal, J. (1999). An interior point algorithm for large-scale nonlinear programming. SIAM Journal on Optimization, 9(4), 877-900.

Esmailzadeh, S., Medina-Cetina, Z., Kang, J. W., & Kallivokas, L. (2015). Varying dimensional Bayesian acoustic waveform inversion for 1D semi-infinite heterogeneous media. Probabilistic Engineering Mechanics, 39, 56-68.

Foresee, F. D., & Hagan, M. T. (1997). Gauss-Newton approximation to Bayesian learning. Paper presented at the Proceedings of International Conference on Neural Networks (ICNN'97).

Lubliner, J., Oliver, J., Oller, S., & Oñate, E. (1989). A plastic-damage model for concrete. International journal of solids and structures, 25(3), 299-326.

MacKay, D. J. (1992). Bayesian interpolation. Neural computation, 4(3), 415-447.

Medina-Cetina, Z., Kang, J. W., Esmailzadeh, S., & Kallivokas, L. (2013). Bayesian inversion of heterogeneous media: Introducing the next generation of integrated studies for offshore site investigations. Paper presented at the Offshore Technology Conference.

Papazafeiropoulos, G., Muñiz-Calvente, M., & Martínez-Pañeda, E. (2017). Abaqus2Matlab: a suitable tool for finite element post-processing. Advances in Engineering Software, 105, 9-16.

Waltz, R. A., Morales, J. L., Nocedal, J., & Orban, D. (2006). An interior algorithm for nonlinear optimization that combines line search and trust region steps. Mathematical programming, 107.

6. EVALUATION OF LATERAL RESPONSE OF URM WALLS SUBJECT TO VERTICAL COMPRESSION STRESS AND LATERAL LOAD

6.1. Introduction

Unreinforced masonry walls consider as complex structures due to the uncertainty of inherent variation of material properties, errors associated with experimental tests, and errors associated with the numerical model. The CDP model with the constitutive material properties that are calibrated in the previous chapter is used to predict the structural response of URM walls that had been tested in the laboratory subject to compressive and lateral loads. Wang, Heath, and Walker (2013) studied the contact behavior between brick units and mortar layers under compression, flexure and shear, and the perforations appears of brick units control the shear strength in which the forces redistributed in both directions normal and tangential along the brick/mortar interface. Sarhosis and Sheng (2014) obtained directly the material parameters for masonry constitutive models from the results of compressive, tensile and shear strength tests on small masonry prisms. The effect of variation in material parameters for small-scale are problematics due to load conditions, raw material and manufacturing methods, the uncertainty of material parameters and boundary conditions(Hendry, 1998; Sarhosis & Sheng, 2014; Vermeltfoort, 1997). On the other hand, constructing small-scale consider less complexity in laboratory which could be controlled to avoid unnecessary devices and human errors and inexpensive compared to large masonry structures (Lignola, Prota, & Manfredi, 2009; Sarhosis & Sheng, 2014). V. Toropov and Garrity (1998) proposed an optimization method to identify material parameters which is based on the responses of relatively ‘‘non-trivial’’ large scale masonry elements. A proposed

method presented by Sarhosis and Sheng (2014) to identify the material parameters for masonry to reflect the complex nature of masonry and the range of stress state. Sarhosis and Sheng (2014) investigated the relative mechanical response masonry wall simulation as a large-scale based on results obtained from small-scale experiments or on the codes of practice or on engineering judgment are used in the model for the simulation of the large experiments. Then, the material parameters are implemented in masonry walls and modified through an optimization process to minimize the errors that express the difference between the responses measured from the large-scale experiments and those obtained from the numerical analysis. Because optimizing the material parameters of large-scale experiments is very expensive especially for masonry structures, the aim of this study is to optimize the material parameters through small-scale (prism) experiments and use these optimized values into simulation of large-scale (wall) experiments to validate experimental observations with numerical results. Also, the hypothesis is the identification of material parameters of small-scale throughout an optimization procedure in which the optimal parameters used for minimizing the errors that express the difference between the responses measured from the large-scale experiments and those obtained from the numerical analysis.

Richart, Moorman, and Woodworth (1932) investigated variation of the material properties, geometry and code specification for mortar and brick unit from individual components to full wall system experimentally in order to determine the factors influence masonry wall strength. Also, Richart et al. (1932) studied the influence the slenderness ratio, opening and load combinations effects in which they found the wall thickness is an important factor in determining the wall strength. The influence of the wall aspect ratio, which is essential to understand shear strength capacity and identify the mechanism failure of URM

walls under lateral loads, is investigated in several studies (Abrams & Shah, 1992; Agnihotri, Singhal, & Rai, 2013; Epperson & Abrams, 1990; Magenes & Calvi, 1997; Salmanpour, Mojsilović, & Schwartz, 2015; Xu & Abrams, 1992).

The results of model prediction showed a good agreement with the experimental data. Numerical simulations of Unreinforced Masonry (URM) walls were also performed for different aspect ratios to evaluate their failure mechanisms. The general procedure of the material parameter identification method and the numerical results are presented. The interface behavior is described by considering a Coulomb-type friction criterion on the mortar bed joints. Based on the shear and normal stress distributions derived with the model, possible failure modes are examined.

In this chapter, the optimal material parameters from chapter four will be used for two purposes: (a) to validate two experimental cases regarding the shear response of URM walls and (b) to discuss different types of failure criteria corresponding to their failure modes. Then, the procedure will be developed to discuss the shear strength in term of a relation between lateral load and vertical compressive stress, aspect ratio, and the material sensitivity on four parameters (e.g., flexural tensile strength, compressive strength, coefficient of friction and cohesion stress).

6.2. Evaluation of Lateral Strength of Unreinforced Masonry Walls

An essential consideration to assess masonry walls is to examine their resistance capability against a lateral force caused by wind or earthquake loads. Flexural cracking, shear sliding, and compressive failure are the most common failure modes that are predominantly a function of in-plane shear capacity of the walls. The feasibility of the evaluation process is verified through comparison with corresponding experimental results

(Abrams & Shah, 1992; Epperson & Abrams, 1990; Xu & Abrams, 1992). The numerical simulations of masonry walls showed a good agreement with experimental observations based on deterministic material parameters obtained from small-scale (prism) simulations as mentioned in chapter four. The essential aspects that control the cracks in masonry walls are, apart from the material parameters, the wall geometry and the ratio of vertical load to lateral load. Therefore, the effect of different parameters is accounted for by performing a parametric study of load combination and wall aspect ratio l/h_{eff} to investigate the crack failure patterns due to flexural cracking, compressive failure and sliding shear failure through varying the tensile strength, compressive strength, and coefficient of friction and shear stress on the intact elements between mortar layers and bricks. The ultimate shear strength is determined from the sum of lateral forces at the top nodes of the masonry wall divided by the gross sectional area.

6.2.1. Mesh Convergence Study

An issue that is usually overlooked in FE simulations and affects accuracy is mesh convergence, namely the mesh refinement that is required, so that the FE solution becomes practically independent of the mesh size. Since the geometry of the wall is simple, i.e. without curved geometry, it is obvious that there are not any geometric constraints on the mesh refinement process. The model WallE3 was used for the mesh convergence study. This FE model of the URM wall was solved for two levels of refinement for the mortar and three levels of refinement for the bricks. The refinements of the mortar and the bricks are independent, thus they yield six refinement cases, as shown in Table 6.1. The naming convention of the six models used for the mesh convergence study is meshRefBXMY, where X is the refinement level of the bricks and Y is the refinement level of the mortar. As X

and/or Y increase, the refinement increases, i.e. the number of nodes and elements of the FE mesh increase, leading to more accurate solutions. X=1 corresponds to discretization of the brick edges in two finite elements. Y=1 corresponds to discretization through the thickness of the mortar in a single finite element. For example, in the model meshRefB1M1 all bricks are discretized in two finite elements per edge (i.e. 4 finite elements per brick), and one element along the mortar thickness. X=2 and X=3 correspond to discretization of three and four elements per edge respectively. Y=2 corresponds to discretization through the thickness of the mortar in two finite elements. It is noted that the aspect ratio of the finite element of the mortar is equal, or as closest as possible to unity, in order to preserve a good mesh quality. Furthermore, special attention has been paid to ensure that hourglassing and shear locking phenomena do not occur in the FE mesh during the solution process (Reddy, 2014). The number of nodes and elements of the bricks and the mortar of each model is shown in Table 6.1.

The naming convention of Table 6.1 is used in the legend of Figure 6.1, where the shear stress – top displacement curves are plotted for the various cases. For reasons of easy comparison, the experimental result has been plotted in Figure 6.1. It is apparent that the cases with increased mesh refinement are closer to the experimental curve than those with the coarse mesh, which shows that the former cases have increased accuracy. In addition, since the numerical results of the refined mesh are in satisfactory agreement with the experimental results, it is justified that a further refinement of the mesh is not necessary. Therefore, the mesh refinement of the case meshRefB3M2 is used for the parametric analysis the results of which are presented in this study.

Table 6.1 Details of the 6 Models Used for the Mesh Refinement Study.

Model	Part	Element type	Elements	Nodes
meshRefB1M1	MORTAR	CPS4R	10108	19570
	BRICKS	CPS4R	1568	3528
meshRefB1M2	MORTAR	CPS4R	34941	50822
	BRICKS	CPS4R	1568	3528
meshRefB2M1	MORTAR	CPS4R	10108	19570
	BRICKS	CPS4R	3528	6272
meshRefB2M2	MORTAR	CPS4R	34941	50822
	BRICKS	CPS4R	3528	6272
meshRefB3M1	MORTAR	CPS4R	10108	19570
	BRICKS	CPS4R	6272	9800
meshRefB3M2	MORTAR	CPS4R	34941	50822
	BRICKS	CPS4R	6272	9800

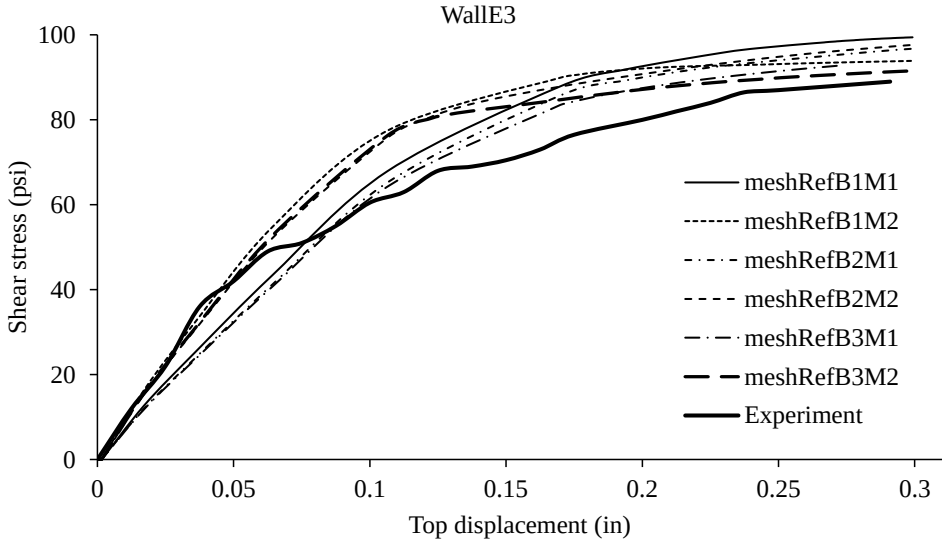

Figure 6.1. Mesh convergence results for the case WallE3 (Epperson & Abrams, 1990).

6.2.2. Masonry Wall Model Validation

To check the validity of optimal material parameters obtained from the NNO algorithm for the prism, two URM walls (referred from now on as “wall 1” and “wall 2”) were simulated and compared to experimental tests by Epperson and Abrams (1990). The geometrical model of URM walls was represented by clay brick panel with same height of 72” height and two different width 114” and 94” for wall 1 and wall 2, respectively. The cross-section area of wall 1 is 1870 in2 and for wall 2 1600 in2 which are tested by vertical compressive stress and lateral load-displacement. The walls are fixed at their bottom and free at their ends. The ABAQUS model of the wall is represented by 2D plane-stress elements (CPS8R). The constitutive behavior of both the bricks and the mortar thickness of 0.75” is defined by the ABAQUS CDP model. The Poisson ratio of the bricks is equal to 0.1 whereas the Poisson ratio of the mortar is 0.2. In addition, the flow potential eccentricity (ϵ) is equal to 0.1 for both the bricks and the mortar layers, and the ratio of initial equibiaxial compressive yield stress to initial uniaxial compressive yield stress (f_b / f_c) is set equal to 1.16 for both the bricks and the mortar. The optimal parameters of the masonry prism that were taken from Table 4.2 of Chapter 4 have been specified in the material definition of the walls which showed a good agreement with experiment tests (see Figure 6.2).

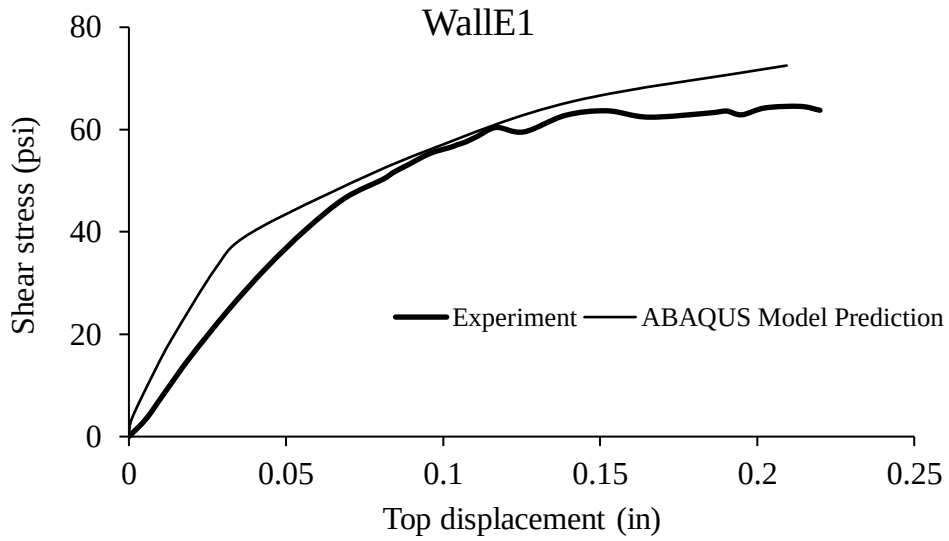

(a)

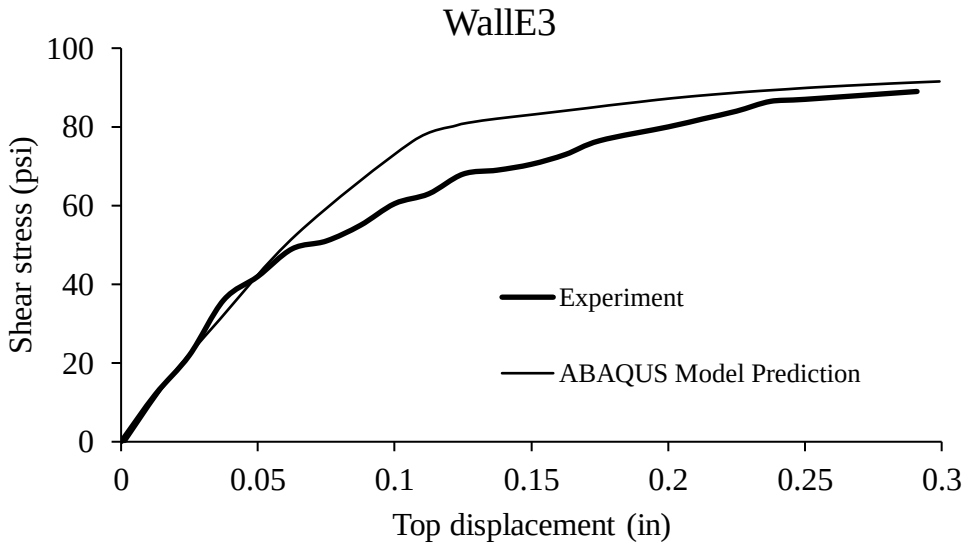

(b)

Figure 6.2. Model validation. a) Wall 1 b) Wall 2 (Epperson & Abrams, 1990).

6.3. Failure Modes and Failure Criteria

6.3.1. Flexural Crack

An important parameter in terms of shear strength is the flexural tension strength which is perpendicular to the bed joints and can affect the distribution of shear and normal stress between masonry layers through flexural cracking. However, the flexural tension strength is more important for URM with aspect ratio $l / h_{eff} = 0.5$ with a relatively low vertical compressive stress (see Figure 6.5c). Increasing lateral loads can significantly propagate the crack towards the toe. Theoretically, if the flexural tensile stress exceeds the allowable flexural tensile strength, the wall cracks propagate near the wall-base.

$$\sigma_y \leq f_t \tag{28}$$

where σ_y is the tension stress at the base of the wall which is normal to the bed joint and f_t is the flexural tensile strength. In general, the flexural crack initiates when the linear stage of the wall response ends. Figure 8 shows that the onset of cracking corresponds to lateral displacement equal to 0.1" which means that the linear stage is between 0-0.1". Also, it is obvious that the flexural failure occurs for low vertical compressive stresses σ_v between 0-50 psi combined with high lateral force. Consequently, as the lateral force applied in-plane of the wall increases, the inelastic (nonlinear) behavior is more pronounced. As a result, when the flexural tensile cracks extend to the toe of the wall, overturning will occur. Overturning can occur only when the unreinforced wall cracks and the following criterion is used to check failure due to overturning:

$$\tau = \frac{\sigma_v}{2}\left(\frac{l}{h_{eff}}\right) \tag{29}$$

Xu and Abrams (1992) presented an equation to evaluate the crack of unreinforced walls due to flexural tensile stress $\tau = \frac{1}{6}(\frac{l}{h_{eff}})(f_t + \sigma_v)$ where τ is the nominal shear stress between the brick and mortar layers.

6.3.2. Shear Sliding

The typical shear failure along the bed joint is due to the high lateral forces that cause high shear stress between the bricks and mortar layers. Also, the shear stress between the layers depends on several factors to resist the shear sliding such as the bond between the layers, friction, cohesion, and material heterogeneities. In this study, the friction a cohesion stress between the elements have been investigated. Failure due to sliding may occur in slender walls with high aspect ratio $l / h_{eff} > 1.5$ (Xu & Abrams, 1992). However, for aspect ratio $l / h_{eff} = 0.5$ shear sliding along the wall length may prevail when it subjected to high lateral force and low vertical compressive stress. Because the failure can extend over the full width, slender walls are most likely to fail in earlier loading stages compared to stocky walls (see Figure 6.5c). A major factor which affects this is the bond between brick and mortar layers; for this reason, friction and cohesion stresses have been studied in detail. According to the Mohr-Coulomb shear friction relationship, the shear failure criterion is as follows:

$$\tau \leq \tau_o + \mu\sigma_y \qquad (30)$$

where τ_o ,is the cohesion stress and μ is the coefficient of friction. The latter have been considered in ABAQUS software in order to investigate the effects of the normal and tangential behavior in the contact interfaces between bricks and mortar layers.

6.3.3. Diagonal Compressive Splitting

The diagonal compressive splitting occurs usually when $l / h_{eff} > 1.25$ which is a common failure mechanism, especially when the wall is subjected to high lateral force and vertical compressive stress. Compressive splitting is the last stage before collapse of the unreinforced walls. In other words, when the wall starts to deflect and a local area of shear sliding starts to form, the diagonal compressive splitting occurs toward the toe causing the wall to overturn. When the URM wall reaches shear sliding failure redistribution of normal and shear stresses takes place which can be induced from the resultant shear force and can generally delay the collapse event (see Figure 6.5b). Consequently, toe crashing or diagonal compression splitting may happen due to redistribution of the stresses. Page (1981) defined the failure criteria of the biaxial stresses and the principal stresses (σ_1, σ_2) with their orientation θ in term of 3D surface stresses. These stresses are the normal, tangential, and shear stress to the bed joint which can be represented by σ_n, σ_t and τ respectively. The failure criteria of biaxial stress is given by:

$$\tau^2 \leq (f_{mt} - \sigma_t)(f_{mn} - \sigma_n) \qquad (31)$$

where f_{mt} and f_{mn} are the compressive strength at the normal and tangential directions at the bed joints respectively, which can be obtained from masonry prism tests. When the normal stress σ_n is larger than the compressive strength f_{mn} crushing occurs at the toe(Xu & Abrams, 1992) (see Figure 6.5a).

6.3.4. Diagonal Tension Cracking

In this mode, the wall tends to crack at the heel due to high lateral forces and lack of diagonal tensile strength such as seismic loads (Council et al., 1999). This type of failure can

occur in the strong brick units and weak mortar which is typically found in walls with aspect ratio $l / h_{eff} > 1.25$. Xu and Abrams (1992) stated that strong mortar and weak units cracked with high vertical compressive stresses while weak mortar strong units cracked with low vertical compressive stresses. Essawy and Drysdale (1986) presented an equation to determine the principal tensile stress according to Mohr's circle at a point:

$$(\frac{\tau}{\sigma_o}) = (1 - \frac{\sigma_t}{\sigma_o})(1 - \frac{\sigma_n}{\sigma_o}) \qquad (32)$$

where σ_o is the diagonal tension strength in which the diagonal crack occurs when diagonal tensile stress is larger than the diagonal tensile strength.

6.4. Influence of Vertical Compressive Stress

In order to understand the effect of vertical compressive stress, a relationship has been considered between the lateral displacement and shear strength. An aspect ratio l / h_{eff} equal to 1.5 is used with compressive strength 1600 psi, coefficient of friction 0.5 and cohesion stress 100 psi. The values of vertical compressive stress applied at the top of the walls range from 50 psi to 250 psi (see Figure 6.3). The variation of vertical compressive stress can significantly affect the failure mode. When low vertical compressive stress is applied at the top of a slender wall with high lateral loads, the shear sliding may predominate the failure modes. The wall with aspect ratio $l / h_{eff} = 0.5$ is more likely to fail by sliding due to its short length. The effect of vertical compressive stress on the shear strength is slightly increased after the shear sliding modes start to propagate between the brick units and bed joints. Consequently, the shear stress is redistributed in some local areas in the normal and tangential directions that can increase the shear strength till a compression failure is reached.

The URM wall with lateral displacement between 0-0.8” exhibits elastic behavior while nonlinear behavior takes place as soon as the wall starts cracking.

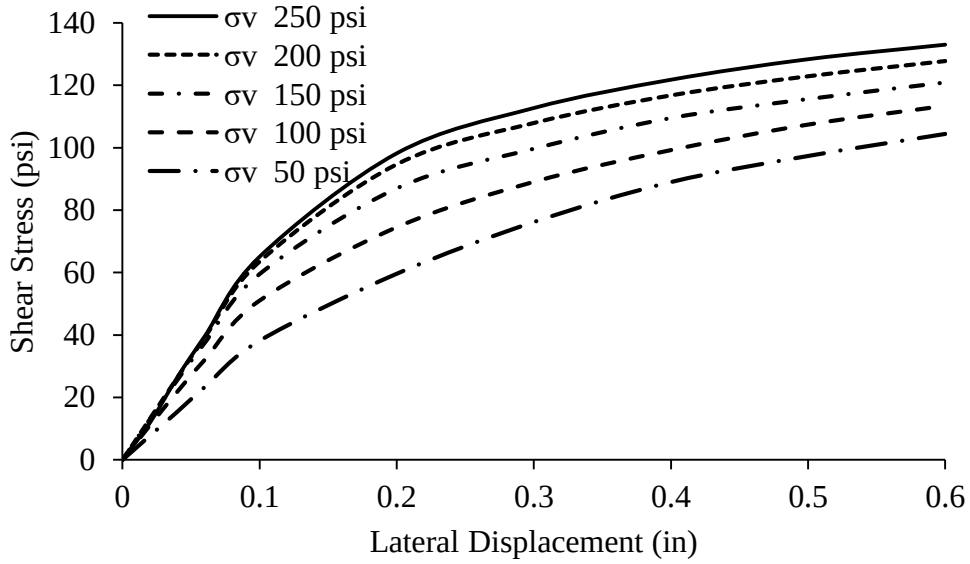

Figure 6.3. Influence of compressive vertical stress on shear strength of URM walls

6.5. Influence of Aspect Ratio

In this section the relationship between the lateral shear load-displacement and shear strength is investigated in terms of the length-to-effective height (aspect) ratio l / h_{eff}. The shear strength is estimated from the summation of lateral forces (e.g., 0, 0.02”, 0.04”, 0.06”, and 0.1”-0.6”) at the top nodes of masonry walls divided by the gross sectional area. The vertical compressive stress, flexural tensile strength and compressive strength are specified equal to 150 psi, 300 psi and 3000 psi respectively. The friction coefficient and cohesion stress are equal to 0.7 and 150 psi respectively. The aspect ratio is the only parameter that is

varied to investigate the effect shear strength capacity (e.g., 0.55, 1.3 and 1.6). The shear strength resistance increases significantly when l / h_{eff} increases (see Figure 6.4). The common failure mechanisms are flexural cracking, shear sliding and compressive splitting which occur in sequence. The higher the aspect ratio, the more failure modes show up during high lateral loads combined with low vertical compression stress. When the aspect ratio is $l / h_{eff} > 1.5$, most failure modes occur during high lateral loading (e.g., rocking, bed joint sliding, diagonal tension splitting and toe crush) (see Figure 6.5a). The sequence of this failure started with cracks usually near the wall base which then propagate across the wall. Then, the wall started unbinding between the brick units and mortar layers in which this stage may extend across the wall length especially with $l / h_{eff} < 1.25$ (see Figure 6.5c). Shear sliding can play a significant role to redistribute the normal and tangential stresses between the bed joints and brick units. Consequently, the propagation of shear sliding forms a typical stair-stepped bed-joint that can enhance a ductile mode with significant hysteretic energy dissipation capability. Masonry walls with $0.5 < l / h_{eff} < 1.5$ may show all failure mechanisms except rocking foundation during high loads (See Figure 6.5b).

6.6. Influence of Material Parametric Sensitivity

In order to investigate the effects of material parameters sensitivity, a relationship between lateral displacement and shear strength has been constructed for URM walls. The shear strength of a cracked wall is calculated by the maximum in-plane lateral force divided by the gross sectional area. In other words, the shear strength is obtained from the sum of

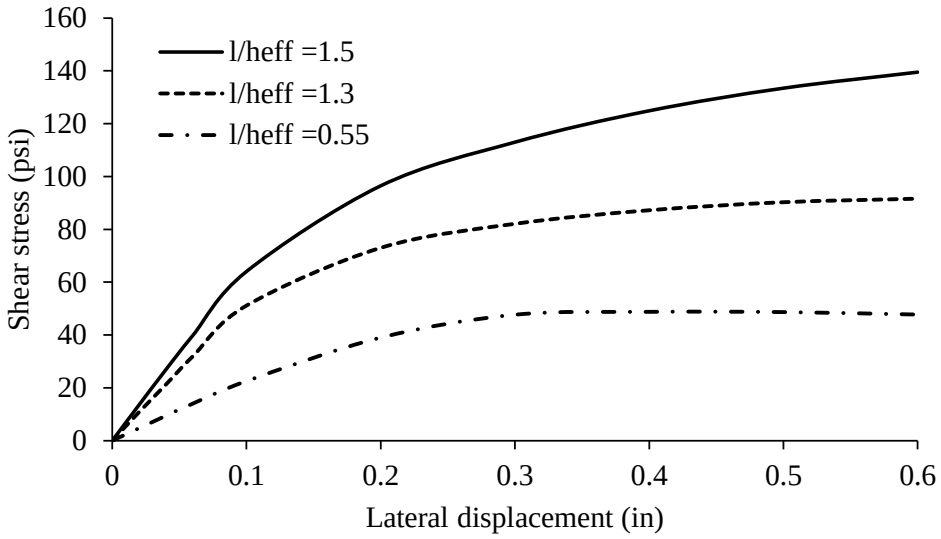

Figure 6.4. Influence Aspect Ratio in Shear Strength of URM walls.

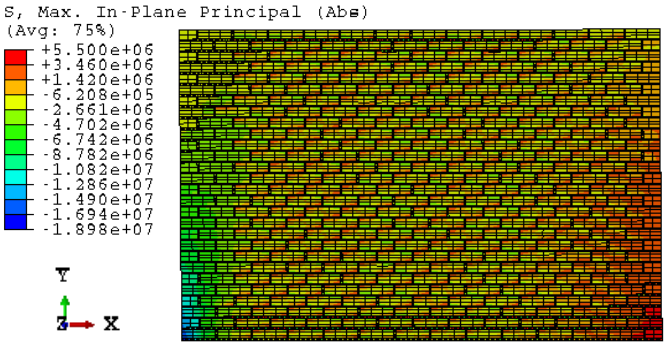

(a)Stocky

Figure 6.5. URM walls simulations in ABAQUS for max. Absolute in-plane principal stress (Pa).

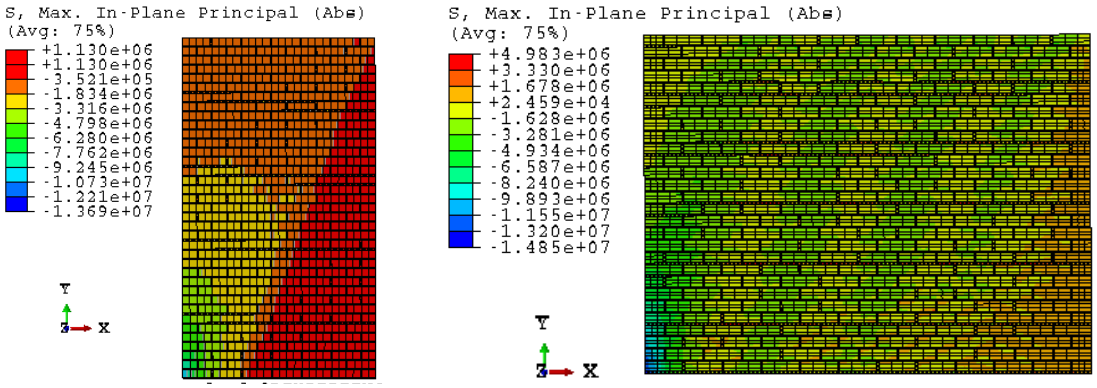

(b) Slender **(c) Square**

Figure 6.5 Continued

lateral force of the top nodes of unreinforced walls divided by their gross sectional area. The masonry wall is simulated in ABAQUS with dimensions of 72” height and 114” length and its gross area is 1870 in2. The wall is subjected to an in-plane lateral load-displacement for example (e.g., 0, 0.02”, 0.04”, 0.06”, and 0.1”-0.6”) and for each simulation the shear strength is determined from the sum of lateral force divided by the gross sectional area. The CDP model is used with the material parameters that have been used for the verification of the wall response in section 5.3.1. In order to understand the post-cracking behavior, it is essential to carry out parametric studies, the parameters of which are the tensile strength, compressive strength, the coefficient of friction and the cohesion between the brick units and mortar layers.

6.6.1. Flexural Tensile Strength

Flexural tensile strength is the most important factor which contributes to the shear resistance and controls the ductility when the masonry walls are subject to in-plane lateral loads. The low vertical compressive stress and high lateral displacement can significantly

affect slender walls. In order to investigate the flexural shear strength, the relationship between the lateral displacement and shear strength is considered. The aspect ratio is 1.5 with 1600 psi as compressive strength and coefficient friction and cohesion stress 0.7 and 100 psi respectively. Flexural tensile strength is the only parameter that is varied (e.g., 10 psi, 50 psi, and 100 psi) to evaluate the shear strength. Figure 11 shows that for higher flexural tensile strength, the masonry wall's resistance to the lateral loads and ductility increase. For lateral displacement equal to 0.8" flexural cracks begin to propagate. In addition, when the wall is subjected to lateral load-displacement equal to 0.5", it failed with 10 psi of flexural tensile strength. Also, the shear sliding failure predominates in the failure stage as illustrated in Figure 6.6 compared to other failure stages. Consequently, the shear

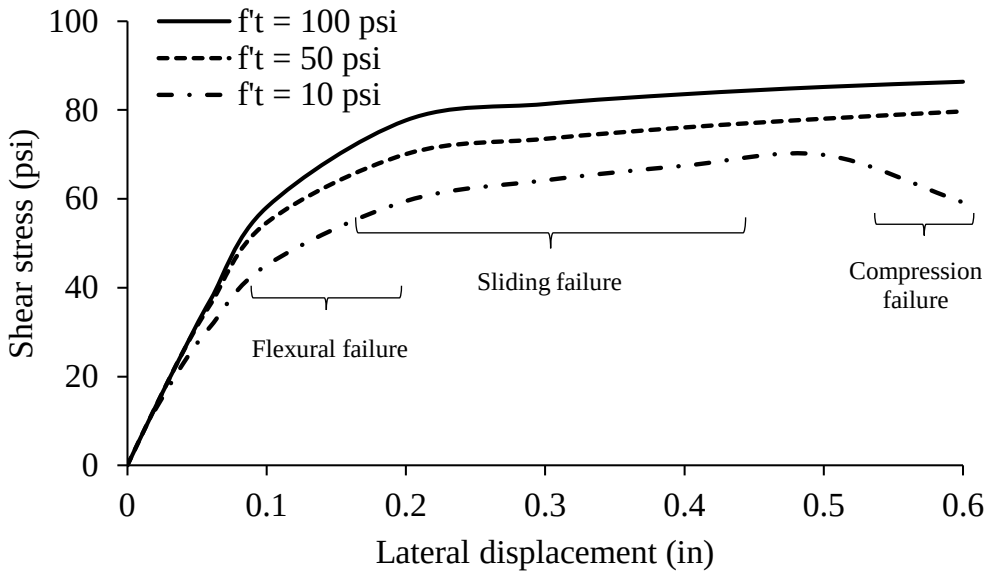

Figure 6.6. Influence of flexural tensile strength on shear strength of URM walls.

sliding between the bed joints increases the resistance against collapse as well as ductility.

6.6.2. Compressive Strength

Compressive strength is an important parameter that controls failure due to vertical compressive stresses. Three values for compressive strength have been considered in the simulation (e.g., 1000 psi, 2000 psi, and 3000 psi). The vertical compressive stress is equal to 150 psi for masonry wall, $l / h_{eff} = 1.5$ and the other parameters are as follows: flexural tensile strength 300 psi, cohesion stress 150 psi and coefficient of friction 0.7. However, when the compressive strength is equal to 1000 psi, the strength of the wall is significantly reduced, and it failed at lateral load-displacement equal to 0.4" (see Figure 6.7). From Figure 6.7 it is noted that flexural cracks were created when the lateral displacement ranges from 0.1" to 0.2" and the shear sliding ranges between 0.2" and 0.4" and then compressive splitting takes place until collapse. The variation of compressive strength demonstrates clearly that all curves start in the same range of flexural cracking and shear sliding whereas the compressive splitting controls the shear strength. Consequently, if the wall does not fail due to the compressive stress, then the shear strength of the wall does not depend on the compressive strength.

6.6.3. Coefficient of Friction and Cohesion Stress

Coefficient of friction and cohesion stress depend on the normal and tangential behavior between the brick units and mortar layers. The Mohr-Coulomb criterion in eq. 30 shows that friction and cohesion affect significantly the shear sliding failure. As these two parameters increase, the shear strength to resist shear sliding failure that propagates along the length of masonry wall increases (see Figure 6.8). When the applied lateral load is low,

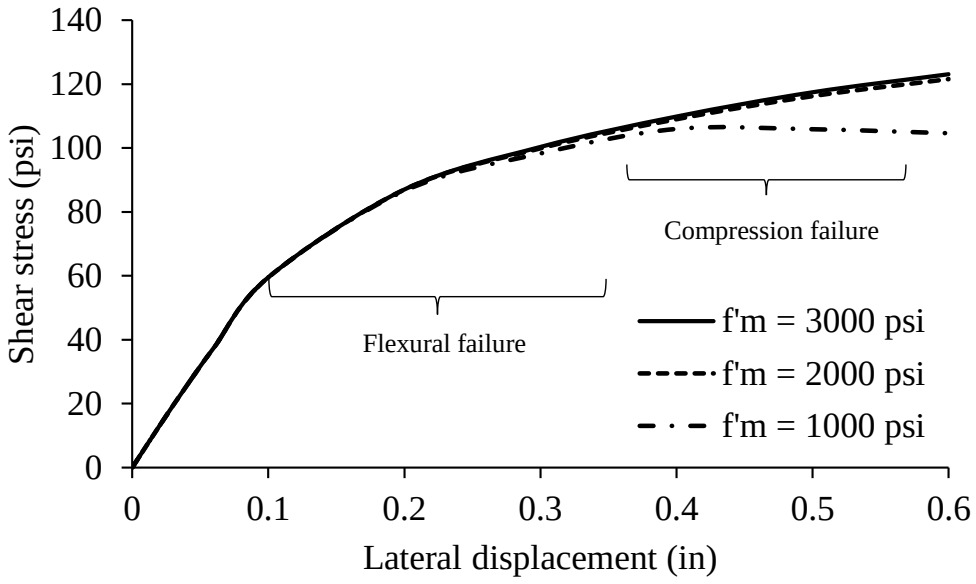

Figure 6.7. Influence of compressive strength on shear strength of URM walls

the variation of the shear strength is slightly changed with respect to high coefficient of friction and cohesion stress. Consequently, in most cases the region of sliding failure varies based on the local values of normal and tangential stresses between the bed joints. To investigate the variation effect of coefficient of friction and cohesion stress URM walls were individually simulated corresponding to parameters and aspect ratio similar to those mentioned above, except for coefficient of friction and cohesion stress which take the values [0.5, 0.7, 0.9] and [100 psi, 150 psi, 200 psi], respectively. Bolhassani, Hamid, Lau, and Moon (2015) tested masonry prisms under diagonal shear and the coefficient of friction values used based on slip-rate data between [0.6-0.8]. The results are slightly change in shear strength from 0.7 to 0.9 while the coefficient of friction is more sensitive for values from 0.5 to 0.7. Consequently, for higher values of the friction coefficient, less variation of shear

strength can be achieved (see Figure 6.8a). The variation of cohesion significantly controls the shear strength when the wall is subjected to in-plane lateral loads. For lower values of cohesion stress the effect on the shear strength becomes more pronounced. Figure 6.8b illustrates that shear sliding begins earlier for cohesion equal to 100 psi compared to the other cohesion values.

6.7. Conclusion

The calibrated material properties that are calculated from the NNO algorithm that is presented in the previous chapter have been inserted in suitable FE models which have shown good agreement with analogous experimental data. Consequently, it is concluded that the proposed NNO algorithm is sufficiently robust and accurate for calibration of constitutive material properties based on experimental data. Apart from this, the influence of various factors on the shear response of URM walls is investigated. It has been found that the shear stress is redistributed in some local areas in the normal and tangential directions that can increase the shear strength till a compression failure is reached. Shear sliding can play a significant role to redistribute the normal and tangential stresses between the bed joints and brick units. Consequently, the propagation of shear sliding forms a typical stair-stepped bed-joint that can enhance a ductile mode with significant hysteretic energy dissipation capability. Generally, the shear sliding between the bed joints increases the resistance against collapse as well as the ductility of the wall.

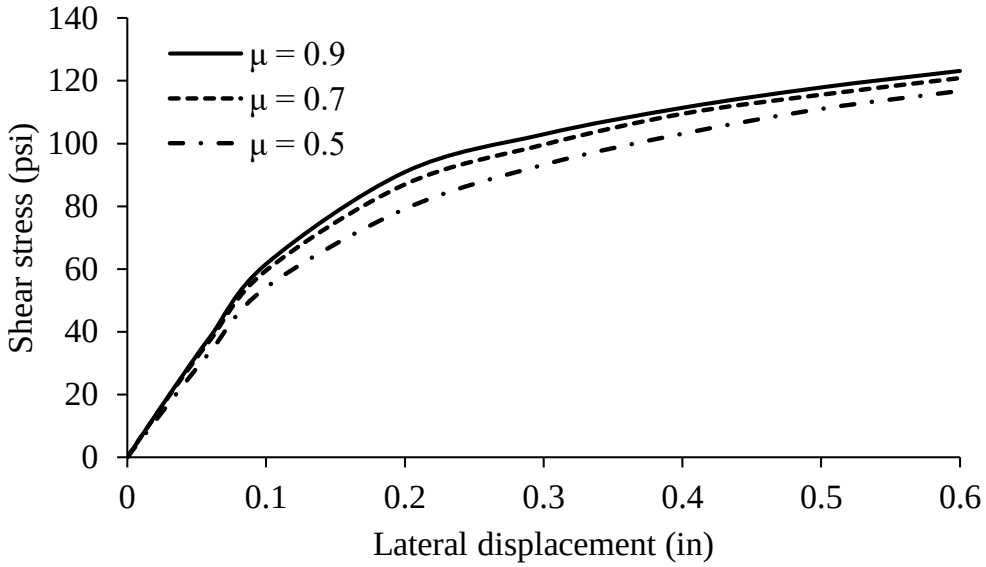

a)

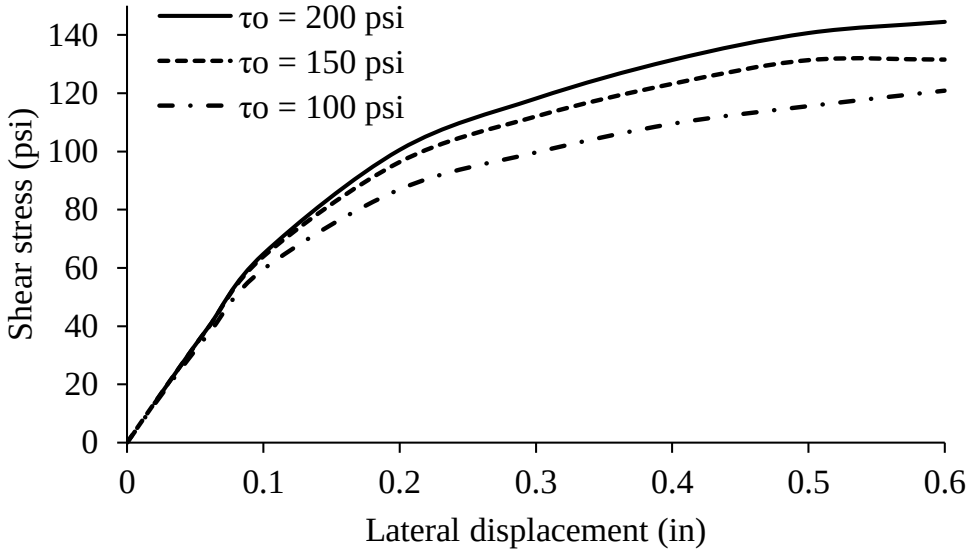

b)

Figure 6.8. Influence of contact properties on shear strength of URM walls: a) friction, b) cohesion stress.

6.8. Reference

Abrams, D. P., & Shah, N. (1992). Cyclic load testing of unreinforced masonry walls. Retrieved from

Agnihotri, P., Singhal, V., & Rai, D. C. (2013). Effect of in-plane damage on out-of-plane strength of unreinforced masonry walls. Engineering Structures, 57, 1-11.

Bolhassani, M., Hamid, A. A., Lau, A. C., & Moon, F. (2015). Simplified micro modeling of partially grouted masonry assemblages. Construction and Building Materials, 83, 159-173.

Council, A. T., Response, P. f., & Agency, U. S. F. E. M. (1999). Evaluation of Earthquake Damaged Concrete and Masonry Wall Buildings: Basic Procedures Manual: The Agency.

Epperson, G. S., & Abrams, D. P. (1990). Nondestructive evaluation of masonry buildings (Vol. 89): University of Illinois at Urbana-Champaign.

Essawy, A. S., & Drysdale, R. G. (1986). Macroscopic failure criterion for masonry assemblages. Paper presented at the Proc., 4th Canadian Masonry Symp.

Hendry, A. W. (1998). Structural masonry: Macmillan International Higher Education.

Lignola, G. P., Prota, A., & Manfredi, G. (2009). Nonlinear analyses of tuff masonry walls strengthened with cementitious matrix-grid composites. Journal of Composites for Construction, 13(4), 243-251.

Magenes, G., & Calvi, G. M. (1997). In-plane seismic response of brick masonry walls. Earthquake engineering & structural dynamics, 26(11), 1091-1112.

Page, A. (1981). The biaxial compressive strength of brick masonry. Proceedings of the Institution of Civil Engineers, 71(3), 893-906.

Richart, F. E., Moorman, R., & Woodworth, P. M. (1932). Strength and stability of concrete masonry walls: a report. Retrieved from

Salmanpour, A. H., Mojsilović, N., & Schwartz, J. (2015). Displacement capacity of contemporary unreinforced masonry walls: an experimental study. Engineering Structures, 89, 1-16.

Sarhosis, V., & Sheng, Y. (2014). Identification of material parameters for low bond strength masonry. Engineering Structures, 60, 100-110.

Toropov, V., & Garrity, S. (1998). Material parameter identification for masonry constitutive models. Paper presented at the Proceedings of the Eighth Canadian Masonry Symposium.

Vermeltfoort, A. (1997). Effects of the width and boundary conditions on the mechanical properties of masonry prisms under compression. Paper presented at the Proc. 11 th Int. Brick/Block Masonry Conference, Shangai.

Wang, J., Heath, A., & Walker, P. (2013). Experimental investigation of brickwork behaviour under shear, compression and flexure. Construction and building materials, 48, 448-456.

Xu, W., & Abrams, D. P. (1992). Evaluation of Lateral Strength and Deflection for Cracked Unreinforced Masonry Walls. Illinois University at Urbana Advanced Construction Technology Center.

7. CONCLUSION – FUTURE STUDY

7.1. Conclusions

- This work introduces the calibration of the Concrete Damaged Plasticity (CDP) material properties in ABAQUS for URM infill walls (e.g. comprised of brick, mortar and concrete) by using stress-strain data of compressive masonry prism experimental tests taken from the literature
- The ABAQUS model with the optimal CDP material parameters showed good agreement with experimental observations. The algorithm of nonlinear least squares proved to be an efficient formulation for capturing optimal parameters.
- The optimal parameters are used as a starting point for the probabilistic calibration of a brick unit and mortar.
- The Markov Chain Monte Carlo approach coupled with Metropolis Hastings criteria (MCMC- MH) algorithm showed a unique capability to fit the experimental observation and validated the stress strain curves when applied for the elastic and inelastic model response.
- Spatial statistical inferences were produced from the solution to the numerical integration of the posterior from the numerical predictions, and the experimental observations.
- Material heterogeneity is studied for a masonry prism using random variables for predicting stress strain curves using the ABAQUS CDP model. Four cases were considered about the inverse problem of calibrating the CDP model parameters. In

each case different material parameter combinations for fitting the experimental stress strain curve were examined.

- A novel Artificial Neural Network Optimization (NNO) algorithm was introduced to calibrate the material parameters in masonry prisms for describing the mechanical response of the Unreinforced Masonry (URM) walls.
- An appealing characteristic of the NNO is its ability to fit numerical model parameters based on experimental data, so that the agreement between simulation and experiment is very good and also requires minimal computational effort.
- The URM walls was validated using the optimal material parameters of a masonry prism. Then, shear strength capacity is evaluated in term of a relationship between the sums of lateral-loads divides by gross sectional area and the maximum lateral displacement.
- Mesh sensitivity is considered in order to examine the convergence accuracy with different levels of mesh refinement between the brick units and mortar layers to preserve a good mesh quality and prevent shear locking and hourglassing phenomena.
- The influence of various factors on the shear response of URM walls is investigated in terms of length-to-effective height "aspect ratios (l / h_{eff})" and vertical compressive stress.
- Parametric studies are carried out to investigate three common failure mechanisms associated with URM walls (e.g., flexural failure, shear sliding, compressive failure).

7.2. Future Study

"It is controversy issues and important tasks for engineers and scientists perform is to model natural phenomena" said by Reddy, 2019. Therefore, there is always a chance to develop a theory to capture the true behavior of a mechanical response; however, the errors between the natural phenomena and the model prediction exist. The possible future studies based on this thesis are threefold:

- Investigate the probabilistic calibration of three material parameters in CDP model (e.g., Young's modulus E viscosity μ , and deviatoric out-of-roundness κ) and the uncertainty associated with the observations and predictions model.
- Determine the optimal parameters associated with failure modes and failure criteria of URM walls (e.g., flexural tensile strength, compressive strength, coefficient of friction and cohesion stress).
- Investigate the correlation between the failure mechanisms (e.g., flexural failure, shear sliding, compressive failure) by using the Markov Chain Monte Carlo approach coupled with Metropolis Hastings criteria (MCMC- MH) algorithm.

APPENDIX A

DATA COLLECTION

Table A-1 Mortar Data

Reference	Spec #	Spec Shape	Dim (in^3)			Material Properties				
				E (psi)	f'c (psi)	Mix	w/c	Material	Load	Days
Fiorato, et al. (1970)	1	Cylinder	4 x 8 x5	1.23E+06	1390		1.35	sand	15,000 Ib /min	25
Mosalam (1996)	1	Cylinder	2x4	2.00E+06	3070 S	S 1 : 0.2: 3.83	1.2	Cement-Lime-sand		28
Mosalam (1996)	1	Cylinder	2x4	6.00E+05	1770	N 1: 0.5:4.5		Cement-Lime-sand		
Fransico (1997)	4	cylinder	2x4		1494	1:0.5:4.5 S		Cement-Lime-sand		28
Blockrad et. al (2009)		Cylinder	4x8	5.00E+05	732	1:1:5 M		Cement-Lime-sand		28
Blockrad et. al (2009)	5	Cylinder	4x8		1160	1:1:5 M		Cement-Lime-Sand	Triaxial load	28
Barbosa et al. (2010)	4	Cylinder	2x4	1.18E+06	1116	1:1.3:5.3	1.4	Cement-Lime-Sand	0.005 mm/s	14
Cheng & Khoo (1972)	6	Cylinder	1.5x4		4949	1 : 0.25 : 3	0.64	Cement-Sand-aggr	0 psi	14

Table A-1 Continued

								Cement-Sand-aggr	282 psi	14
								Cement-Sand-aggr	590 psi	14
								Cement-Sand-aggr	896 psi	14
					1033	1 : 1 : 6	1.25	Cement-Sand-aggr	1206 psi	14
									1510 psi	14
Gonçalves et al., (2007)	4	Cylinder	2x4	3858004	7992	1:1.5 c/agg	0.4	cement - sand		28
Gonçalves et al., (2007)	4	Cylinder	2x4	3567928	5932	1:1.5 c/agg	0.5	cement - sand		28
Mohamad et al. (2006)		Cylinder	2x4	1.63E+06	2886	1:1/4:3		Cement-Lime-Sand		28
Mohamad et al., (2006)		Cylinder	2x4	584937	609.2	1:1:6,		Cement-Lime-Sand		28
Mohamad et al., (2016)		Cylinder	2x4	1.86E+06	2944	1:1/4:3		Cement-Lime-Sand		28
Mohamad et al., (2016)		Cylinder	2x4	6.96E+05	1073	1:0.5:4.5		Cement-Lime-Sand		28

Table A-1 Continued

Mohamad et al., (2016)		Cylinder	2x4	4.64E+05	652.7	1:1:6,		Cement-Lime-Sand		28
Ciornei (2012)	5	cube	2x2x2		1407					66
Nguyen (2014)	2	cube	2x2x2		1200			Cement-Lime-Sand	0.0001 in/s	28
Kaushik, et al. (2007)	3	cube	2x2x2	79034.4	450	1 : 0 : 6	0.7	Cement-Lime-Sand		28
	3	cube	2x2x3	543876	2175	1 : 0.5 : 4.5	0.7	Cement-Lime-Sand		28
	3	cube	2x2x2	478611	2200	1 : 0 : 3	0.7	Cement-Lime-Sand		28
Bu et al., (2016)	3	cube	2x2x6	6584.71	5E+06		0.4			
				5859.53	4E+06		0.45			
				5337.39	3E+06		0.5			
Singh & Munjal (2016)	3	cube	2x8	478611	3023	1 : 0 : 3	0.7	Cement-Lime-Sand		28
					2355	1:1:4,	0.7	Cement-Lime-Sand		28
					1836		0.8	Cement-Lime-Sand		28

Table A-2 Brick Data

Reference	Spec #	Dim (in^3)	type	Material Prop.	
				E (psi)	f'c (psi)
Mosalam (1996)		7.5x15.5	concrete block	1.41E+06	
Barbosa et al. (2010)		5.5x7.5x15	concrete block		1624.4
Andreas (2009)	8	7.6x3.6x3.4	concrete bricks		1377
Mohamad et al., (2016)	10	5.5x7.5x15	concrete bricks	2987777	
Singh & Munjal (2016)	1	8x4x4	concrete bricks		2422.13
Kaushik et al., (2007)	10	9x4x3	clay bricks	7.63E+05	2567.15
				7.30E+05	2335.1
				1.09E+06	4191.57
				9.48E+05	2987.76

Table A-2 Continued

				8.84E+05	3016.77
Blockrad (2009)	2	4.5×3.75×2.25	clay bricks	3.00E+06	4840
Singh & Munjal (2016)	3	9x4.5x3	clay bricks		1595.42
					1934.8
					1195.11

Table A-3 Concrete Data

Reference	**Spec #**	**Spec Shape**	**Dim (in^3)**				**Material Prop.**		
				f'c (psi)	Mix	w/c	Material	Load	Days
Fiorato (1970)	1	Cylinder	4 x8 x5	5510	1:1:4 M	0.8	fine & coarse aggregate	75,000 Ib /min	25
Mehrabi (1996)	3	cube	6x6x6	3900					28
Stavridis (2009)	3	Cylinder	6x12	5500					28

Table A-3 Continued

Nguyen (2014)	5	Cylinder	2x8	3000					28
Hognstad et al., (1955)	5	Cylinder	6x12	4000					28
Smith & Young (1956)		Cylinder							45